Biogeosciences Discuss., 9, 5579–5623, 2012
www.biogeosciences-discuss.net/9/5579/2012/
doi:10.5194/bgd-9-5579-2012

Biogeosciences Discussions

Modelling contrasting responses of wetland productivity to changes in water table depth

R. F. Grant[1], A. R. Desai[2], and B. N. Sulman[2]

[1]Department of Renewable Resources, University of Alberta, Edmonton, AB, T6G2E3, Canada
[2]University of Wisconsin-Madison Department of Atmospheric and Oceanic Sciences, 1225 W. Dayton St, Madison, WI 53706, USA

Received: 15 April 2012 – Accepted: 18 April 2012 – Published: 14 May 2012

Correspondence to: R. F. Grant (robert.grant@ales.ualberta.ca)

Published by Copernicus Publications on behalf of the European Geosciences Union.

Abstract

Responses of wetland productivity to changes in water table depth (WTD) are controlled by complex interactions among several soil and plant processes, and hence are site-specific rather than general in nature. Hydrological controls on wetland productivity were studied by representing these interactions in connected hummock and hollow sites in the ecosystem model *ecosys*, and by testing CO_2 and energy fluxes from the model with those measured by eddy covariance (EC) during years with contrasting WTD in a shrub fen at Lost Creek, WI. Modelled interactions among coupled processes for O_2 transfer, O_2 uptake, C oxidation, N mineralization, N uptake and C fixation by diverse microbial, root, mycorrhizal and shoot populations enabled the model to simulate complex responses of CO_2 exchange to changes in WTD that depended on the WTD at which change was occurring. At the site scale, greater WTD caused the model to simulate greater CO_2 influxes and effluxes over hummocks vs. hollows, as has been found at field sites. At the landscape scale, greater WTD caused the model to simulate greater diurnal CO_2 influxes and effluxes under cooler weather when water tables were shallow, but also smaller diurnal CO_2 influxes and effluxes under warmer weather when water tables were deeper, as was also apparent in the EC flux measurements. At an annual time scale, these diurnal responses to WTD in the model caused lower net primary productivity (NPP) and heterotrophic respiration (R_h), but higher net ecosystem productivity (NEP = NPP – R_h), to be simulated in a cooler year with a shallower water table than in a warmer year with a deeper one. This difference in NEP was consistent with those estimated from gap-filled EC fluxes in years with different water tables at Lost Creek and at similar boreal fens elsewhere. In sensitivity test of the model, annual NEP declined with increasing WTD in a year with a shallow water table, but rose in a year with a deeper one. The model thus provided an integrated set of hypotheses for explaining site-specific and sometimes contrasting responses of wetland productivity to changes in WTD as found in different field experiments.

BGD
9, 5579–5623, 2012

1 Introduction

The productivity of wetland ecosystems is strongly affected by changes in water table depth (WTD). However these effects are complex and site-specific because they arise from numerous interactions among physical and biological processes that control carbon and nutrient transformations in soils. Lowering shallow water tables has been found to increase soil respiration (Flanagan and Syed, 2011; Silvola et al., 1996) through the effects of increased access to O_2 on microbial activity in drained soil (Moore and Dalva, 1993). However lowering deeper water tables has been found not to affect, or even to reduce, soil respiration (Lafleur et al., 2005; Muhr et al., 2011; Scanlon and Moore, 2000) because effects on microbial activity from increased uptake of O_2 in deeper drained soil may be offset by those from reduced access to substrates in dry surface soil (Dimitrov et al., 2010a).

The relationship between WTD and soil respiration therefore depends on the hydrological and biological properties of wetland soils. Those with large water holding capacity and low macroporosity drain more slowly, and so maintain soil wetness through capillary rise, enabling soil respiration to increase as water tables deepen. Soils with low water holding capacity and large macroporosity drain more rapidly, and so are less able to maintain surface wetness through capillary rise, causing soil respiration not to increase, or even to decrease, as water tables deepen. The extent to which respiration increases in soils drained by deepening water tables also depends upon the lability vs. recalcitrance (Muhr et al., 2011; Nadelhoffer et al., 1991) and on the temperature (Blodau et al., 2007) of the deeper drained soil organic carbon (SOC).

More rapid soil respiration with increased WTD can hasten nutrient mineralization and uptake, and thereby increase primary productivity. Wood and foliar growth are more rapid on soils with lower water tables because nutrient mineralization and consequently nutrient uptake are more rapid, as evidenced by higher foliar nutrient concentrations and CO_2 assimilation rates measured in spruce on drained vs. undrained peatlands (Macdonald and Lieffers, 1990) or in a treed fen over declining water tables

BGD
9, 5579–5623, 2012

(Flanagan and Syed, 2011). Lowering of water tables has caused annual basal area increments of black spruce to more than double (Lieffers and Macdonald, 1990) and annual tree ring growth to increase by several times (Dang and Lieffers, 1989) at different boreal sites. More rapid nutrient uptake and growth with lower water tables have been attributed to higher soil temperatures (Lieffers and Rothwell, 1987) and lower soil water contents (Lieffers, 1988). More rapid nutrient uptake and growth can also be attributed to more rapid root O_2 uptake and hence activity, particularly in roots with low internal porosity which rely more on soil transport for O_2 uptake. However in soils with rapid drainage and low water holding capacity, lower water tables can reduce productivity by causing surface drying and hence water stress in shallow-rooted vegetation such as moss (Dimitrov et al., 2011).

Responses of respiration and productivity to changes in water table thus depend upon soil and plant properties as well as on WTD, and consequently differ among wetlands (Adkinson et al., 2011; Sulman et al., 2010). Mathematical models may provide a means to understand and eventually to predict these responses, but only if they represent the basic processes by which these responses are determined. Water table effects on soil respiration are usually represented in models by lower rate constants for anoxic decomposition (St-Hilaire et al., 2010), or by scalar functions that reduce rate constants for decomposition at high soil water contents or potentials (e.g., Bond-Lamberty et al., 2007; Zhang et al., 2002). Water table effects on productivity are sometimes represented by time-dependent scalar functions that reduce productivity in wet soils through a driver variable such as stomatal conductance (e.g., Bond-Lamberty et al., 2007; Sonnentag et al., 2008). However these scalar functions do not simulate the physical and biological processes by which suppression of decomposition and productivity occur in wetland soils, but rather the effects of these processes.

Even so, these functions are not widely implemented in mathematical models used to study ecosystem behavior. In a recent review of seven widely used ecosystem models, Sulman et al. (2012) found only one which included processes to limit productivity in wet soils. Furthermore, most ecosystem models do not simulate the hydrological

BGD
9, 5579–5623, 2012

processes that control WTD and hence the soil wetness that drives these functions, but rather require WTD as an input (e.g., St-Hilaire et al., 2010; Frolking et al., 2002). This requirement limits the predictive capabilities of these models.

The key processes needed in models used for studies of wetland productivity are the transport, uptake and reduction of O_2 in soil as affected by soil water content. Higher water tables are thought to decrease respiration by reducing O_2 uptake used to drive oxidation-reduction reactions by soil microbes and roots. Energy yield from oxidation when coupled to reduction of O_2 exceeds that from oxidation when coupled to reduction of other electron acceptors (Brock and Madigan, 1991). Reduced O_2 uptake therefore slows processes driven by this energy, including microbial and root growth, decomposition and nutrient mineralization, and hence nutrient uptake and plant productivity. On the other hand, lower water tables are thought to decrease respiration by reducing microbial access to substrate in desiccated near-surface soil (Dimitrov et al., 2010a), thereby slowing oxidation-reduction reactions and hence microbial growth and activity. Models used to study water table effects on wetland respiration and productivity therefore should explicitly simulate (1) the transformations and energy yields of oxidation-reduction reactions by microbes and roots, (2) controls on the rates of these reactions exerted by the transfers of water and of the reactants and products of these reactions, particularly O_2, through soil and roots, and (3) the effects of these reactions on soil nutrient transformations and root nutrient uptake. These reactions, as well as their controls and effects, need to be simulated in dynamic aerobic and anaerobic zones determined by water table position calculated from vertical and lateral water transfers.

These processes are implemented to varying degrees in transient variably saturated flow models (e.g., Langergraber and Šimůnek, 2005) used to study respiration in constructed wetlands. The full implementation of these processes would avoid the arbitrary scalar functions described above which are used to represent these effects in some current ecosystem models. Such implementation is attempted in the general-purpose model *ecosys*, in which a comprehensive set of oxidation-reduction reactions in soil

BGD
9, 5579–5623, 2012

(obligate aerobic, facultative anaerobic and obligate anaerobic heterotrophic decomposition, heterotrophic and autotrophic methanogenesis, autotrophic methanotrophy, autotrophic nitrification and heterotrophic diazotrophy) and roots are calculated from reaction kinetics driven by oxidation-reduction energy yields (Grant, 1998, 1999; Grant and Pattey, 2003; Grant et al., 2006, 2008, 2009a, 2010a,b). All reactants and products of these reactions undergo convective-dispersive transfer through, and volatilization-dissolution exchange between gaseous and aqueous phases of soil and roots in three-dimensional soil landscapes, thereby controlling aqueous concentrations and hence oxidation-reduction rates (Dimitrov et al., 2010a, 2011; Grant, 2004; Grant and Roulet, 2002). These rates drive those of soil nutrient transformations and hence root nutrient uptake, thereby controlling primary productivity (Grant et al., 2009a, 2010a,b). All algorithms used to simulate these transformations and transfers are parameterized from basic research conducted independently of the model, allowing *ecosys* to avoid arbitrary parameterizations of anaerobic effects on respiration and productivity used in earlier models. Furthermore, the model includes a full set of vertical and lateral water flows used to calculate WTD (Dimitrov et al., 2010b; Grant, 2004), enabling the simulation of all key processes by which WTD affects wetland respiration and productivity.

The absence of these processes in most ecosystem models prevents them from simulating changes in respiration and productivity observed with changes in WTD, limiting their ability to simulate wetland behavior (Sulman et al., 2012). The objective of this study is to determine whether implementing these processes in a more detailed ecosystem model such as *ecosys* would enable simulation of the complex changes in wetland respiration and productivity observed with changes in WTD. For example, with increasing WTD the model should be able to simulate increases in respiration from more rapid O_2 uptake and reduction under some conditions, but decreases in respiration from soil drying under others. With increasing WTD the model should also be able to simulate increases in productivity from more rapid nutrient mineralization and uptake under some conditions, but reduced productivity from water stress under others. To accomplish this, CO_2 fluxes modelled over a shrub fen at Lost Creek, WI, were compared

BGD
9, 5579–5623, 2012

with those measured by eddy covariance (EC) at hourly, seasonal and annual time scales during several years with differing temperature, precipitation and WTD.

2 Methods

2.1 Model development

2.1.1 General

The key algorithms governing the modelling of ecological controls on CO_2 exchange in *ecosys* are described in the Supplement to this article, in which equations and variables referenced below are described and listed in Appendices A–F. Algorithms which govern the transport, uptake and reduction of O_2 in soil are particularly relevant to controls on CO_2 exchange in wetlands, and so are described here in further detail. All model parameters in *ecosys* are derived from independent experiments and so remain unchanged in this study from those used in earlier studies (e.g., Dimitrov et al., 2010a,b, 2011; Grant, 2004; Grant et al., 2008, 2009a,b, 2010a,b, 2011, 2012) as given in the Supplement.

2.1.2 Heterotrophic respiration

Organic transformations in *ecosys* occur in five organic matter–microbe complexes (coarse woody litter, fine non-woody litter, animal manure, particulate organic carbon (POC), and humus), each of which consists of five organic states (three decomposition substrates: solid organic C, sorbed organic C and microbial residue C, as well as the decomposition product: dissolved organic C (DOC), and the decomposition agent: microbial biomass) in a surface residue layer and in each soil layer. The decomposition rates of each of the three substrates and resulting production of DOC in each complex is a first-order function of the active biomasses M of diverse heterotrophic microbial functional types, including obligate aerobes (bacteria and fungi), facultative anaerobes

BGD
9, 5579–5623, 2012

(denitrifiers), obligate anaerobes (fermenters), heterotrophic (acetotrophic) and autotrophic (hydrogenotrophic) methanogens, and aerobic and anaerobic heterotrophic diazotrophs (non-symbiotic N_2 fixers) [A1, A2]. Decomposition rates are also Monod functions of substrate C concentrations in soil [A3], calculated from the fraction of substrate mass colonized by M [A4].

Growth of M by each microbial functional type [A25] is calculated from its uptake of DOC [A21], driven by energy yields from growth respiration (R_g) [A20] remaining after subtracting maintenance respiration (R_m) [A18] from heterotrophic respiration (R_h) [A11] driven by DOC oxidation [A13]. This oxidation may be limited by microbial O_2 reduction [A14] driven from microbial O_2 demand [A16] and constrained by aqueous O_2 concentrations ($[O_{2s}]$) [A17]. These concentrations are maintained by convective-dispersive transport of O_2 from the atmosphere to gaseous and aqueous phases the soil surface layer [D15], by convective-dispersive transport of O_2 through gaseous and aqueous phases in adjacent soil layers [D16, D19], and by dissolution of O_2 from gaseous to aqueous phases within each soil layer [D14a].

Under dryland conditions, rapid O_2 diffusivity in the gaseous phase (D_g in [D17]) allows O_2 demand by aerobic functional types to be met almost entirely from $[O_{2s}]$ [A17] as long as some air-filled porosity θ_g is present. However with higher water tables, θ_g above the water table may decline to values at which D_g may reduce gaseous O_2 transport [D16], while θ_g below the water table is zero and so prevents gaseous O_2 transport. Under these conditions, $[O_{2s}]$ relies more on O_2 transport through the slower aqueous phase [D19]. Consequent declines in $[O_{2s}]$ slow O_2 uptake [A17] and hence R_h [A14], R_g [A20] and growth of M [A25]. Lower M in turn slows decomposition of organic C [A1, A2] and production of DOC which further slows R_h [A13], R_g and growth of M. Although some microbial functional types can sustain DOC oxidation by reducing alternative electron acceptors (e.g. methanogens reducing acetate or CO_2 to CH_4 in Grant, 1998, and denitrifiers reducing NO_x to N_2O or N_2 in Grant et al., 2006), lower energy yields from these reactions reduce DOC uptake from R_g, and hence M growth, organic C decomposition and subsequent DOC oxidation. Slower decomposition of

BGD
9, 5579–5623, 2012

organic C under low [O_{2s}] also causes slower decomposition of organic N and P [A7] and production of DON and DOP, which causes slower uptake [A22] and growth [A29] of microbial N and P. This slower growth causes slower mineralization of NH_4^+, NO_3^- and $H_2PO_4^-$ [A26], and hence lower aqueous concentrations.

2.1.3 Autotrophic respiration

Growth of root and shoot phytomass in each plant population is calculated from its assimilation of the nonstructural C product of CO_2 fixation (σ_C) [C20]. Assimilation is driven by growth respiration (R_g) [C17] remaining after subtracting maintenance respiration (R_m) [C16] from autotrophic respiration (R_a) [C13] driven by oxidation of σ_C [C14]. This oxidation in roots may be limited by root O_2 reduction [C14b] which is driven by root O_2 demand to sustain C oxidation and nutrient uptake [C14e], and constrained by O_2 uptake controlled by concentrations of aqueous O_2 in the soil ([O_{2s}]) and roots ([O_{2r}]) [C14d]. Values of [O_{2s}] are maintained by convective-dispersive transport of O_2 through soil gaseous and aqueous phases and by dissolution of O_2 from soil gaseous to aqueous phases. Values of [O_{2r}] are maintained by convective-dispersive transport of O_2 through the root gaseous phase [D16d] and by dissolution of O_2 from root gaseous to aqueous phases [D14b] through processes analogous to those described under Sect. 2.1.2 above. This transport depends on species-specific values used for root air-filled porosity (θ_{pr}) [D17b].

Under dryland conditions, rapid O_2 diffusivity in the soil gaseous phase usually allows root O_2 demand to be almost entirely met from [O_{2s}] [C14c,d] as long as some air-filled porosity θ_g is present. However with higher water tables, reduced soil O_2 transport forces root O_2 uptake to rely more on [O_{2r}] and hence on root O_2 transport. If this transport is inadequate, declines in [O_{2r}] slow O_2 uptake [C14c,d] and hence R_a [C14b], R_g [C17] and root growth [C20b].

BGD
9, 5579–5623, 2012

2.1.4 Primary productivity

When higher water tables reduce soil O_2 transport and root O_2 uptake, commensurate reductions in root C oxidation slow root growth and root N and P uptake [C23b, d, f]. Root uptake is further slowed by reductions in aqueous concentrations of NH_4^+, NO_3^- and $H_2PO_4^-$ [C23a, c, e] from slower mineralization of organic N and P as described in Sect. 2.1.2 above. Slower root uptake reduces concentrations of nonstructural N and C products of root uptake (σ_N and σ_P) with respect to that of σ_C in leaves [C11], thereby slowing CO_2 fixation [C6] and hence productivity.

Thus water table effects on R_h, R_a and productivity in *ecosys* are not explicitly parameterized from ecosystem-level observations, but instead are governed by O_2 transport and uptake through processes parameterized from basic research.

2.1.5 Water table depth

The position of the water table arises from influxes vs. effluxes of water in vertical and lateral directions within the landscape and through surface and subsurface boundaries in one-, two- or three-dimensions. Vertical surface boundary influxes from precipitation or irrigation are provided as inputs to the model. Vertical surface boundary effluxes from transpiration [B1] and evaporation [D6] are calculated from energy balances for canopy, snow, residue and soil surfaces [D11] coupled with subsurface water transfers through root [B5] and soil [D7] profiles. Lateral surface runoff within the landscape and across lower surface boundaries is modelled using Manning's equation [D1] with surface water velocity [D3] calculated from surface geometry [D5] and slope [D6], and with surface water depth [D2] calculated from surface water balance [D4] using kinematic wave theory. Vertical and lateral subsurface water flows within the landscape [D7] are calculated from Richard's equation using bulk soil water potentials ψ_s of adjacent cells if both source and destination cells are unsaturated [D9a], or from Green-Ampt equation using ψ_s beyond the wetting front of the unsaturated cell if either source or destination cell is saturated [D9b] (Grant et al., 2004). Vertical and lateral subsurface water

BGD
9, 5579–5623, 2012

flows can also occur within the landscape through macropores using Poiseuille-Hagen theory for laminar flow in tubes, depending on inputs for macropore volume fraction (Dimitrov et al., 2010b).

Lateral flows through subsurface boundaries are controlled by the depth of and distance to an external water table used to represent watershed effects on landscape hydrology (Fig. 1). The depth of this external water table is calculated as the average of a fixed value provided to the model, and the WTD in the boundary grid cells through which lateral flows occur. The external water table can therefore rise and fall with changes in landscape surface water exchange. Lateral subsurface flows from boundary grid cells are calculated from their ψ_s and lateral hydraulic conductivities, and from external hydraulic gradients determined by elevation differences and lateral distances between these grid cells and the external water table [D10]. The WTDs within the boundary grid cells are calculated from the uppermost position in the soil profiles at which discharge to, or recharge from, the external water table is occurring. The WTDs in the modelled landscape are not therefore prescribed, but are controlled by vertical surface boundary fluxes, and by lateral surface and subsurface boundary fluxes.

2.2 Model experiment

2.2.1 Site conditions

Model algorithms for the effects of hydrology on wetland respiration and productivity were tested with CO_2 fluxes measured by EC over a minerotrophic wetland dominated by alder (*Alnus incana* sp. *rugosa*) and willow (*Salix* sp.) shrubs with an understory of sedges (*Carex* sp.), near Lost Creek, WI, (46° 4.90′ N, 89° 58.70′ W) during six years (2001–2006) with contrasting weather and hydrology. The site and EC flux measurements are described in further detail by Sulman et al. (2009).

BGD
9, 5579–5623, 2012

2.2.2 Model runs

Wetland microtopography was simulated by two interconnected soil profiles representing a hummock and a hollow, with equal areas and identical properties except for the absence of the upper 0.075 m in the hollow (Fig. 1). Based on site observations of WTD, the external water table was set to a depth of 0.6 m at a distance of 500 m from the modelled landscape (Fig. 1). Both the hummock and the hollow were seeded with the same populations of shrubs and sedges, properties of which were unchanged from those in earlier studies (e.g., Dimitrov et al., 2011; Grant et al., 2003, 2011, 2012). Shrubs and sedges used common values for parameters in all autotrophic C transformations [C1–C23], except for 0.1 and 0.2 (Visser et al., 2000), respectively for θ_{pr} in root O_2 transport [D17d]. The model was run for 105 yr under repeating 7-yr sequences of hourly-averaged weather data (solar radiation, air temperature, wind speed, humidity and precipitation) recorded at nearby Willow Creek in 2000, and at Lost Creek from 2001 to 2006. This period allowed CO_2 exchange in the model to achieve stable values through successive weather sequences. Model results for the final 6 yr of the run were compared with measurements at Lost Creek from 2001 to 2006.

2.2.3 Model testing

Hourly CO_2 fluxes modelled over hummocks and hollows were averaged and then regressed on hourly-averaged EC CO_2 fluxes, of which both 1/2-hourly values were measured rather than gap-filled, for each year of measurement. Model performance was evaluated from regression intercepts ($a \rightarrow 0$), slopes ($b \rightarrow 1$) and correlation coefficients ($R^2 \rightarrow 1$).

2.2.4 Model sensitivity to WTD

To examine sensitivity of modelled CO_2 exchange and productivity to changes in WTD, the final 6 yr of the model run described above were repeated with the depth of the

BGD
9, 5579–5623, 2012

external water table raised from 0.6 to 0.3 m, or lowered to 0.9 m, but with everything else unchanged.

3 Results

3.1 Modelled vs. measured CO_2 fluxes

Regressions of hourly modelled CO_2 fluxes vs. hourly-averaged measured CO_2 fluxes gave intercepts within 0.1 $\mu mol\,m^{-2}\,s^{-1}$ of zero, and slopes within 0.1 of one, indicating minimal bias in modelled values for all years of the study except 2004 when variation in CO_2 fluxes was overestimated (Table 1). Values for coefficients of determination (R^2) and root mean squares for differences between modelled and EC fluxes (RMSD) were ca. 0.7 ($P < 0.0001$) and 2 $\mu mol\,m^{-2}\,s^{-1}$. Much of the unexplained variance in EC fluxes could be attributed to a random error of ca. 20 % in EC methodology (Wesely and Hart, 1985). This attribution was corroborated by root mean squares for error (RMSE) for EC measurements at LC calculated from Richardson et al. (2006) that were similar to RMSD, indicating that further constraint in model testing could not be achieved without further precision in EC measurements.

3.2 Water table and seasonal net ecosystem productivity

The water table measured at Lost Creek from 2001 to 2006 typically remained within 0.2 m of hummock surfaces until May, but descended to depths varying from 0.4 to 0.7 m during July through September before rising gradually thereafter (Fig. 2). These seasonal trends in WTD were simulated from transfers of water in vertical [B1] and lateral [D1, D10] directions through surface and subsurface boundaries (Fig. 1) as described under Sect. 2.1 above. WTD in the model was close to that measured in unfrozen soil during most years, but remained lower than that measured in unfrozen soil during 2001 and 2003, and in frozen soil during most years of the study (Fig. 2).

BGD
9, 5579–5623, 2012

The lower WTD modelled in frozen soil was attributed to lower ψ_s calculated in the presence of ice which increased the depth at which a free water surface was detected in frozen soil.

Net ecosystem productivity (NEP), calculated from daily sums of gap-filled EC fluxes at Lost Creek from 2001 through 2006, remained negative (net C emissions) until warming in May, rose rapidly during late May and June to reach 2–4 $g\,C\,m^{-2}\,d^{-1}$ (net C uptake) during late June and July, then declined gradually during August, becoming negative again after late September (Fig. 2). These seasonal trends in NEP were modelled from changes in net CO_2 exchange driven by those in GPP [C1], R_a [C13] and R_h [A11] with changes in weather and hydrology, as described under Sect. 2.1 above. Because CO_2 fluxes in the model were consistent with those measured by EC (Table 1), net C uptake modelled during growing seasons was similar to that calculated from gap-filled EC. However net C emissions modelled during late spring and early autumn were consistently larger than those calculated from gap-filled EC.

3.3 Water table and diurnal CO_2 exchange

Changes in WTD were found to have contrasting effects on ecosystem CO_2 exchange, depending on the WTD at which changes occurred. To investigate relationships between WTD and ecosystem CO_2 exchange, diurnal CO_2 fluxes were examined during selected intervals with different WTD and weather in 2002 and 2006, when seasonal WTD was shallowest and deepest, respectively during the study period (Fig. 2e, q).

These fluxes were first examined during mid-May 2002 vs. 2006 when the water table was shallowest (Fig. 2e, q) and the weather was cool (Fig. 3a, d). Only very low CO_2 influxes and effluxes were modelled and measured in 2002 (Fig. 3c) when the water table was near the surface (Fig. 2e). Larger CO_2 influxes and effluxes were modelled and to a lesser extent measured under comparable weather (Fig. 3a, d) in 2006 (Fig. 3f) when the water table was about 0.2 m below the surface (Fig. 2q). In both years, low LE effluxes modelled and measured during May delayed soil drying and water table decline.

BGD
9, 5579–5623, 2012

CO_2 fluxes were then examined during mid-August 2002 vs. 2006 when WTD and weather were near respective seasonal averages (Fig. 4). CO_2 effluxes modelled over a WTD just below 0.2 m in 2002 (Fig. 2e) were slightly less than those modelled under comparable weather conditions (Fig. 4a, d) over a WTD of 0.7 m in 2006 (Fig. 2q) (−4 vs. −5 $\mu mol\,m^{-2}\,s^{-1}$ in Fig. 4c, f). Peak CO_2 influxes modelled over the shallower water table in 2002 were slightly smaller than those over the deeper water table in 2006 (13 vs. 14 $\mu mol\,m^{-2}\,s^{-1}$ in Fig. 4c, f), even though greater effluxes of LE vs. H indicated better hydration in 2002 (Fig. 4b, e). In both years CO_2 influxes and effluxes modelled over hollows were smaller than those over hummocks (Fig. 4 c, f). However these small differences in CO_2 fluxes modelled with landscape position or WTD could not be clearly resolved in the EC measurements.

CO_2 fluxes were then examined during late June–early July 2002 vs. 2006 when different WTD under comparable warming events (Fig. 5a, d) enabled interactive effects of WTD and temperature on CO_2 exchange to be investigated (Fig. 5c, f). Warming in 2002 over a WTD just above 0.2 m (Fig. 2e) caused rises in LE but not in H (Fig. 5b), indicating that the fen surface remained well hydrated. Warming also caused sharp rises in CO_2 effluxes and only slight declines CO_2 influxes (Fig. 5c), indicating that both respiration and productivity, estimated from differences between diurnal influxes and effluxes, rose with warming over a shallower water table. However the same warming in 2006 over a WTD of ca. 0.7 m (Fig. 2q) during a dry period (Fig. 2p) caused much smaller rises in LE, and larger rises in H (Fig. 5e), indicating some drying of the fen surface. In both years, Bowen ratios (β = H/LE) declined as LE rose with warming at hourly and daily time scales, but remained consistently larger in 2006 vs. 2002 (Fig. 6a, b), indicating constraints on LE imposed by soil drying over the deeper water table. Warming in 2006 caused much smaller rises in CO_2 effluxes, but sharper declines in CO_2 influxes than did similar warming in 2002 (Fig. 5f), indicating that both respiration and productivity were constrained by soil drying during warming over a deeper water table. Thus CO_2 exchange responded differently to a lower water table under warmer weather which induced surface drying (Fig. 5) than under cooler weather which did not

BGD
9, 5579–5623, 2012

(Figs. 3 and 4). The constraint of surface drying on R_h was later alleviated by several precipitation events (Fig. 7a) that raised effluxes of LE vs. H (Fig. 7b), and sharply raised effluxes of CO_2, causing a brief but pronounced decline in NEP (Fig. 2f).

The effects of WTD on CO_2 effluxes in Figs. 3–5 were modelled through the effects of WTD on $[O_{2s}]$. The near-surface water table in May 2002 (Fig. 2e) caused $[O_{2s}]$ in the model to decline sharply with depth under hummocks and hollows (Fig. 8a), thereby strongly limiting C oxidation and hence CO_2 effluxes (Fig. 3c). The slightly deeper water table in May 2006 (Fig. 2q) caused $[O_{2s}]$ to decline slightly less sharply with depth, partially alleviating O_2 limitation to C oxidation (Fig. 3f). Deepening water tables in summer 2002 allowed $[O_{2s}]$ to decline less sharply with depth than in May (Fig. 8b, c), enabling more rapid C oxidation (Figs. 4c and 5c). The very deep water tables in summer 2006 (Fig. 2q) allowed $[O_{2s}]$ to remain close to atmospheric equivalents through most of the rooting zone (Fig. 8b, c), largely alleviating O_2 limitation to C oxidation (Figs. 4f and 5f). The sharp declines in $[O_{2s}]$ in the model occurred at depths which approached to those of the water table (Fig. 2), indicating the effectiveness of saturated soil in reducing O_2 concentrations.

3.4 Water table and annual C balances

Annual totals of GPP, R_a, NPP and R_h modelled over hummocks and hollows exhibited interannual variability associated with mean annual temperature (MAT), precipitation, WTD and landscape position (Table 2). Annual NPP modelled in 2001 gave peak above-ground phytomasses for shrubs and sedges of 401 and 110 $g\,C\,m^{-2}$, comparable to ones of 414 and 79 $g\,C\,m^{-2}$ (assuming 50 % C in DM) reported in Sulman et al. (2009). Losses of CH_4 and of dissolved organic and inorganic C (DOC and DIC) also varied with MAT, precipitation, WTD and landscape position (Table 2), and caused net ecosystem C balance (NECB = NEP – CH_4 – DOC – DIC) to be 15–25 % less than NEP. Although greater WTD in 2006 vs. 2002 caused diurnal CO_2 influxes both to increase (Figs. 3 and 4) and decrease (Fig. 5) depending on WTD and weather, at an annual time scale variation in GPP and NPP appeared to be driven more by variation in

BGD
9, 5579–5623, 2012

MAT than in WTD. Thus GPP and NPP declined with MAT from 2001 to 2003 and rose with MAT from 2004 to 2006 (Table 2), as has been modelled and measured at several boreal sites in North America during this period (Grant et al., 2009a,b; Krishnan et al., 2008).

However variation in annual R_h appeared to be driven more by variation in WTD than in MAT (Table 2). Greater WTD in 2006 vs. 2002 caused diurnal CO_2 effluxes driven largely by R_h to increase under seasonally average weather (Figs. 3 and 4) and to decrease under warmer weather (Fig. 5). However these decreases in CO_2 effluxes were modelled infrequently so that at an annual time scale the shallower water table in 2002 reduced R_h and the deeper water tables thereafter increased R_h (Table 2). Consequently annual NECB in the model was greatest in 2002 with the shallowest water table and hence lowest R_h, and smallest in 2004 with the lowest MAT and hence NPP.

Landscape position had a large effect on ecosystem productivity in the model. Greater annual GPP, R_a, R_h and hence NECB were modelled over greater WTD in hummocks vs. hollows (Table 2), driven by greater diurnal CO_2 fluxes (Figs. 3–5). The greater GPP was attributed to improved nutrient status in hummocks, apparent as greater foliar N contents in Table 2. This improved nutrient status allowed greater dominance of shrub over sedge, apparent as greater GPP and NPP ratios, to be modelled in hummocks than in hollows (Table 2). Greater effluxes of CH_4, DOC and DIC were modelled in years with greater precipitation and shallower water tables such as 2002, and from hollows vs. hummocks in all years of the study (Table 2).

3.5 Sensitivity of CO_2 exchange to water table

The responses of CO_2 exchange to seasonal and interannual changes in WTD (Figs. 1–7) determined those to long-term changes in WTD caused by raising or lowering the external water table. Raising the external water table by 0.3 m slowed discharge and hastened recharge through the lateral boundaries of the modelled landscape (Fig. 1), and thereby raised the internal water table from that in the earlier model

BGD
9, 5579–5623, 2012

run (Fig. 9a, c). Conversely lowering the external water table by 0.3 m hastened discharge and slowed recharge, and thereby lowered the internal water table. Subsidence of the fen surface with drainage was not modelled, so that WTD in these runs referred to an unchanged surface elevation. These changes in WTD had contrasting effects on NEP modelled at different times of the year in 2002 and 2006. In 2002, lowering the water table decreased NEP until the end of June, increased it slightly during July and early August, but decreased it again thereafter (Fig. 9b). In 2006, lowering the water table decreased NEP until the end of May, but increased NEP thereafter (Fig. 9d). In general, lowering the water table reduced NEP when the WTD was less than ca. 0.2 m, and increased NEP when WTD was greater.

A transition from increases to decreases in NEP with deeper water tables occurred in late August 2002 (Fig. 9b). The cause of this transition was investigated by examining the diurnal CO_2 exchange modelled during the period in which the transition occurred (Fig. 10). Lowering the water table (Fig. 10a) increased daytime near-surface soil temperatures (Fig. 10b) and both influxes and effluxes of CO_2 (Fig. 10c). Precipitation on DOY 232 (Fig. 2d) raised all water tables by ca. 0.1 m so that the shallowest water table rose above 0.2 m (Fig. 10a). This rise caused CO_2 effluxes to decrease, and consequently CO_2 influxes to increase, over the shallower water table with respect to those over the deeper (Fig. 10c). These decreased effluxes were modelled from lower $[O_{2s}]$ in a shallower aerobic zone following the rise in water table (Fig. 11a, b). These changes in CO_2 effluxes vs. influxes with WTD caused the transition from increases to decreases in NEP with deeper water tables in late August 2002 (Fig. 9b). Lowering the much deeper water table during the same period in 2006 (Fig. 10d) had little effect on near-surface soil temperatures (Fig. 10e) or on CO_2 effluxes (Fig. 10e), but increased CO_2 influxes and hence NEP (Fig. 9d).

3.6 Sensitivity of annual C balances to water table

Responses of NEP to changes in WTD at seasonal (Fig. 9) and diurnal (Fig. 10) time scales were aggregated to the annual time scale for 2001 to 2006 in Table 3. Lowering

BGD
9, 5579–5623, 2012

the water table increased GPP and NPP of shrub, and to a lesser extent of sedge, in each year of the study. Lowering the water table also increased R_h in each year of the study, but more in years with shallow water tables such as 2002 (as in Fig. 10c) and less in years with deeper water tables such as 2006 (as in Fig. 10f). These increases in R_h were greater than those in NPP when WTD was small so that lowering the water table reduced NECB during 2002 (as in Fig. 9b). However these increases in R_h were less those in NPP when WTD was large so that lowering the water table increased NECB during 2006 (as in Fig. 9d). Increases in R_h were similar to those in NPP during years with intermediate WTD, so that lowering the water table had smaller effects on NECB during the other years of the study. Lowering the water table also decreased CH_4 emissions, particularly during 2002 (Table 3).

4 Discussion

4.1 Model processes by which WTD affects CO_2 exchange

The modeling of WTD effects on peatland CO_2 exchange in *ecosys* is based on the explicit coupling of oxidation-reduction reactions which drive C and N transformations in soil, roots and mycorrhizae with gaseous and aqueous transfers of the substrates and products of these reactions through soil and root profiles with dynamic WTD. This coupling allowed the model to simulate complex responses of CO_2 exchange to changes in WTD. The processes by which this simulation was accomplished are described below.

4.1.1 CO_2 effluxes and WTD

Rates of C oxidation and hence of CO_2 effluxes by microbial, root and mycorrhizal populations in *ecosys* are governed by their rates of O_2 reduction [A14, C14b]. These rates are in turn governed by [O_{2s}] [A17a, b; C14c, d] determined by convective and dispersive transport from the atmosphere through gaseous [D16a–d] and aqueous [D19] phases in soil and roots, by dissolution from gaseous to aqueous phases in soil and

BGD
9, 5579–5623, 2012

roots [D14a, b], and by diffusion to and uptake at microbial [A17a, b], root and mycorrhizal [C14c, d] surfaces. Above the water table, [O_{2s}] was well above the Michaelis-Menten constant used for microbial, root and mycorrhizal uptake (0.064 g O_2 m^{-3} in [A17a] and [C14c]) (Figs. 8 and 11), so that C oxidation was not much limited by O_2 reduction. Below the water table, [O_{2s}] declined sharply to values that were two orders of magnitude smaller than this constant, so that C oxidation was strongly limited by O_2 reduction. Although C oxidation in *ecosys* is also coupled with reduction of DOC by anaerobic heterotrophic fermenters, generating CO_2, H_2 and acetate that drives heterotrophic and autotrophic CH_4 production (Grant, 1998) (Tables 2 and 3), the energy yield from reduction of DOC is much smaller than that of O_2 (Brock and Madigan, 1991), and so drove slower microbial growth [A21] and hence C oxidation [A13].

Under the site conditions presented to the model in this study, [O_{2s}] above the Michaelis-Menten constant to a depth of ca. 0.2 m (e.g., Fig. 8b) was sufficient to sustain rapid rates of C oxidation and hence CO_2 effluxes (e.g., Fig. 5c). Shallower aerobic zones (e.g., Fig. 8a) reduced CO_2 effluxes (e.g., Fig. 3c, f), while deeper aerobic zones (e.g., Fig. 8c) increased CO_2 effluxes only slightly (Fig. 4c, f). Deeper water tables also raised soil temperatures [D12] (Fig. 10b) by reducing water contents, further contributing to increases in rates of C oxidation through Arrhenius functions for R_h [A6] and R_a [C22a, b]. These model processes thus enabled the simulation of greater CO_2 effluxes over deeper water tables vs. smaller effluxes over shallower, particularly within the upper 0.2 m of the soil profile, consistent with greater effluxes measured with greater WTD at Lost Creek (Sulman et al., 2009) and elsewhere (e.g., Moore and Dalva, 1993; Moore and Roulet, 1993; Silvola et al., 1996). The model processes were also able to simulate greater R_h and hence greater CO_2 effluxes, as well as smaller CH_4 effluxes, over greater WTD in hummocks vs. hollows (Figs. 3–5; Table 2), as has been reported from field sites (Strack and Waddington, 2007).

However smaller CO_2 effluxes were modelled and measured over deeper water tables (Fig. 5c, f) during periods of high temperature (Fig. 5d) and low precipitation (Fig. 2p) when drying, evidenced by higher Bowen ratios (Fig. 6), limited C oxidation

BGD
9, 5579–5623, 2012

in surface soil and litter (Fig. 7c). Drying of surface soil and litter was modelled when capillary rise of water [D7] plus diffusive transfer of vapor [D16] from wetter soil below failed to replace evaporative transfer of vapor to the atmosphere above [D6]. Surface drying therefore depended on soil hydraulic properties (Fig. 1) as well as on weather. Limitations to C oxidation caused by drying were modelled from functions for competitive inhibition of heterotrophic decomposers exacerbated by low water content [A3, A5], and for constraints to microbial growth from low water potentials [A15], which together slowed R_h in dry soil and litter (Grant et al., 2012). These limitations were rapidly alleviated by rainfall and consequent surface wetting (Fig. 7), enabling the simulation of CO_2 emission pulses commonly observed after rainfall on dry soil (Huxman et al., 2004).

These model processes thus enabled the simulation of smaller CO_2 effluxes sometimes measured over deeper water tables. By simulating rises in CO_2 effluxes when shallower water tables were lowered (Fig. 10c), and no change or declines in CO_2 effluxes when deeper water tables were lowered (Fig. 10f), the model explained apparently contradictory increases, no changes, and decreases of soil respiration that have been observed with increases in WTD (e.g., Lafleur et al., 2005a; Silviola et al., 1996). This model explanation was accomplished without arbitrary parameterizations of aerobic vs. anaerobic respiration used in other wetland models (e.g., St-Hilaire et al., 2010). The complex response to WTD of respiration in *ecosys* was also demonstrated by Dimitrov et al. (2010a) in an ombrotrophic bog with very different hydrologic characteristics to those of the fen at Lost Creek.

4.1.2 CO_2 influxes and WTD

The effects of WTD on CO_2 influxes were driven in large part by those on CO_2 effluxes. Over deeper water tables, increases in $[O_{2s}]$ (e.g., Fig. 8a) raised rates of C oxidation by microbial populations [A13, A14] which drove more rapid microbial growth [A25] and hence nutrient mineralization [A26]. Increases in $[O_{2s}]$ also raised rates of C oxidation by root and mycorrhizal populations [C14a, b] which drove more rapid root and mycorrhizal growth [C20b] and hence nutrient uptake [C23]. Greater rates of nutrient

BGD
9, 5579–5623, 2012

uptake increased foliar nutrient contents [C12] (Tables 2 and 3) and hence increased rates of CO_2 fixation [C6a, C7, C11]. These greater uptake rates were consistent with the experimental findings of Laiho et al. (2003) that N uptake by vascular plants was more rapid in drained vs. undrained boreal peatlands. These model processes enabled greater CO_2 influxes and hence greater NPP to be simulated over deeper vs. shallower water tables, consistent with greater influxes and NPP measured with greater WTD at Lost Creek (Sulman et al., 2009) (e.g., Fig. 3c, f; Table 2). These processes also enabled the simulation of greater CO_2 influxes and hence greater NPP over greater WTD in hummocks vs. hollows (Figs. 3–5; Table 2), as has been reported from field sites (Strack and Waddington, 2007). This simulation was accomplished without arbitrary parameterizations of productivity under aerobic vs. anaerobic conditions used in other wetland models (e.g., Bond-Lamberty et al., 2007; Sonnentag et al., 2008).

However smaller CO_2 influxes were sometimes modelled and measured over deeper water tables (Fig. 5c, f) under high temperature (Fig. 5d) and surface drying (Fig. 6), as was also measured in a boreal peatland by Shurpali et al. (1995). These smaller influxes were modelled from coupled processes for root water uptake [B6] and canopy transpiration [B1] that lowered canopy water potential [B14], conductance [B2] and hence CO_2 fixation [C2, C6a, C7] as soil water potentials declined with drying when upward water movement from the saturated soil zone [D7, D16] failed to maintain near-surface water contents (Grant et al., 2012). Similar declines in CO_2 influxes measured by EC and modelled by *ecosys* over lower WTD in an ombrotrophic bog were also attributed by Dimitrov et al. (2011) to water stress in moss caused by near-surface soil drying. Corresponding declines in CO_2 influxes have also been measured at WTDs below 0.2–0.5 m in a boreal fen by Sonnentag et al. (2010). The warm, dry weather and deeper water tables during which these smaller influxes were modelled did not occur frequently enough at Lost Creek to lower annual GPP and NPP, both of which rose with deeper water tables in all years of the study (Tables 2 and 3). However if warming events over deeper water tables were to occur more frequently under proposed climate change, these adverse effects on annual GPP and NPP might become more apparent.

BGD
9, 5579–5623, 2012

4.1.3 Net CO_2 exchange and WTD

The combined effects of WTD on CO_2 effluxes and influxes caused greater NECB to be modelled in a cooler year with shallower water table such as 2002 than in a warmer year with a deeper one such as 2006 (Table 2). However the lowest NECB in this study was modelled in 2004 with an average WTD but the lowest MAT, so that annual NECB was better correlated with MAT than with annual average WTD as found by Lafleur et al. (2005). Sulman et al. (2009) calculated slightly greater NEP in 2002 than in 2006, and lower NEP in 2004, from gap-filled EC fluxes at Lost Creek, which was consistent with model results, and so also did not find a correlation between annual WTD and NEP. However their annual NEP was generally larger than annual NECB modelled here, in part because they did not account for losses as CH_4, DOC and DIC (Table 2), and in part because CO_2 effluxes measured by EC during peak emission periods in late spring and early autumn were smaller than those modelled (Fig. 2). The comparatively low annual NECB modelled here reflects the growth habit of the shrub–sedge plant functional types at Lost Creek in which there was no long-term accumulation of woody C. Correlations of annual NECB with MAT and WTD among years were complicated by the effects on R_h of changes in litter stocks carried over from previous years with differing productivity.

Differences among annual NECB with WTD in the model were consistent with experimental findings from an open peatland in nearby Minnesota over which a net C uptake of $32\,g\,m^{-2}$ was measured from May to October in a wet year and a net C emission of $71\,g\,m^{-2}$ was measured during the same period in a dry year (Shurpali et al., 1995). Differences in the model were also consistent with experimental findings from a boreal fen over which a net C uptake of $92\,g\,m^{-2}$ was measured in a wetter year and a net C emission of $31\,g\,m^{-2}$ was measured during a drier year with earlier snowmelt (Joiner et al., 1999). Contrasting changes in annual NECB modelled when water tables were lowered at smaller vs. greater WTD (e.g. 2002 vs. 2006 in Table 3) were consistent with the findings of Minkkinen et al. (2002) that peat C accumulation

BGD
9, 5579–5623, 2012

rates usually increase but may decrease with drainage of boreal wetlands in Finland. The contributions of DOC losses to NECB in the model (Tables 2 and 3) were similar to ones of 8–11 $g C m^{-2} yr^{-1}$ or about 17 % of NEP measured in a boreal fen by Strack et al. (2008).

4.2 Sensitivity of species composition to changes in water table

Changes in water table had different effects on CO_2 exchange by shrubs and sedges in the model. Larger root porosity θ_{pr} [D17d] used for sedges as described in Sect. 2.2 above enabled more rapid O_2 uptake through sedge root axes [D16d], particularly when [O_{2s}] and hence [O_{2r}] [D14] were low. Consequently O_2 uptake [C14c] and hence C oxidation [C14b] by sedge roots were less dependent on convection-dispersion [D16a–c] and diffusion [C14d] through soil to root surfaces. Therefore GPP and NPP of sedges increased while those of shrubs decreased in hollows vs. hummocks where the water tables were shallower (Table 2). At the landscape scale, GPP and NPP of sedges declined less than did those of shrubs when water tables were raised (Table 3) and root O_2 uptake became more dependent on root O_2 transport. Conversely productivity of sedge rose less than that of shrubs when water tables were lowered (Table 3), which was consistent with declines in graminoid biomass and increases in shrub biomass observed after lowering water tables in boreal peatlands from chronosequence studies by Laiho et al. (2003), drainage studies by Weltzin et al. (2003) and natural drying by Sonnentag et al. (2010). Thus θ_{pr} was a key attribute for plant adaptation to wetland conditions in *ecosys*, allowing changes in species composition with changes in WTD. Such changes in composition are an important adaptive response that reduces the impact of changes in hydrology on wetland productivity. At the present stage of model development, this attribute is not dynamic, although θ_{pr} has been found to rise in anoxic soils (Visser et al., 2000).

BGD
9, 5579–5623, 2012

5 Conclusions

The model was able to simulate complex responses of CO_2 exchange to changes in WTD at diurnal, seasonal and annual time scales that were consistent with those observed at LC and at similar sites elsewhere. However these responses required the explicit modeling of key processes, particularly O_2 transport, uptake and reduction, by which CO_2 exchange is determined in wetlands, and which need to be included in models used to study wetland productivity. At the diurnal time scale:

(1) Soil CO_2 effluxes rose with increased WTD over shallow water tables (Fig. 4) because increased [O_{2s}] (Figs. 8 and 11) hastened microbial and root oxidation-reduction reactions by raising energy yields [A20]. This response required explicit modeling of coupled transport and uptake processes for O_2 through soil and roots [A17, C14, D16, D19] which were parameterized independently of the model.

(2) Soil CO_2 effluxes declined with increased WTD over deeper water tables (Fig. 5) because surface drying slowed microbial oxidation-reduction reactions [A3, A5]. This response required modeling of coupled transport [D7] and evaporation [D6] processes for water through soil and surface litter from water potential gradients determined by peat hydrologic properties.

(3) Soil CO_2 influxes usually rose with increased WTD (Figs. 4 and 10) because more rapid microbial and root oxidation-reduction reactions from (1) drove more rapid N mineralization [A25] and uptake [C23]. This response required modeling a comprehensive set of soil and plant N transformations fully coupled to those of C.

(4) Soil CO_2 influxes sometimes declined with increased WTD over deeper water tables during warming events (Fig. 5) because drying soils forced lower canopy water potential [B14] and hence CO_2 fixation [C2, C6a, C7]. This response required modeling the effects on CO_2 fixation of plant water status solved from

BGD
9, 5579–5623, 2012

hydraulically-driven water transport along soil-plant-atmosphere water potential gradients [B14].

At the annual time scale, the combined responses (1) to (4) caused

(5) NECB to be greater in years with shallow water tables and smaller in years with deeper water tables (Table 2),

(6) NECB to decline with increases in WTD in years with shallow water tables and to rise with increases in WTD in years with deeper water tables (Table 3), indicating that deepening water tables may reduce NECB only to a certain depth, below which further deepening may not.

Supplementary material related to this article is available online at: http://www.biogeosciences-discuss.net/9/5579/2012/ bgd-9-5579-2012-supplement.pdf.

Acknowledgements. Field research was funded by DOE BER NICCR 050516Z19 and NSF BIO DEB-0845166. Computational facilities for *ecosys* were provided by the University of Alberta and by the Compute Canada high performance computing infrastructure.

References

Adkinson, A. C., Syed, K. H., and Flanagan, L. B.: Contrasting responses of growing season ecosystem CO_2 exchange to variation in temperature and WTD in two peatlands in Northern Alberta, Canada, J. Geophys. Res, 116, G01004, doi:10.1029/2010JG001512, 2011.

Blodau, C., Roulet, N. T., Heitmann, T., Stewart, H., Beer, J., Lafleur, P., and Moore, T. R.: Belowground carbon turnover in a temperate ombrotrophic bog, Global Biogeochem. Cy., 21, GB1021, doi:10.1029/2005GB002659, 2007.

Boelter, D. H.: Physical properties of peats as related to degree of decomposition, Soil Sci. Soc. Am. Proc., 33, 606–609, 1969.
Bond-Lamberty, B., Gower, S. T., and Ahl, D. E.: Improved simulation of poorly drained forests using Biome-BGC, Tree Physiol., 27, 703–715, 2007.
Brock, T. D. and Madigan, M. T.: Biology of Microorganisms, 6th edn., Prentice Hall, New Jersey, USA, 1991.
Dang, Q. L. and Lieffers, V. J.: Assessment of patterns of response of tree ring growth of black spruce following peatland drainage, Can. J. For. Res., 19, 924–929, 1989.
Dimitrov, D. D., Grant, R. F., LaFleur, P. M., and Humphreys, E.: Modelling the effects of hydrology on ecosystem respiration at Mer Bleue bog. J. Geophys. Res.-Biogeosci., 115, G04043, doi:10.1029/2010JG001312, 2010a.
Dimitrov, D. D., Grant, R. F., LaFleur, P. M., and Humphreys, E.: Modelling subsurface hydrology of Mer Bleue bog, Soil Sci. Soc. Amer. J., 74, 680–694, 2010b.
Dimitrov, D. D., Grant, R. F., LaFleur, P. M., and Humphreys, E.: Modelling the effects of hydrology on gross primary productivity and net ecosystem productivity at Mer Bleue bog, J. Geophys. Res.-Biogeosci., 116, G04010, doi:10.1029/2010JG001586, 2011.
Flanagan, L. B. and Syed, K. H.: Stimulation of both photosynthesis and respiration in response to warmer and drier conditions in a boreal peatland ecosystem, Glob. Change Biol., 17, 2271–2287, doi:10.1111/j.1365-2486.2010.02378.x, 2011.
Frolking, S., Roulet, N. T., Moore, T. R., Lafleur, P. M., Bubier, J. L., and Crill, P. M.: Modelling the seasonal to annual carbon balance of Mer Bleue bog, Ontario, Canada, Global Biogeochem. Cy., 16, doi:10.1029/2001GB1457, 2002.
Grant, R. F.: Simulation of methanogenesis in the mathematical model ecosys, Soil Biol. Biochem., 30, 883–896, 1998.
Grant, R. F.: Simulation of methanotrophy in the mathematical model ecosys, Soil Biol. Biochem., 31, 287–297, 1999.
Grant, R. F.: Modelling topographic effects on net ecosystem productivity of boreal black spruce forests, Tree Physiol., 24, 1–18, 2004.
Grant, R. F. and Pattey, E.: Modelling variability in N_2O emissions from fertilized agricultural fields, Soil Biol. Biochem., 35, 225–243, 2003.
Grant, R. F. and Roulet, N. T.: Methane efflux form boreal wetlands: theory and testing of the ecosystem model ecosys with chamber and tower flux measurements, Global Biogeochem. Cy., 16, 1054, doi:10.1029/2001GB001702, 2002.

BGD
9, 5579–5623, 2012

Grant, R. F., Oechel, W. C., Ping, C., and Kwon, H.: Carbon balance of coastal arctic tundra under changing climate, Glob. Change Biol., 9, 16–36, 2003.
Grant, R. F., Pattey, E. M., Goddard, T. W., Kryzanowski, L. M., and Puurveen, H.: Modelling the effects of fertilizer application rate on nitrous oxide emissions from agricultural fields, Soil Sci. Soc. Amer. J., 70, 235–248, 2006.
Grant, R. F., Barr, A. G., Black, T. A., Margolis, H. A., Dunn, A. L., Metsaranta, J., Wang, S., McCaughey, J. H., and Bourque, C. P.-A.: Interannual variation in net ecosystem productivity of Canadian forests as affected by regional weather patterns – a Fluxnet-Canada synthesis, Agr. Forest Meteorol., 149, 2022–2039, 2009a.
Grant, R. F., Margolis, H. A., Barr, A. G., Black, T. A., Dunn, A. L., Bernier, P. Y., and Bergeron, O.: Changes in net ecosystem productivity of boreal black spruce stands in response to changes in temperature at diurnal and seasonal time scales, Tree Physiol., 29, 1–17, 2009b.
Grant, R. F., Barr, A. G., Black, T. A., Margolis, H. A., McCaughey, J. H., and Trofymow, J. A.: Net ecosystem productivity of temperate and boreal forests after clearcutting – a Fluxnet-Canada synthesis, Tellus B, 62, 475–496, 2010a.
Grant, R. F., Jassal, R. S., Black, T. A., and Bruemmer, C.: Changes in net CO_2 and N_2O exchange with fertilization of Douglas fir: mathematical modelling in ecosys, J. Geophys. Res., 115, G04009, doi:10.1029/2009JG001094, 2010b.
Grant, R. F., Humphreys, E. R., Lafleur, P. M., and Dimitrov, D. D.: Ecological controls on net ecosystem productivity of a mesic arctic tundra under current and future climates. J. Geophys. Res.-Biogeosci., 116, G01031, doi:10.1029/2010JG001555, 2011.
Grant, R. F., Baldocchi, D. D., and Ma, S.: Ecological controls on net ecosystem productivity of a Mediterranean grassland under current and future climates, Agr. Forest Meteorol., 152, 189–200, 2012.
Huxman, T. E., Snyder, K. A., Tissue, D., Leffler, A. J., Ogle, K., Pockman, W. T., Sandquist, D. R., Potts, D. L., and Schwinning, S.: Precipitation pulses and carbon fluxes in semiarid and arid ecosystems, Oecologia, 141, 254–268, 2004.
Joiner, D. W., Lafleur, P. M., McCaughey, J. H., and Bartlett, P. A.: Interannual variability in carbon dioxide exchanges at a boreal wetland in the BOREAS northern study area, J. Geophys. Res., 104, 27663–27672, 1999.

BGD
9, 5579–5623, 2012

Krishnan, P., Black, T. A., Barr, A. G., Grant, N. J., Gaumont-Guay, D., Nesic, Z.: Factors controlling the interannual variability in the carbon balance of a southern boreal black spruce forest, J. Geophys. Res., 113, D09109, doi:10.1029/2007JD008965, 2008.

Lafleur, P. M., Moore, T. R., Roulet, N. T., and Frolking, S.: Ecosystem respiration in a cool temperate bog depends on peat temperature but not on water table, Ecosystems, 8, 619–629, 2005.

Laiho, R., Vasander, H., Penttilä, T., and Laine, J.: Dynamics of plantmediated organic matter and nutrient cycling following water-level drawdown in boreal peatlands, Global Biogeochem. Cy., 17, 1053, doi:10.1029/2002GB002015, 2003.

Langergraber, G. and Šimůnek, J.: Modeling variably saturated water flow and multicomponent reactive transport in constructed wetlands, Vadose Zone J., 4, 924–938, 2005.

Lieffers, V. J.: Sphagnum and cellulose decomposition in drained and natural areas of an Alberta peatland, Can. J. Soil Sci., 68, 755–761, 1988.

Lieffers, V. J. and Macdonald, S. E.: Growth and foliar nutrient status of black spruce and tamarack in relation to depth of water table in some Alberta peatlands, Can. J. For. Res., 20, 805–809, 1990.

Lieffers, V. J. and Rothwell, R. L.: Effects of drainage on substrate temperature and phenology of some trees and shrubs in an Alberta peatland, Can. J. For. Res., 17, 97–104, 1987.

Macdonald, S. E. and Lieffers, V. J.: Photosynthesis, water relations and foliar nitrogen of *Picea mariana* and *Larix laricina* from drained and undrained peatlands, Can. J. For. Res., 20, 995–1000, 1990.

Minkkinen, K., Korhonen, R., Savolainen, I., and Laine, J.: Carbon balance and radiative forcing of Finnish peatlands 1900–2100 – the impact of forestry drainage, Glob. Change Biol., 8, 785–799, 2002.

Moore, T. R. and Dalva, M.: The influence of temperature and water-table position on carbon dioxide and methane emissions from laboratory columns of peatland soils, J. Soil Sci., 44, 651–664, 1993.

Moore, T. R. and Roulet, N. T.: Methane flux: water table relations in northern wetlands, Geophys. Res. Lett., 20, 587–590, 1993.

Muhr, J., Höhle, J., Otieno, D. O., and Borken, W.: Manipulative lowering of the water table during summer does not affect CO_2 emissions and uptake in a fen in Germany, Ecol. Appl., 21, 391–401, 2011.

Nadelhoffer, K. J., Giblin, A. E., Shaver, G. R., and Laundre, J. A.: Effects of temperature and substrate quality on element mineralization in six arctic soils, Ecology, 72, 242–253, 1991.

Päivänen, J.: Hydraulic conductivity and water retention in peat soils, Acta Forest. Fenn., 129, 1–70, 1973.

Richardson, A. D., Hollinger, D. Y., Burba, G. G., Davis, K. J., Flanagan, L. B., Katul, G. G., Munger, J. W., Ricciuto, D. M., Stoy, P. C., Suyker, A. E., Verma, S. B., and Wofsy, S. C.: A multi-site analysis of random error in tower-based measurements of carbon and energy fluxes, Agr. Forest Meteorol., 136, 1–18, 2006.

Saxton, K. E., Rawls, W. J., Romberger, J. S., and Papendick, R. I.: Estimating generalized soil-water characteristics from texture, Soil Sci. Soc. Amer. J., 50, 1031–1036, 1986.

Scanlon, D. and Moore, T. R.: Carbon dioxide production from peatland soil profiles: the influence of temperature, oxic/anoxic conditions and substrate, Soil Sci., 165, 153–160, 2000.

Shurpali, N. J., Verma, S. B., and Kim, J.: Carbon dioxide exchange in a peatland ecosystem, J. Geophys. Res., 100, 14319–14326, 1995.

Silvola, J., Alm, J., Ahlholm, U., Nykanen, H., and Martikainen, P. J.: CO_2 fluxes from peat in boreal mires under varying temperature and moisture conditions, J. Ecol., 84, 219–228, 1996.

Sonnentag, O., Chen, J. M., Roulet, N. T., Ju, W., and Govind, A.: Spatially explicit simulation of peatland hydrology and carbon dioxide exchange: influence of mesoscale topography, J. Geophys. Res., 113, G02005, doi:10.1029/2007JG000605, 2008.

Sonnentag, O., Kamp, G. V. D., Barr, A. G., and Chen, J. M.: On the relationship between water table depth and water vapor and carbon dioxide fluxes in a minerotrophic fen, Glob. Change Biol., 16, 1762–1776, doi:10.1111/j.1365-2486.2009.02032.x, 2010.

St-Hilaire, F., Wu, J., Roulet, N. T., Frolking, S., Lafleur, P. M., Humphreys, E. R., and Arora, V.: McGill wetland model: evaluation of a peatland carbon simulator developed for global assessments, Biogeosciences, 7, 3517–3530, doi:10.5194/bg-7-3517-2010, 2010.

Strack, M. and Waddington, J. M.: Response of peatland carbon dioxide and methane fluxes to a water table drawdown experiment, Global Biogeochem. Cy., 21, 13 pp., GB1007, doi:10.1029/2006GB002715, 2007.

Strack, M., Waddington, J. M., Bourbonniere, R. A., Buckton, E. L., Shaw, K., Whittington, P., and Price, J. S.: Effect of water table drawdown on peatland dissolved organic carbon export and dynamics, Hydrol. Proc., 22, 3373–3385, 2008.

BGD
9, 5579–5623, 2012

Sulman, B. N., Desai, A. R., Cook, B. D., Saliendra, N., and Mackay, D. S.: Contrasting carbon dioxide fluxes between a drying shrub wetland in Northern Wisconsin, USA, and nearby forests, Biogeosciences, 6, 1115–1126, doi:10.5194/bg-6-1115-2009, 2009.

Sulman, B. N., Desai, A. R., Saliendra, N. Z., Lafleur, P. M., Flanagan, L. B., Sonnentag, O., Mackay, D. S., Barr, A. G., and Kamp, G. V. D.: CO_2 fluxes at northern fens and bogs have opposite responses to inter-annual fluctuations in water table, Geophys. Res. Lett., 37, L19702, doi:10.1029/2010GL044018, 2010.

Sulman, B. N., Desai, A. R., Schroeder, N. M., Ricciuto, D., Barr, A. G., Richardson, A. D., Flanagan, L. B., Lafleur, P. M., Tian, H., Chen, G., Grant, R. F., Poulter, B., Verbeeck, H., Ciais, P., Peylin, P., Ringeval, B., Baker, I. T., Schaefer, K., Luo, Y., and Weng, E.: Impact of hydrological variations on modeling of peatland CO_2 fluxes: results from the North American Carbon Program site synthesis, J. Geophys. Res.-Biogeosci., in press., 2012.

Visser, E. J. W., Colmer, T. D., Blom, C. W. P. M., and Voesenek, L. A. C. J.: Changes in growth, porosity, and radial oxygen loss from adventitious roots of selected mono- and dicotyledonous wetland species with contrasting types of aerenchyma, Plant Cell Environ., 23, 1237–1245, 2000.

Weltzin, J. F., Bridgham, S. D., Pastor, J., Chen, J., and Harth, C.: Potential effects of warming and drying on peatland plant community composition, Glob. Change Biol., 9, 141–151, 2003.

Wesely, M. L. and Hart, R. L.: Variability of short term eddy-correlation estimates of mass exchange, in: The Forest–Atmosphere Interaction, Hutchinson, B. A. and Hicks, B. B. (eds.), D. Reidel, Dordrecht, 591–612, 1985.

BGD
9, 5579–5623, 2012

Table 1. Statistics from regressions of simulated on measured (a, b), and measured on simulated (R^2, RMSD), hourly CO_2 fluxes over a boreal fen at Lost Creek, WI. All measured values were recorded at $u^* > 0.2\,\mathrm{m\,s^{-1}}$.

	n	$a^\dagger$ $\mu\mathrm{mol\,m^{-2}\,s^{-1}}$	$b^\dagger$	$R^{2\ddagger}$	RMSD‡ $\mu\mathrm{mol\,m^{-2}\,s^{-1}}$	RMSE $\mu\mathrm{mol\,m^{-2}\,s^{-1}}$
2001	6366	0.0	0.94	0.65	2.1	2.2
2002	6796	0.0	1.05	0.75	1.9	2.1
2003	5509	−0.1	0.96	0.72	2.2	2.5
2004	4695	−0.2	1.22	0.73	1.5	2.2
2005	4251	0.1	0.98	0.72	2.7	2.5
2006	4576	0.1	1.06	0.73	2.5	2.4

† $y = a + bx$ from regression of simulated y on measured x.
‡ R^2 = coefficient of determination and RMSD = root mean square for error from regression of measured y on simulated x.

BGD
9, 5579–5623, 2012

Table 2. Landscape position, mean annual temperature (MAT), total precipitation, average WTD from hummock surface between DOY 120 and 300 (modelled/measured), foliar N content at anthesis, gross primary productivity (GPP), autotrophic respiration (R_a), net primary productivity (NPP), heterotrophic respiration (R_h), methane emissions (CH_4), export of dissolved organic and inorganic C (DOC + DIC), and net ecosystem carbon balance (NECB = NEP − CH_4 − DOC − DIC) modelled for a boreal fen at Lost Creek, WI.

Year	Position	MAT °C	Precip. mm yr^{-1}	Water Table mod./mes. m	Foliar N shrub/sedge g N (kg C)$^{-1}$	GPP shrub/sedge	R_a shrub/sedge	NPP shrub/sedge g C m^{-2} yr^{-1}	R_h	CH_4	DOC + DIC	NECB
2001	hummock				27/28	1136/171	493/080	643/091	722	2.9	0	9
	hollow				20/24	494/374	226/167	268/207	532	5.4	15	−77
	average	**5.6**	**865**	**0.33/0.12**	**23/26**	**815/273**	**360/124**	**456/149**	**627**	**4.2**	**8**	**−34**
2002	hummock				32/34	1064/153	465/074	599/079	599	3.3	−2	79
	hollow				23/32	521/383	231/187	290/196	395	3.8	26	61
	average	**4.9**	**965**	**0.17/0.07**	**28/33**	**793/268**	**348/131**	**445/138**	**497**	**3.6**	**12**	**70**
2003	hummock				32/29	1017/146	446/063	571/083	650	1.7	−1	4
	hollow				22/31	479/380	227/177	252/203	489	2.1	9	−45
	average	**4.1**	**692**	**0.49/0.31**	**27/30**	**748/263**	**337/120**	**411/143**	**570**	**1.9**	**4**	**−21**
2004	hummock				27/24	972/125	404/052	568/073	683	0.8	0	−43
	hollow				21/26	482/362	207/154	275/208	520	1.1	15	−53
	average	**4.0**	**814**	**0.32/0.35**	**24/25**	**727/244**	**306/103**	**421/141**	**602**	**1.0**	**8**	**−48**
2005	hummock				31/25	1231/142	547/066	684/076	654	2.1	0	103
	hollow				22/29	554/403	251/187	303/216	497	2.8	18	1
	average	**5.7**	**790**	**0.30/0.35**	**27/27**	**893/273**	**399/127**	**494/146**	**576**	**2.5**	**9**	**52**
2006	hummock				30/24	1174/136	503/060	671/076	695	2.0	−3	52
	hollow				22/27	587/388	263/178	324/210	525	2.1	9	−2
	average	**6.1**	**665**	**0.60/0.49**	**26/26**	**881/262**	**383/119**	**498/143**	**610**	**2.1**	**3**	**25**

BGD
9, 5579–5623, 2012

Table 3. External WTD, mean annual temperature (MAT), total precipitation, average WTD from hummock surface between DOY 120 and 300, foliar N content at anthesis, gross primary productivity (GPP), autotrophic respiration (R_a), net primary productivity (NPP), heterotrophic respiration (R_h), methane emissions (CH_4), export of dissolved organic and inorganic C (DOC+DIC), and net ecosystem carbon balance (NECB = NEP−CH_4−DOC−DIC), averaged for hummock and hollow landscape positions, modelled for a boreal fen at Lost Creek, WI. Values at 0.60 m in bold are the same as those in Table 2.

Year	External Water Table m	MAT °C	Precip. mm yr^{-1}	Water Table m	Foliar N shrub/sedge g N (kg C)$^{-1}$	GPP shrub/sedge	R_a shrub/sedge	NPP shrub/sedge g C m^{-2} yr^{-1}	R_h	CH_4	DOC + DIC	NECB
2001	0.30	5.6	865	0.25	22/26	762/279	338/125	424/154	580	6.8	8	−17
	0.60			**0.33**	**23/26**	**815/273**	**360/124**	**456/149**	**627**	**4.2**	**8**	**−34**
	0.90			0.45	25/27	861/299	377/137	484/162	660	2.0	9	−25
2002	0.30	4.9	965	0.14	26/33	760/263	336/127	424/136	426	7.2	18	109
	0.60			**0.17**	**28/33**	**793/268**	**348/131**	**445/138**	**497**	**3.6**	**12**	**70**
	0.90			0.33	30/35	832/295	366/142	466/153	570	1.9	12	36
2003	0.30	4.1	692	0.43	24/29	717/252	328/119	389/133	538	4.4	7	−27
	0.60			**0.49**	**27/30**	**748/263**	**337/120**	**411/143**	**570**	**1.9**	**4**	**−21**
	0.90			0.73	30/29	822/282	359/124	463/158	591	0.6	1	27
2004	0.30	4.0	814	0.26	22/25	690/238	297/102	393/136	557	1.3	8	−36
	0.60			**0.32**	**24/25**	**727/244**	**306/103**	**421/141**	**602**	**1.0**	**8**	**−48**
	0.90			0.36	25/25	768/247	317/105	451/142	656	0.6	5	−68
2005	0.30	5.7	790	0.21	25/27	793/249	362/114	431/135	507	3.8	7	48
	0.60			**0.30**	**27/27**	**893/273**	**399/127**	**494/146**	**576**	**2.5**	**9**	**52**
	0.90			0.36	29/27	938/276	416/129	522/147	627	1.8	8	32
2006	0.30	6.1	665	0.57	24/25	784/257	352/121	432/136	564	2.7	1	0
	0.60			**0.60**	**26/26**	**881/262**	**383/119**	**498/143**	**610**	**2.1**	**3**	**25**
	0.90			0.74	29/27	925/285	396/131	529/154	620	1.6	5	56

BGD
9, 5579–5623, 2012

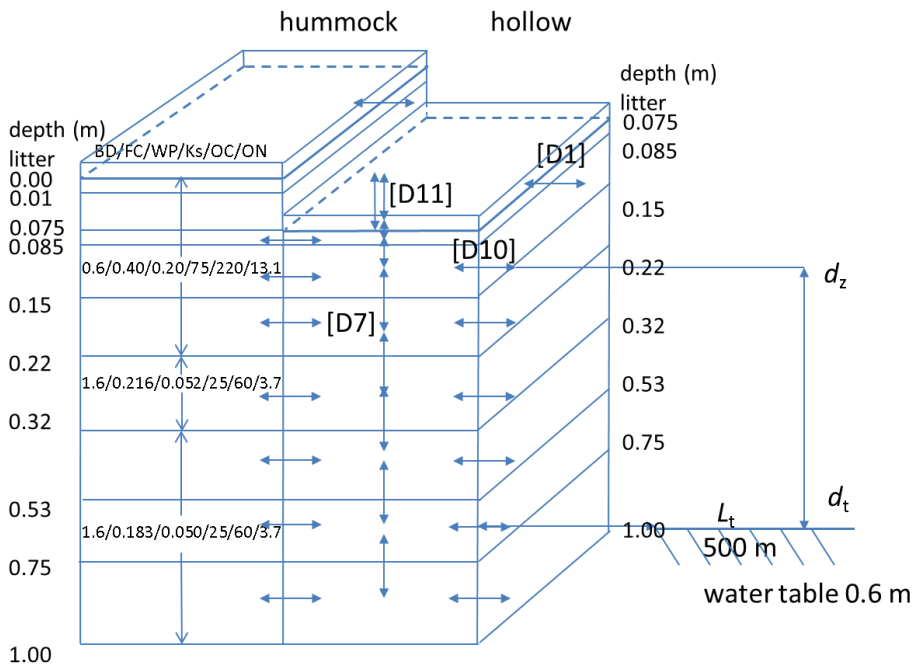

Fig. 1. Schematic representation of wetland landscape in *ecosys*. Depths are from the hummock surface to the bottom of each soil layer. Numbers in each soil layer are BD: Bulk density ($Mg\,m^{-3}$), FC: field capacity ($m^3\,m^{-3}$), WP: wilting point ($m^3\,m^{-3}$), Ks: saturated hydraulic conductivity ($mm\,h^{-1}$), OC: organic carbon ($kg\,Mg^{-1}$), ON: organic nitrogen ($kg\,Mg^{-1}$). Values for BD, OC and ON were measured at the field site. Values for FC, WP and Ks in the organic layers were derived from generalized relationships in Boelter (1969) and Päivänen (1973), and those in the mineral layers from pedotransfer functions in Saxton et al. (1986). Expressions in square brackets refer to equations in the Supplement by which indicated fluxes are calculated.

BGD
9, 5579–5623, 2012

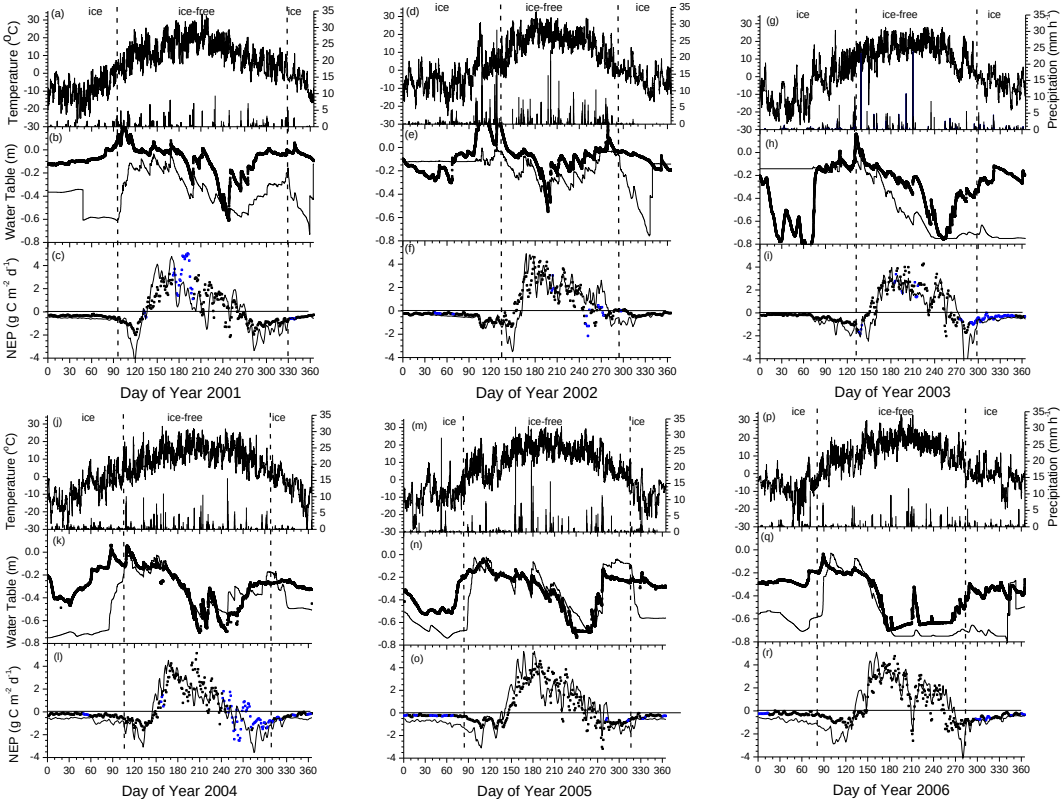

Fig. 2. Hourly air temperatures and precipitation, water table depth and net ecosystem productivity measured (symbols) and modelled (lines) from 2001 to 2006 at Lost Creek, WI. Open symbols represent daily totals calculated from more than 24 gap-filled 1/2-hourly values.

BGD
9, 5579–5623, 2012

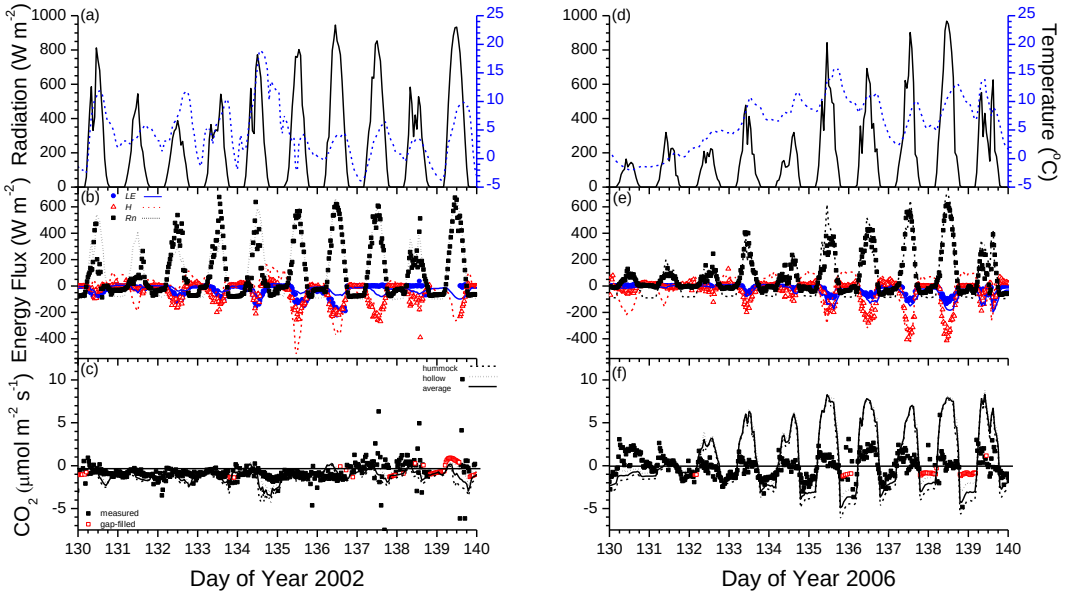

Fig. 3. Radiation and air temperature, energy and CO_2 fluxes measured (symbols) and modelled (lines) from DOY 131 to 140 with high water table in 2002 (0.0 m in Fig. 2) and lower water table in 2006 (0.2 m in Fig. 2). Positive values represent downward fluxes, negative values represent upward fluxes.

BGD
9, 5579–5623, 2012

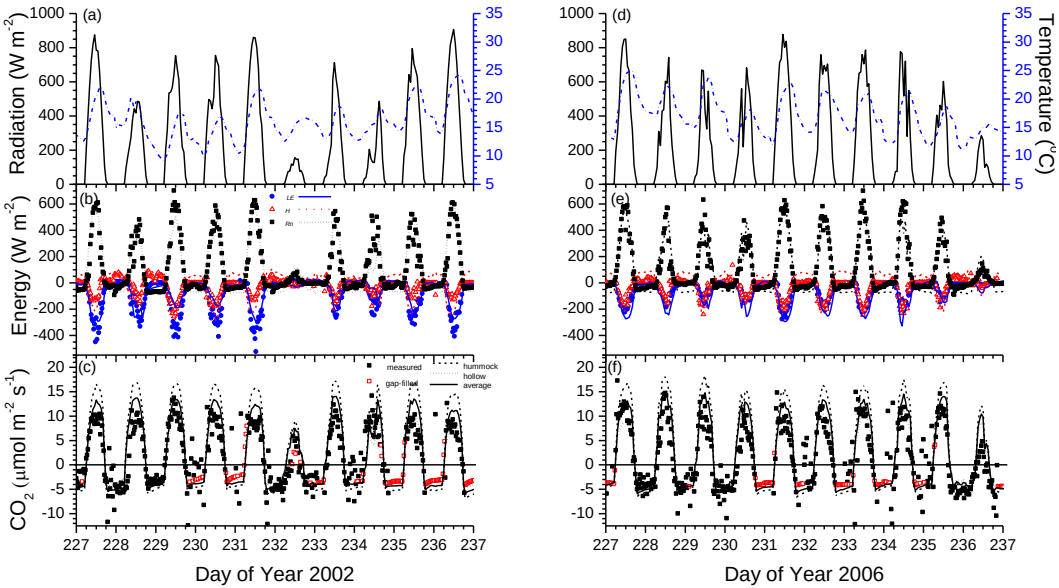

Fig. 4. Radiation and air temperature, energy and CO_2 fluxes measured (symbols) and modelled (lines) from DOY 228 to 237 with high water table in 2002 (0.2 m in Fig. 2) and low water table in 2006 (0.7 m in Fig. 2). Positive values represent downward fluxes, negative values represent upward fluxes.

BGD
9, 5579–5623, 2012

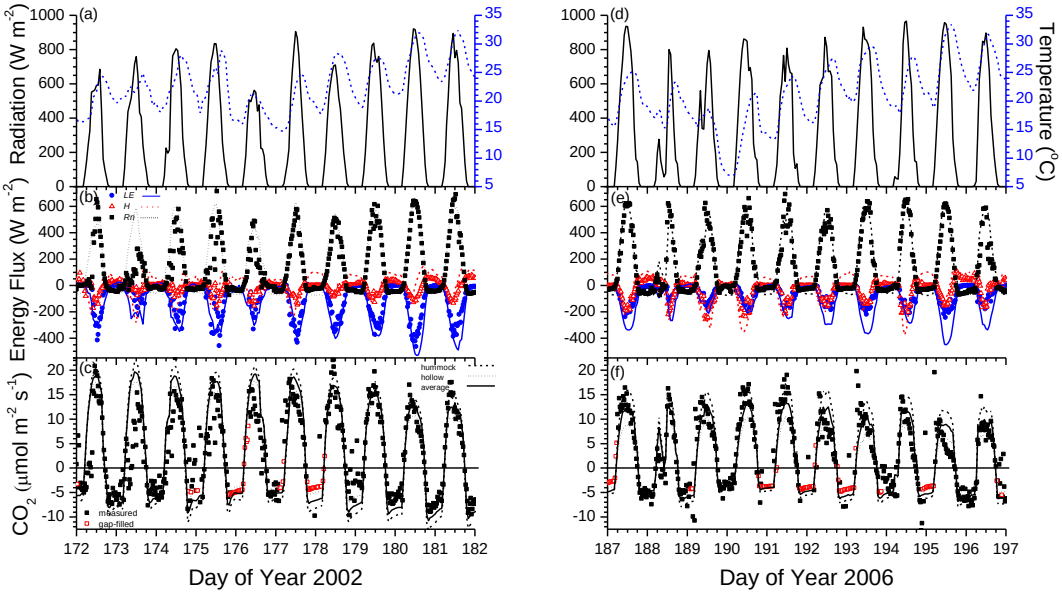

Fig. 5. Radiation and air temperature, energy and CO_2 fluxes measured (symbols) and modelled (lines) during warming events with high water table from DOY 173 to 182 in 2002 (0.2 m in Fig. 2) and low water table from DOY 188 to 197 in 2006 (0.7 m in Fig. 2). Positive values represent downward fluxes, negative values represent upward fluxes.

BGD
9, 5579–5623, 2012

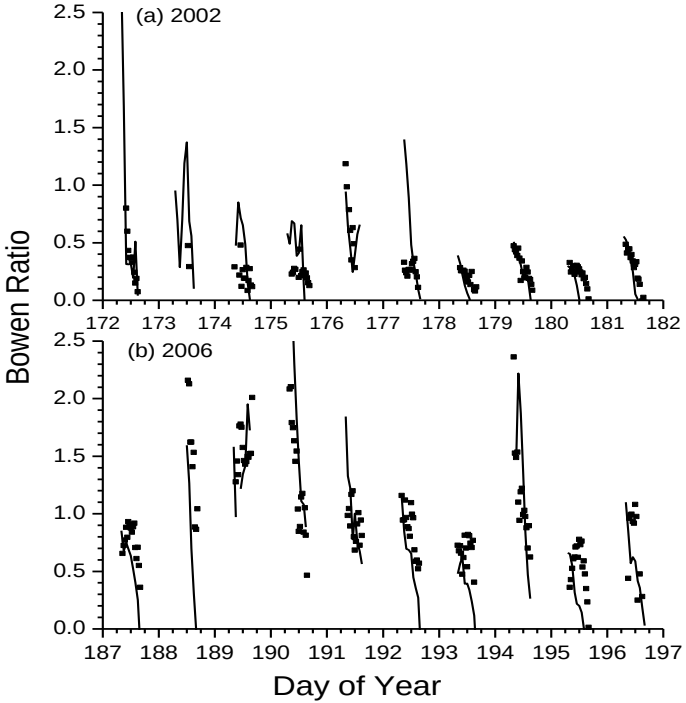

Fig. 6. Bowen Ratios measured (symbols) and modelled (lines) during warming events with high water table from DOY 173 to 182 in 2002 (0.2 m in Fig. 2) and low water table from DOY 188 to 197 in 2006 (0.7 m in Fig. 2) when net radiation > 250 W m^{-2}.

BGD
9, 5579–5623, 2012

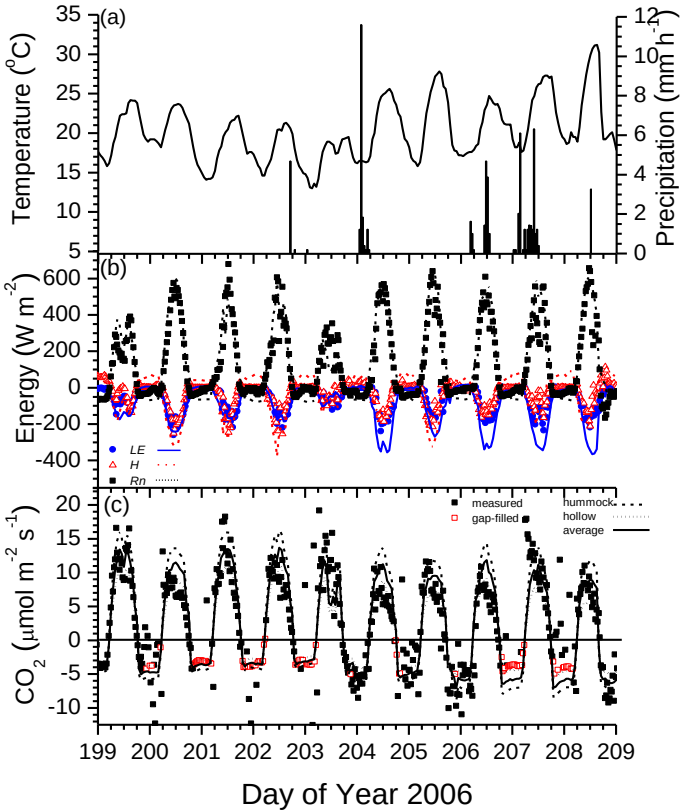

Fig. 7. Air temperature and precipitation, and energy and CO_2 fluxes measured (symbols) and modelled (lines) before and after precipitation events with a low water table from DOY 200 to 209 in 2006 (0.7 m in Fig. 2). Positive values represent downward fluxes, negative values represent upward fluxes.

BGD
9, 5579–5623, 2012

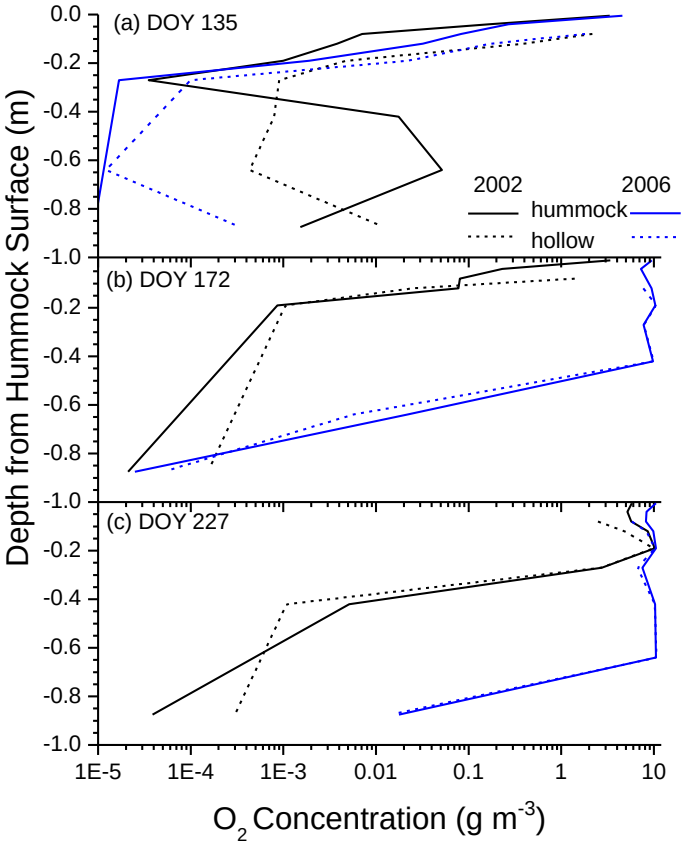

Fig. 8. Vertical profiles of aqueous O_2 concentration ($[O_{2s}]$) modelled below hummocks and hollows on DOY 135, 172 and 227 of 2002 and 2006.

BGD
9, 5579–5623, 2012

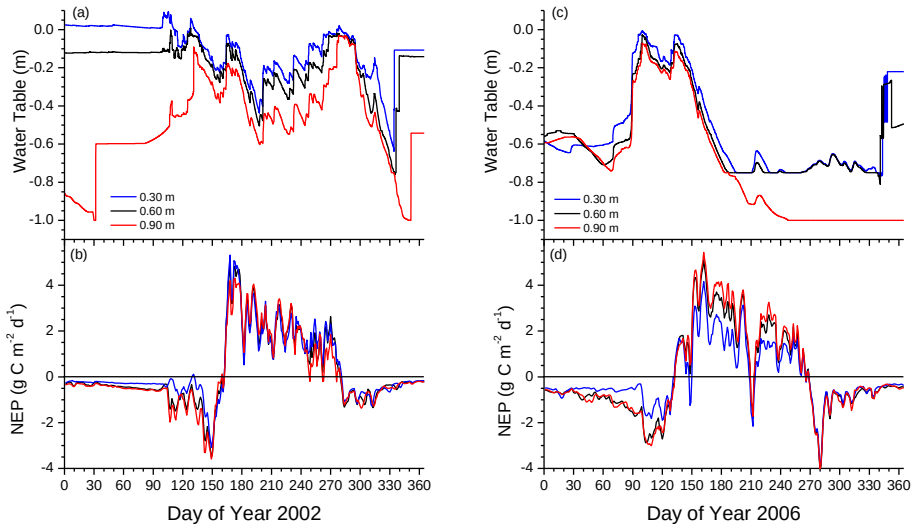

Fig. 9. Changes in water table depth and net ecosystem productivity (NEP) modelled by raising or lowering the depth of the external water table from 0.6 m (Fig. 1) to 0.3 m or 0.9 m in 2002 and 2006. WTD and NEP modelled at 0.6 m are the same as those in Fig. 2.

BGD
9, 5579–5623, 2012

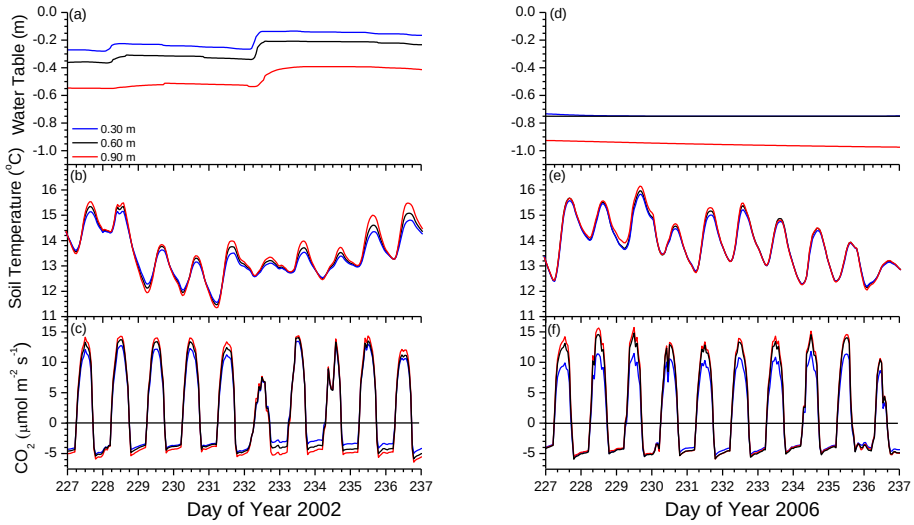

Fig. 10. Changes in water table depth, soil temperatures at 0.12 m, and CO_2 fluxes modelled from DOY 228 to 237 in 2002 and 2006 by raising or lowering the depth of the external water table from 0.6 m (Fig. 1) to 0.3 m or 0.9 m. CO_2 fluxes modelled at 0.6 m are the same as those in Fig. 4.

BGD
9, 5579–5623, 2012

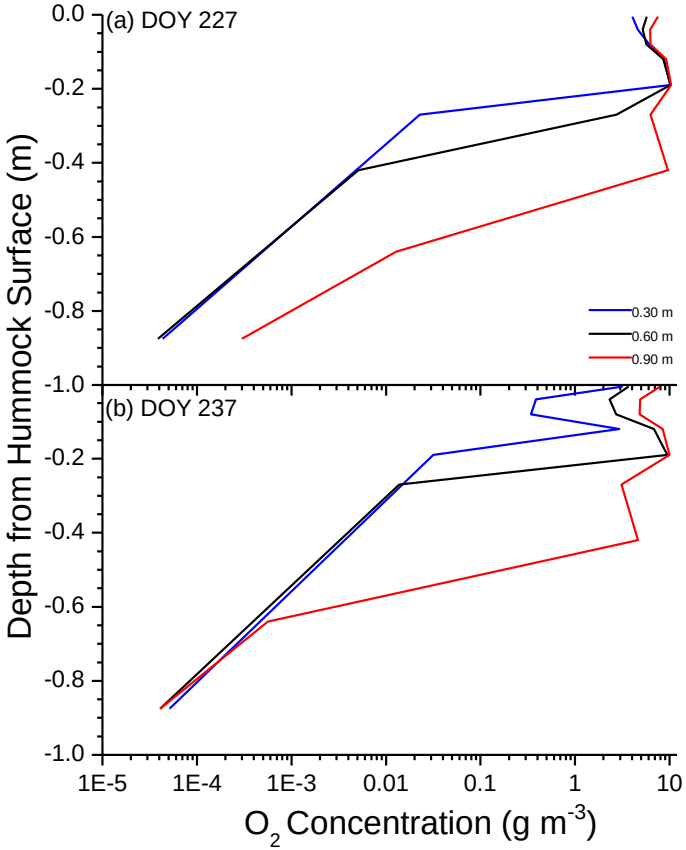

Fig. 11. Vertical profiles of aqueous O_2 concentration ($[O_{2s}]$) modelled below hummocks on DOY 227 and 237 in 2002 by raising or lowering the depth of the external water table from 0.6 m (Fig. 1) to 0.3 m or 0.9 m.

BGD
9, 5579–5623, 2012

SUPPLEMENTAL MATERIAL

Model Development

General

E*cosys* is an hourly time-step model with multiple canopy and soil layers that provide a framework for different plant and microbial populations to acquire, transform and exchange resources (energy, water, C, N and P). The model is constructed from algorithms representing basic physical, chemical and biological processes that determine process rates in plant and microbial populations interacting within complex biomes. These algorithms interact to simulate complex ecosystem behaviour across a wide range of spatial and biological scales. The model is designed to represent terrestrial ecosystems under range of natural and anthropogenic disturbances and environmental changes at patch (spatially homogenous one-dimensional) and landscape (spatially variable two- or three-dimensional) scales. A comprehensive description of *ecosys* with a detailed listing of inputs, outputs, governing equations, parameters, results and references can be found in Grant (2001). A more detailed description of model algorithms and parameters most relevant to simulating temperature, water and nutrient effects on *NEP* is given below, with reference to equations and variable definitions in Appendices A, B, C and D below.

Appendix A: Soil C, N and P Transformations

Decomposition

Organic transformations in *ecosys* occur in five organic matter–microbe complexes (coarse woody litter, fine non-woody litter, animal manure, particulate organic matter (POM), and humus) in each soil layer. Each complex consists of five organic states: solid organic matter, dissolved organic matter, sorbed organic matter, microbial biomass, and microbial residues, among which C, N, and P are transformed. Organic matter in litter and manure complexes are partitioned from proximate analysis results into carbohydrate, protein, cellulose, and lignin components of differing vulnerability to hydrolysis. Organic matter in POM, humus, microbial biomass and microbial residues in

all complexes are also partitioned into components of differing vulnerability to hydrolysis.

The rate at which each component of each organic state in each complex is hydrolyzed during decomposition is a first-order function of the active biomass M of all heterotrophic microbial populations [A1,A2]. The rate at which each component is hydrolyzed is also a Monod function of substrate concentration [A3,A5], calculated from the fraction of substrate mass colonized by M [A4]. Hydrolysis rates are controlled by T_s through an Arrhenius function [A6] and by soil water content (θ) through its effect on aqueous microbial concentrations [M] [A3,A5] in surface litter and in a spatially resolved soil profile. T_s and θ are calculated from surface energy balances and from heat and water transfer schemes through canopy–snow–residue–soil profiles as described in *Energy Exchange* above. Release of N and P from hydrolysis of each component in each complex is determined by its N and P concentrations [A7] which are determined from those of the originating litterfall as described in *Autotrophic Respiration and Growth* above. Most non-lignin hydrolysis products are released as dissolved organic C, N and P (DOC, DON, and DOP) which are adsorbed or desorbed according to a power function of their soluble concentrations [A8 – A10].

Microbial Growth

The DOC decomposition product is the substrate for heterotrophic respiration (R_h) by all M in each substrate-microbe complex [A13]. Total R_h for all soil layers [A11] drives CO_2 emission from the soil surface through volatilization and diffusion. R_h may be constrained by microbial N or P concentrations, T_s, DOC and O_2 [A12 - A14]. O_2 uptake by M is driven by R_h [A16] and constrained by O_2 diffusivity to microbial surfaces [A17], as described for roots in *Autotrophic Respiration and Growth* above. Thus R_h is coupled to O_2 reduction by all aerobic M according to O_2 availability. R_h not coupled with O_2 reduction is coupled with the sequential reduction of NO_3^-, NO_2^-, and N_2O by heterotrophic denitrifiers, and with the reduction of organic C by fermenters and acetotrophic methanogens. In addition, autotrophic nitrifiers conduct NH_4^+ and NO_2^-

oxidation, and NO_2^- reduction, and autotrophic methanogens and methanotrophs conduct CH_4 production and oxidation.

All microbial populations undergo maintenance respiration R_m [A18,A19], depending on microbial N and T_s as described earlier for plants. R_h in excess of R_m is used in growth respiration R_g [A20], the energy yield ΔG of which drives growth in biomass M from DOC uptake according to the energy requirements of biosynthesis [A21, A22]. R_m in excess of R_h causes microbial dieback. M also undergoes first-order decomposition D_m [A23]. Internal retention and recycling of microbial N and P during decomposition [A24] is modelled whenever these nutrients constrain R_h [A12]. Changes in M arise from differences between gains from DOC uptake and losses from $R_m + R_g + D_m$ [A25].

Microbial Nutrient Exchange

During these changes, all microbial populations seek to maintain set minimum ratios of C:N or C:P in M by mineralizing or immobilizing NH_4^+, NO_3^-, and $H_2PO_4^-$ [A26], thereby controlling solution $[NH_4^+]$, $[NO_3^-]$ and $[H_2PO_4^-]$ that determine root and mycorrhizal uptake in *Nutrient Uptake and Translocation* above. If immobilization is inadequate to maintain these minimum ratios, then biomass C:N or C:P may rise, but R_h is constrained by N or P present in the lowest concentration with respect to that at the minimum ratio [A12]. Non-symbiotic heterotrophic diazotrophs can also fix aqueous N_2 [A27] to the extent that immobilization is inadequate to maintain their set minimum C:N, but at an additional respiration cost [A28]. Changes in microbial N and P arise from DON and DOP uptake plus NH_4^+, NO_3^-, and $H_2PO_4^-$ immobilization and N_2 fixation, less NH_4^+, NO_3^-, and $H_2PO_4^-$ mineralization and microbial N and P decomposition [A29].

Humification

C, N and P decomposition products in each organic matter–microbe complex are gradually stabilized into more recalcitrant organic forms with lower C:N and C:P ratios. Products from lignin hydrolysis [A1,A7] combine with some of the products from protein

and carbohydrate hydrolysis in the litterfall and manure complexes and are transferred to the POM complex [A31–A34]. Microbial decomposition products [A23, A24] from all complexes are partitioned between the humus complex and microbial residues in the originating complex according to soil clay content [A35, A36].

Appendix B: Soil-Plant Water Relations

Canopy Transpiration

Canopy energy exchange in *ecosys* is calculated from an hourly two-stage convergence solution for the transfer of water and heat through a multi-layered multi-population soil-root-canopy system. The first stage of this solution requires convergence to a value of canopy temperature T_c for each plant population at which the first-order closure of the canopy energy balance (net radiation R_n, latent heat flux LE [B1a,b], sensible heat flux H [B1c], and change in heat storage G) is achieved. These fluxes are controlled by aerodynamic (r_a) [B3] and canopy stomatal (r_c) [B2] resistances. Two controlling mechanisms are postulated for r_c which are solved in two successive steps:

(1) At the leaf level, leaf resistance r_l [C4] controls gaseous CO_2 diffusion through each leaf surface when calculating CO_2 fixation [C1] from concurrent solutions for diffusion V_g [C2] and carboxylation V_c [C3]. The value of r_l is calculated from a minimum leaf resistance r_{lmin} [C5] for each leaf surface that allows a set ratio for intercellular to canopy CO_2 concentration C_i':C_b to be maintained at V_c under ambient irradiance, air temperature T_a, C_a and zero canopy water potential (ψ_c) (V_c'). This ratio will be allowed to vary diurnally as described in *Gross Primary Productivity* below when ψ_c is solved in the second stage of the convergence solution, described under *Water Relations* below. Values of r_{lmin} are aggregated by leaf surface area to a canopy value r_{cmin} for use in the energy balance convergence scheme [B2a].

(2) At the canopy level, r_c rises from r_{cmin} at zero ψ_c from step (1) above through an exponential function of canopy turgor potential ψ_t [B2b] calculated from ψ_c and

osmotic water potential ψ_π [B4] during convergence for transpiration vs. water uptake.

Root and Mycorrhizal Water Uptake

Root and mycorrhizal water uptake U [B5] is calculated from the difference between canopy water potential ψ_c and soil water potential ψ_s across soil and root hydraulic resistances Ω_s [B9] and Ω_r [B10 – B12] in each rooted soil layer [B6]. Root resistances are calculated from root radial [B10] and from primary [B11] secondary [B12] axial resistivities using root lengths and surface areas from a root system submodel [B13] driven by exchange of nonstructural C, N and P along concentration gradients generated by uptake vs. consumption of C, N and P in shoots and roots (Grant, 1998).

Canopy Water Potential

After convergence for T_c is achieved, the difference between canopy transpiration E_c from the energy balance [B1] and total root water uptake U_c [B5] from all rooted layers in the soil is tested against the difference between canopy water content from the previous hour and that from the current hour [B14]. This difference is minimized in each iteration by adjusting ψ_c which in turn determines each of the three terms in [B14]. Because r_c and T_c both drive E_c, the canopy energy balance described under *Canopy Transpiration* above is recalculated for each adjusted value of ψ_c during convergence.

Appendix C: Gross Primary Productivity and Autotrophic Respiration

C_3 Gross Primary Productivity

After successful convergence for T_c and ψ_c (described in *Plant Water Relations* above), V_c is recalculated from that under zero ψ_c (V_c') to that under ambient ψ_c. This recalculation is driven by stomatal effects on V_g [C2] from the increase in r_{lmin} at zero ψ_c [C5] to r_c at ambient ψ_c [C4], and by non-stomatal effects f_ψ [C9] on CO_2- and light-limited carboxylation V_b [C6] and V_j [C7] (Grant and Flanagan, 2007). The recalculation of V_c is accomplished through a convergence solution for C_i and its aqueous counterpart

C_c at which V_g [C2] equals V_c [C3] (Grant and Flanagan, 2007). The CO_2 fixation rate of each leaf surface at convergence is added to arrive at a value for gross primary productivity (*GPP*) by each plant population in the model [C1]. The CO_2 fixation product is stored in nonstructural C pools σ_C in each branch.

GPP is strongly controlled by nutrient uptake U_{NH_4}, U_{NO_3} and U_{PO_4} [C23], products of which are added to nonstructural N (σ_N) and P (σ_P) in root and mycorrhizal layers where they are coupled with σ_C to drive growth of branches, roots and mycorrhizae as described in *Growth and Senescence* below. Low σ_N:σ_C or σ_P:σ_C in branches indicate excess CO_2 fixation with respect to N or P uptake for phytomass growth. Such ratios in the model have two effects on GPP:

(1) They reduce activities of rubisco [C6a] and chlorophyll [C7a] through product inhibition [C11], thereby simulating the suppression of CO_2 fixation by leaf σ_C accumulation widely reported in the literature.

(2) They reduce the structural N:C and P:C ratios at which leaves are formed because σ_C, σ_N and σ_P are the substrates for leaf growth. Lower structural ratios cause a proportional reduction in areal concentrations of rubisco [C6b] and chlorophyll [C7b], reducing leaf CO_2 fixation.

Autotrophic Respiration

The temperature-dependent oxidation of these nonstructural pools (R_c) [C14], plus the energy costs of nutrient uptake [C23], drive autotrophic respiration (R_a) [C13] by all branches, roots and mycorrhizae. R_c by roots and mycorrhizae is constrained by O_2 uptake U_{O2} [C14b] calculated by solving for aqueous O_2 concentrations at root and mycorrhizal surfaces [O_{2r}] at which convection + radial diffusion through the soil aqueous phase plus radial diffusion through the root aqueous phase [C14d] equals active uptake driven by O_2 demand from R_c [C14c] (Grant, 2004). These diffusive fluxes are in turn coupled to volatilization – dissolution between aqueous and gaseous phases in soil and root [D14]. The diffusion processes are driven by aqueous O_2 concentrations sustained by transport and dissolution of gaseous O_2 through soil and roots (Grant 2004), and are governed by lengths and surface areas of roots and mycorrhizae (Grant, 1998).

Thus R_c is coupled to O_2 reduction by all root and mycorrhizal populations according to O_2 availability. R_c is first used to meet maintenance respiration requirements (R_m), calculated independently of R_c from the N content in each organ, and a function of T_c or T_s [C16]. Any excess of R_c over R_m is expended as growth respiration R_g, constrained by branch, root or mycorrhizal ψ_t [C17]. When R_m exceeds R_c, the shortfall is met by the respiration of remobilizable C (R_s) in leaves and twigs or roots and mycorrhizae [C15].

Growth and Senescence

R_g drives the conversion of branch σ_C into foliage, twigs, branches, boles and reproductive material according to organ growth yields Y_g and phenology-dependent partitioning coefficients [C20], and the conversion of root and mycorrhizal σ_C into primary and secondary axes according to root and mycorrhizal growth yields. Growth also requires organ-specific ratios of nonstructural N (σ_N) and P (σ_P) from U_{NH_4}, U_{NO_3} and U_{PO_4} [C23] which are coupled with σ_C to drive growth of branches, roots and mycorrhizae.

The translocation of σ_C, σ_N and σ_P among branches and root and mycorrhizal layers is driven by concentration gradients generated by production of σ_C from branch GPP and of σ_N and σ_P from root and mycorrhizal uptake vs. consumption of σ_C, σ_N and σ_P from R_c, R_g and phytomass growth (Grant 1998). Low σ_N:σ_C or σ_P:σ_C in mycorrhizae and roots indicates inadequate N or P uptake with respect to CO_2 fixation. These ratios affect translocation of σ_C, σ_N and σ_P by lowering mycorrhizal – root – branch concentration gradients of σ_N and σ_P while raising branch – root – mycorrhizal concentration gradients of σ_C. These changes slow transfer of σ_N and σ_P from root to branch and hasten transfer of σ_C from branch to root, increasing root and mycorrhizal growth at the expense of branch growth, and thereby raising N and P uptake [C23] with respect to CO_2 fixation. Conversely, high σ_N:σ_C or σ_P:σ_C in roots and mycorrhizae indicate excess N or P uptake with respect to CO_2 fixation. Such ratios reduce specific activities of root and mycorrhizal surfaces for N or P uptake through a product inhibition function as has been observed experimentally. These changes hasten transfer of σ_N and

σ_P from root to branch and slow transfer of σ_C from branch to root, increasing branch growth at the expense of root and mycorrhizal growth, and thereby slowing N and P uptake Thus the modelled plant translocates σ_C, σ_N and σ_P among branches, roots and mycorrhizae to maintain a functional equilibrium between acquisition and use of C, N and P by different parts of the plant.

R_g is limited by ψ_t [C17], and because branch ψ_t declines relatively more with soil drying than does root ψ_t, branch R_g also declines relatively more with soil drying than does root R_g, slowing oxidation of σ_C in branches and allowing more translocation of σ_C from branches to roots. This change in allocation of σ_C enables more root growth to reduce Ω_s, Ω_r and Ω_a, and hence increase U [B6], thereby offsetting the effects of soil drying on ψ_t. Thus the modelled plant translocates σ_C, σ_N and σ_P among branches, roots and mycorrhizae to maintain a functional equilibrium between acquisition and use of water.

R_s [C15] drives the withdrawal of remobilizable C, N and P (mostly nonstructural protein) from leaves and twigs or roots and mycorrhizae into σ_N and σ_P, and the loss of associated non-remobilizable C, N and P (mostly structural) as litterfall [C18]. Provision is also made to withdraw remobilizable N or P from leaves and twigs or roots and mycorrhizae when ratios of σ_N:σ_C or σ_P:σ_C become smaller than those required for growth of new phytomass. This withdrawal drives the withdrawal of associated remobilizable C, and the loss of associated non-remobilizable C, N and P as litterfall. Environmental constraints such as water, heat, nutrient or O_2 stress that reduce σ_C and hence R_c with respect to R_m therefore hasten litterfall.

R_a of each branch or root and mycorrhizal layer is the total of R_c and R_s, and net primary productivity (NPP) is the difference between canopy GPP [C1] and total R_a of all branches and root and mycorrhizal layers [C13]. Phytomass net growth is the difference between gains driven by R_g and Y_g, and losses driven by R_s and litterfall [C20]. These gains are allocated to leaves, twigs, wood and reproductive material at successive branch

nodes, and to roots and mycorrhizae at successive primary and secondary axes, driving leaf expansion [C21a] and root extension [C21b]. Losses from remobilization and litterfall in shoots start at the lowest node of each branch at which leaves or twigs are present, and proceed upwards when leaves or twigs are lost. Losses in roots and mycorrhizae start with secondary axes and proceeds to primary axes when secondary axes are lost.

Root and Mycorrhizal Nutrient Uptake

Root and mycorrhizal uptake of N and P U_{NH_4}, U_{NO_3} and U_{PO_4} is calculated by solving for solution [NH_4^+], [NO_3^-] and [$H_2PO_4^-$] at root and mycorrhizal surfaces at which radial transport by mass flow and diffusion from the soil solution to these surfaces [C23a,c,e] equals active uptake by the surfaces [C23b,d,f]. Path lengths and surface areas for U_{NH_4}, U_{NO_3} and U_{PO_4} are calculated from a root and mycorrhizal growth submodel driven by exchange of nonstructural C, N and P along concentration gradients generated by uptake vs. consumption of C, N and P in shoots and roots (Grant, 1998). A product inhibition function is included to avoid uptake in excess of nutrient requirements [C23g].

C_4 Gross Primary Productivity

C_4 Mesophyll

In C_4 plants, the mesophyll carboxylation rate is the lesser of CO_2- and light-limited reaction rates [C26] (Berry and Farquhar, 1978). The CO_2-limited rate is a Michaelis-Menten function of PEP carboxylase (PEPc) activity and aqueous CO_2 concentration in the mesophyll [C29] parameterized from Berry and Farquhar (1978) and from Edwards and Walker (1983). The light-limited rate [C30] is a hyperbolic function of absorbed irradiance and mesophyll chlorophyll activity [C31] with a quantum requirement based on 2 ATP from Berry and Farquhar (1978). PEPc [C32] and chlorophyll [C33] activities are calculated from specific activities multiplied by set fractions of leaf surface N density, and from functions of C_4 product inhibition (Jiao and Chollet, 1988; Lawlor, 1993) [C34], ψ_c ([C35] as described in Grant and Flanagan, 2007) and T_c [C36]. Leaf surface N density is controlled by leaf structural N:C and P:C ratios

calculated during leaf growth from leaf non-structural N:C and P:C ratios arising from root N and P uptake (Grant, 1998) vs. CO_2 fixation.

C_4 Mesophyll-Bundle Sheath Exchange

Differences in the mesophyll and bundle sheath concentrations of the C_4 carboxylation product drive mesophyll-bundle sheath transfer (Leegood, 2000) [C37]. The bundle sheath concentration of the C_4 product drives a product-inhibited decarboxylation reaction (Laisk and Edwards, 2000) [C38], the CO_2 product of which generates a concentration gradient that drives leakage of CO_2 from the bundle sheath to the mesophyll [C39]. CO_2 in the bundle sheath is maintained in 1:50 equilibrium with HCO_3^- (Laisk and Edwards, 2000). At this stage of model development, the return of a C_3 decarboxylation product from the bundle sheath to the mesophyll is not simulated. Parameters used in Eqs. [C37 – C39] allowed mesophyll and bundle sheath concentrations of C_4 carboxylation products from [C40 – C41] to be maintained at values consistent with those in Leegood (2000), bundle sheath concentrations of CO_2 (from Eq. [C42]) to be maintained at values similar to those reported by Furbank and Hatch (1987), and bundle sheath CO_2 leakiness [C39]), expressed as a fraction of PEP carboxylation, to be maintained at values similar to those in Williams et al. (2001), in sorghum as described in Grant et al. (2004).

C_4 Bundle Sheath

A C_3 model in which carboxylation is the lesser of CO_2- and light-limited reaction rates (Farquhar et al., 1980) has been parameterized for the bundle sheath of C_4 plants [C43] from Seeman et al. (1984). The CO_2-limited rate [C44] is a Michaelis-Menten function of RuBP carboxylase (RuBPc) activity and bundle sheath CO_2 concentration [C42]. The light-limited rate [C45] is a hyperbolic function of absorbed irradiance and activity of chlorophyll associated with the bundle sheath with a quantum yield based on 3 ATP [C46]. The provision of reductant from the mesophyll to the bundle sheath in NADP-ME species is not explicitly simulated. RuBPc [C47] and chlorophyll [C48] activities are the products of specific activities and concentrations multiplied by set

fractions of leaf surface N density, and from functions of C_3 product inhibition (Bowes, 1991; Stitt, 1991) [C49], ψ_c (Eq. A12 from Grant and Flanagan, 2007) and T_c [C36].

Rates of C_3 product removal are controlled by phytomass biosynthesis rates driven by concentrations of nonstructural products from leaf CO_2 fixation and from root N and P uptake. If biosynthesis rates are limited by nutrient uptake, consequent depletion of nonstructural N or P and accumulation of nonstructural C will constrain specific activities of RuBP and chlorophyll [C47 – C49], and thereby slow C_3 carboxylation [C43], raise bundle sheath CO_2 concentration [C42], accelerate CO_2 leakage [C39], slow C_4 decarboxylation [C38], raise C_4 product concentration in the bundle sheath [C41], slow C_4 product transfer from the mesophyll [C37], raise C_4 product concentration in the mesophyll [C40], and slow mesophyll CO_2 fixation [C32 – C35]. This reaction sequence simulates the progressive inhibition of C_3 and C_4 carboxylation hypothesized by Sawada et al. (2002) following partial removal of C sinks in C_4 plants.

Appendix D: Soil Water, Heat, Gas and Solute Fluxes

Surface Water Flux

Surface runoff is modelled using Manning's equation [D1] with surface water velocity v [D3] calculated from surface geometry [D5a] and slope [D5b], and with surface water depth d [D2] calculated from surface water balance [D4] using kinematic wave theory.

Subsurface Water Flux

Subsurface water flow [D7] is calculated from Richard's equation using bulk soil water potentials ψ_s of both cells if both source and destination cells are unsaturated [D9a], or Green-Ampt equation using ψ_s beyond the wetting front of the unsaturated cell if either source or destination cell is saturated [D9b] (Grant et al., 2004). Subsurface water flow can also occur through macropores using Poiseulle-Hagen theory for laminar flow in tubes (Dimitrov et al., 2010), depending on inputs for macropore volume fraction.

Exchange with Water Table

If a water table is present in the model, subsurface boundary water fluxes between saturated boundary grid cells and a fixed external water table are calculated from lateral hydraulic conductivities of the grid cells, and from elevation differences and lateral distances between the grid cells and the external water table [D10]. These terms are determined from set values for the depth d_t of, and lateral distance L_t to, an external water table.

Surface Heat Flux

Surface heat fluxes (G) arising from closure of the energy balance at snowpack, surface litter and soil surfaces [D11] (Grant et al., 1999) drive conductive – convective fluxes among snowpack, surface litter and soil layers [D12]. These fluxes drive freezing – thawing (Q_f) and changes temperatures (T) in snowpack, surface litter and soil layers [D13].

Gas Flux

All gases undergo volatilization – dissolution between the gaseous and aqueous phases in the soil [D14a] and root [D14b], and between the atmosphere and the aqueous phase at the soil surface [D15a], driven by gaseous – aqueous concentration differences calculated from solubility coefficients and coupled to diffusive uptake by roots [C14] and microbes [A17]. Gases also undergo convective - conductive transfer among soil layers driven by gaseous concentration gradients and diffusivities [D16a,b,c] calculated from air-filled porosities [D17a,b,c], and from each rooted soil layer directly to the atmosphere through roots driven by gaseous concentration gradients and diffusivities [D16d] calculated from root porosities [D17d]. Gases may also bubble upwards from soil zones in which the total partial pressure of all aqueous gases exceeds atmospheric pressure [D18].

Solute Flux

All gaseous and non-gaseous solutes undergo convective - dispersive transfer among soil layers driven by aqueous concentration gradients and dispersivities [D19] calculated from water-filled porosity [D20] and water flow length [D21].

Appendix E: Solute Transformations

Precipitation - Dissolution Equilibria

Solution [NH_4^+], [NO_3^-] and [$H_2PO_4^-$] that drive U_{NH_4}, U_{NO_3} and U_{PO_4} [C23] are controlled by precipitation, adsorption and ion pairing reactions (Grant et al., 2004; Grant and Heaney, 1997), including precipitation-dissolution of $Al(OH)_3$, $Fe(OH)_3$, $CaCO_3$, $CaSO_4$, $AlPO_4$, $FePO_4$, $Ca(H_2PO_4)_2$, $CaHPO_4$, and $Ca_5(PO_4)_3OH$ [E1 – E9], cation exchange between Ca^{2+}, NH_4^+ and other cations [E10 – E15], anion exchange between adsorbed and soluble $H_2PO_4^-$, HPO_4^{2-} and OH^- [E16 – E20], and ion pairing [E22 – E55].

Key governing equations for simulating net ecosystem productivity in *ecosys*. Variables input to the model appear in bold with values given in the **Definition of Variables** below.

Appendix F: N_2 Fixation

Rhizobial Growth

Modelling the activity of symbiotic N_2 fixing bacteria in roots follows a protocol similar to that of non-symbiotic N_2 fixing bacteria in soil. Respiration demand is driven by specific activity, microbial biomass M_n, and nonstructural C concentration [χ_n] in root nodules [F1], and is constrained by temperature [F2] and microbial N or P status [F3]. Nodule respiration R is constrained by the extent to which O_2 uptake meets O_2 demand [F4] imposed by respiration demand [F5]. O_2 uptake is in turn constrained by rhizosphere [O_{2r}] [F6a] which is controlled by radial diffusion of O_2 through soil water to roots and

nodules [F6b]. Soil water [O_2] is maintained by dissolution of O_2 from soil air which is in turn maintained by soil-atmosphere gas exchange and vertical diffusion (Grant, 2004). R_h is first allocated to maintenance respiration R_m [F7 – F8] and the remainder if any is allocated to growth respiration R_g [F9]. If R_m exceeds R_h, the shortfall is made up from respiration of microbial protein C, forcing senescence and litterfall of associated non-protein C [F10 – F11].

N_2 Fixation

N_2 fixation V_{N_2} is driven by R_g [F12], but is constrained by accumulation of nonstructural N ν_n with respect to nonstructural C and P also required for microbial growth in the nodule [F13]. Nonstructural N ν_{nd} is the product of V_{N_2}, so that [F12] simulates the inhibition of N_2 fixation by its product (Postgate, 1998). The value of V_{N_2} is also limited by the additional N needed to maintain bacterial N content [N_n'] of M_n [F12], so that N_2 fixation is constrained by the need of nodule bacteria for N not met from other sources (Postgate, 1998). Respiration required for N_2 fixation R_{N_2} [F14] is subtracted from R_g [F15] when calculating microbial growth [F16 – F18]. Microbial senescence drives N and P litterfall [F19 – F20].

Nodule – Root Exchange

Exchange of nonstructural C, N and P between roots and nodules is driven by concentration gradients [F21 – F23] created by generation, transfer and consumption of nonstructural C, N and P in shoots, roots, mycorrhizae and nodules. Nonstructural C is generated in shoots and transferred along concentration gradients to roots and thence to nodules [F21]. Nonstructural P is generated in roots and transferred along concentration gradients to shoots and nodules [F23]. Nonstructural N is generated in roots through mineral uptake and in nodules through gaseous fixation [F22]. Nonstructural C, N and P in nodules is determined by root-nodule exchange, by nodule respiration and fixation, and by remobilization from nodule litterfall [F24 – F26].

Root nonstructural N (ν_r) may rise if high mineral N concentrations in soil sustain rapid N uptake by roots. Large ν_r suppresses or even reverses the transfer of ν_n from nodule to root [F22], raising ν_n [F25] and hence suppressing V_{N_2} [F12 – F13]. Large ν_r also accelerates the consumption of χ_r, slowing its transfer to nodules [F21], reducing χ_n [F24] and hence slowing nodule growth [F1]. Conversely, slow root N uptake caused by low soil mineral N concentrations would lower ν_{rt} and raise χ_{rt}, hastening the transfer of ν_n from nodule to root and of χ_{rt} from root to nodule, lowering ν_n, raising χ_n, and accelerating V_{N_2}. However [F13] also allows V_{N_2} to be constrained by nonstructural C and P concentrations arising from CO_2 fixation and root P uptake.

Appendix A: Soil C, N and P Transformations

Decomposition

$D_{Si,j,l,\mathrm{C}} = D'_{Si,j,l,\mathrm{C}} \Sigma_n M_{i,n,a,l,\mathrm{C}} \; f_{\mathrm{tg}l}$	decomposition of litter, SOC	[A1]
$D_{Zi,j,l,\mathrm{C}} = D'_{Zi,j,l,\mathrm{C}} \Sigma_n M_{i,n,a,l,\mathrm{C}} \; f_{\mathrm{tg}l}$	decomposition of microbial residues	[A2]
$D'_{Si,j,l,\mathrm{C}} = \{\boldsymbol{D}_{Sj,\mathrm{C}}[S_{i,j,l,\mathrm{C}}]\}/\{[S_{i,j,l,\mathrm{C}}] + \boldsymbol{K}_{\mathbf{m}D}(1.0 + [\Sigma_n M_{i,n,a,l,\mathrm{C}}]/\boldsymbol{K}_{\mathbf{i}D})\}$	substrate and water constraint on D from colonized substrate mass	[A3]
$\delta S_{i,j,k,l,\mathrm{C}}/\delta t = \boldsymbol{\beta} \Sigma_n (U_{i,n,l\mathrm{C}} - R_{\mathrm{h}i,n,l}) (S'_{i,j,k,l,\mathrm{C}}/ S'_{i,j,l,\mathrm{C}}) \{(S'_{i,j,l,\mathrm{C}}/S_{i,j,l,\mathrm{C}})/(S'_{i,j,l,\mathrm{C}}/S_{i,j,l,\mathrm{C}} + \boldsymbol{K}_{\mathbf{i}S})\}$	substrate mass determined by microbial growth into uncolonized substrate mass	[A4]
$D'_{Zi,j,l,\mathrm{C}} = \{\boldsymbol{D}_{Zj,\mathrm{C}}[Z_{i,j,l,\mathrm{C}}]\}/\{[Z_{i,j,l,\mathrm{C}}] + \boldsymbol{K}_{\mathbf{m}D}(1.0 + [\Sigma_n M_{i,n,a,l,\mathrm{C}}]/\boldsymbol{K}_{\mathbf{i}D})\}$	substrate and water constraint on D from microbial residues	[A5]
$f_{\mathrm{tg}l} = T_{\mathrm{s}l}\{e^{[B - \boldsymbol{H}_{\mathbf{a}}/(\boldsymbol{R}T_{\mathrm{s}l})]}\}/\{1 + e^{[(\boldsymbol{H}_{\mathbf{dl}} - \boldsymbol{S}T_{\mathrm{s}l})/(\boldsymbol{R}T_{\mathrm{s}l})]} + e^{[(\boldsymbol{S}T_{\mathrm{s}l} - \boldsymbol{H}_{\mathbf{dh}})/(\boldsymbol{R}T_{\mathrm{s}l})]}\}$	Arrhenius function for D and R_{h}	[A6]
$D_{Si,j,l,\mathrm{N,P}} = D_{Si,j,l,\mathrm{C}}(S_{i,j,l,\mathrm{N,P}}/S_{i,j,l,\mathrm{C}})$	N and P coupled with C during D	[A7a]
$D_{Zi,j,l,\mathrm{N,P}} = D_{Zi,j,l,\mathrm{C}}(Z_{i,j,l,\mathrm{N,P}}/Z_{i,j,l,\mathrm{C}})$		[A7b]
$Y_{i,l,\mathrm{C}} = \boldsymbol{k}_{\mathbf{ts}}(aF_{\mathrm{s}}[Q_{i,l,\mathrm{C}}]^{\boldsymbol{b}} - X_{i,l,\mathrm{C}})$	Freundlich sorption of DOC	[A8]
$Y_{i,l,\mathrm{N,P}} = Y_{i,l,\mathrm{C}}(Q_{i,l,\mathrm{N,P}}/Q_{i,l,\mathrm{C}})$	($Y_{i,l,\mathrm{C}} > 0$) adsorption of DON, DOP	[A9]
$Y_{i,l,\mathrm{N,P}} = Y_{i,l,\mathrm{C}}(X_{i,l,\mathrm{N,P}}/X_{i,l,\mathrm{C}})$	($Y_{i,l,\mathrm{C}} < 0$) desorption of DON, DOP	[A10]

Microbial Growth

$R_{\mathrm{h}} = \Sigma_i \Sigma_n \Sigma_l R_{\mathrm{h}i,n,l}$		[A11]
$\boldsymbol{R}_{\mathrm{h}i,n,l} = \boldsymbol{R}'_{\mathrm{h}n} \min\{C_{\mathrm{N}i,n,l,a}/\boldsymbol{C}_{\mathbf{N}j}, C_{\mathrm{P}i,n,l,a}/\boldsymbol{C}_{\mathbf{P}j}\}$	R_{h} constrained by microbial N, P	[A12]
$R_{\mathrm{h}}'_{i,n,l} = M_{i,n,a,l,\mathrm{C}} \{\boldsymbol{R}_{\mathrm{h}i,n,l} [Q_{i,l,\mathrm{C}}]\}/\{(\boldsymbol{K}_{\mathbf{mQC}} + [Q_{i,l,\mathrm{C}}])\} f_{\mathrm{tg}l} \; f_{\psi gl}$	R_{h} constrained by substrate DOC	[A13]

$R_{hi,n,l} = R_h'_{i,n,l}\,(U_{O2i,n,l}/U'_{O2i,n,l})$	R_h constrained by O_2	[A14]
$f_{\psi gl} = 1.0 - 6.67(1.0 - e^{(M\psi_s/(\boldsymbol{R}T_{sl})})$	ψ_s constraints on microbial growth	[A15]
$U'_{O2i,n,l} = 2.67R_h'_{i,n,l}$	O_2 demand driven by potential R_h	[A16]
$U_{O2i,n,l} = U'_{O2i,n,l}[O_{2mi,n,l}]/([O_{2mi,n,l}] + \boldsymbol{K_{O_2}})$	active uptake coupled with radial diffusion of O_2	[A17a]
$= 4\pi n\, M_{i,n,a,l,C}\, D_{sO2l}[\boldsymbol{r_m} r_{wl}/(r_{wl} - \boldsymbol{r_m})]([O_{2sl}] - [O_{2mi,n,l}]$		[A17b]
$R_{mi,n,j,l} = \boldsymbol{R}_m M_{i,n,j,l,N}\, f_{tml}$		[A18]
$f_{tml} = e^{[\boldsymbol{y}(T_{sl} - 298.16)]}$		[A19]
$R_{gi,n,l} = R_{hi,n,l} - \Sigma_j\, R_{mi,n,j,l}$		[A20]
$U_{i,n,lC} = \min(R_{hi,n,l}, \Sigma_j\, R_{mi,n,j,l}) + R_{gi,n,l}\,(1 + \boldsymbol{\Delta G}/\boldsymbol{E_m})$	DOC uptake driven by R_g	[A21]
$U_{i,n,lN,P} = U_{i,n,l} Q_{i,l,N,P}/Q_{i,l,C}$	DON,DOP uptake driven by $U_{i,n,lC}$	[A22]
$D_{Mi,n,j,l,C} = \boldsymbol{D}_{Mi,j} M_{i,n,j,C}\, f_{tg}$	first-order decay of microbial C,	[A23]
$D_{Mi,n,j,N,P} = \boldsymbol{D}_{Mi,j} M_{i,n,j,l,N,P}\, f_{tgl}\, f_{di,n,lN,P}$	partial release of microbial N, P	[A24]
$\delta M_{i,n,j,l,C}/\delta t = F_j\, U_{i,n,lC} - F_j R_{hi,n,l} - D_{Mi,n,j,l,C}$	$[R_{hi,n,l} > R_{mi,n,j,l}]$ growth	[A25a]
$\delta M_{i,n,j,l,C}/\delta t = F_j\, U_{i,n,lC} - R_{mi,n,j,l} - D_{Mi,n,j,l,C}$	$[R_{hi,n,l} < R_{mi,n,j,l}]$ senescence	[A25b]

Microbial Nutrient Exchange

$U_{NH4i,n,j,l} = (M_{i,n,j,l,C}\, \boldsymbol{C_{Nj}} - M_{i,n,j,l,N})$	$U_{NH_4} < 0$ mineralization	[A26a]
$U_{NH_4 i,n,j,l} = \min\{(M_{i,n,j,l,C}\, \boldsymbol{C_{Nj}} - M_{i,n,j,l,N}),$ $\boldsymbol{U'_{NH_4}} A_{i,n,j,l}\,([NH_4^+{}_{i,n,j,l}] - [\boldsymbol{NH_4^+}_{mn}])/([NH_4^+{}_{i,n,j,l}] - [\boldsymbol{NH_4^+}_{mn}] + \boldsymbol{K_{NH_4}})\}$	$U_{NH_4} > 0$ immobilization	[A26b]
$U_{NO_3 i,n,j,l} = \min\{(M_{i,n,j,l,C}\, \boldsymbol{C_{Nj}} - (M_{i,n,j,l,N} + U_{NH_4 i,n,j,l})),$ $\boldsymbol{U'_{NO_3}} A_{i,n,i,l}\,([NO_3^-{}_{i,n,j,l}] - [\boldsymbol{NO_3^-}_{mn}])/([NO_3^-{}_{i,n,i,l}] - [\boldsymbol{NO_3^-}_{mn}] + \boldsymbol{K_{NO_3}})\}$	$U_{NO_3} > 0$ immobilization	[A26c]

$U_{PO4i,n,j,l} = (M_{i,n,j,l,C}\, \boldsymbol{C_{Pj}} - M_{i,n,j,l,P})$	$U_{PO_4} < 0$	mineralization	[A26d]
$U_{PO4i,n,j,l} = \min\{(M_{i,n,j,l,C}\, \boldsymbol{C_{Pj}} - M_{i,n,j,l,P}),$ $\boldsymbol{U'_{PO_4}}\, A_{i,n,j,l}\, \boldsymbol{([H_2PO_4^-{}_{i,n,j,l}]-[H_2PO_4^-{}_{mn}])/([H_2PO_4^-{}_{i,n,j,l}]-[H_2PO_4^-{}_{mn}] + K_{PO_4})\}}$	$U_{PO_4} > 0$	immobilization	[A26e]
$\Phi_{i,n=f,j,l} = max\{0, M_{i,n=f,j,l,C}\boldsymbol{C_{Nj}} - M_{i,n=f,j,l,N} - max\{0, U_{i,n=f,j,l,N}\}\}$	N_2 fixation driven by N deficit of diazotrophic population		[A27]
$R_{\Phi i,n=f,j,l} = \boldsymbol{E_\Phi}\, \Phi_{i,n=f,j,l}$			[A28]
$\delta M_{i,n,j,l,N}/\delta t = F_j U_{i,n,l,N} + U_{NH_{4i,n,j,l}} + U_{NO_{3i,n,j,l}} + \Phi_{i,n=f,j,l} - D_{Mi,n,j,l,N}$	growth *vs*. losses of microbial N, P		[A29a]
$\delta M_{i,n,j,l,P}/\delta t = F_j U_{i,n,l,P} + U_{PO_{4i,n,j,l}} - D_{Mi,n,j,l,p}$			[A29b]
$M_{i,n,a,l,C} = M_{i,n,j=labile,l,C} + M_{i,n,j=resistant,l,C} F_r/F_l$			[A30]

Humification

$H_{Si,j=lignin,l,C} = D_{Si,j=lignin,l,C}$	decomposition products of litter added to POC depending on lignin		[A31]
$H_{Si,j=lignin,l,N,P} = D_{Si,j=lignin,l,N,P}$			[A32]
$H_{Si,j\neq lignin,l,C} = H_{Si,j=lignin,l,C}\, \boldsymbol{L_{hj}}$			[A33]
$H_{Si,j\neq lignin,l,N,P} = H_{Si,j\neq lignin,l,C}\, S_{i,l,N,P}/S_{i,l,C}$			[A34]
$H_{Mi,n,j,l,C} = D_{Mi,n,j,l,C}\, \boldsymbol{F_h}$	decomposition products of microbes added to humus depending on clay		[A35]
$H_{Mi,n,j,l,N,P} = H_{Mi,n,j,l,C} M_{i,n,j,l,N,P}/M_{i,n,j,l,C}$			[A36]

Definition of Variables in Appendix A

Variable	Definition	Unit	Equation	Value	Reference
		subscripts			
i	substrate-microbe complex: coarse woody litter, fine non-woody litter, POC, humus				
j	kinetic component: labile, resistant, active				
l	soil or litter layer				
n	microbial functional type: heterotrophic (bacteria, fungi), autotrophic (nitrifiers, methanotrophs), diazotrophic, obligate aerobe, facultative anaerobes (denitrifiers), obligate anaerobes (methanogens)				
		variables			
A	microbial surface area	$m^2\ m^{-2}$	[A26]		
a	total substrate + residue C = ($[S_{i,j,C}]$ +$[Z_{i,j,C}]$)	g C Mg^{-1}	[A8]		
$\boldsymbol{B}$	parameter such that f_{tg} = 1.0 at T_l = 298.15 K		[A6]	26.230	
$\boldsymbol{b}$	Freundlich exponent for sorption isotherm		[A8]	0.85	Grant et al. (1993a,b)
$\boldsymbol{\beta}$	specific colonization rate of uncolonized substrate	-	[A4]	5.0	Grant et al. (2010)
$C_{N,Pi,n,a,l}$	ratio of $M_{i,n,a,N,P}$ to $M_{i,n,a,C}$	g N or P g C^{-1}	[A12]		
$\boldsymbol{C}_{\mathbf{N,P}j}$	maximum ratio of $M_{i,n,j,N,P}$ to $M_{i,n,j,C}$ maintained by $M_{i,n,j,C}$	g N or P g C^{-1}	[A12,A26,A27]	0.22 and 0.13 (N), 0.022 and 0.013 (P) for j = labile and resistant, respectively	Grant et al. (1993a,b)

$\boldsymbol{D}_{Mi,j}$	specific decomposition rate of $M_{i,n,j}$ at 30°C	g C g C^{-1} h^{-1}	[A23,A24]	0.0125 and 0.00035 for j = labile and resistant, respectively	Grant et al. (1993a,b)
$D_{Mi,n,j,l,\mathrm{C}}$	decomposition rate of $M_{i,n,j,l,\mathrm{C}}$	g C m^{-2} h^{-1}	[A23,A25,A35]		
$D_{Mi,n,j,l,\mathrm{N,P}}$	decomposition rate of $M_{i,n,j,l,\mathrm{N,P}}$	g N or P m^{-2} h^{-1}	[A24,A29]		
$D_{\mathrm{sO2}l}$	aqueous dispersivity–diffusivity of O_2 during microbial uptake in soil	m^2 h^{-1}	[A17]		
$D_{Si,j,l,\mathrm{C}}$	decomposition rate of $S_{i,j,l,\mathrm{C}}$ by $\Sigma_n M_{i,n,a,l}$ producing Q in [A13]	g C m^{-2} h^{-1}	[A1,A7a,A31]		
$\boldsymbol{D}_{Sj,\mathrm{C}}$	specific decomposition rate of $S_{i,j,l,\mathrm{C}}$ by $\Sigma_n M_{i,n,a,l}$ at 25°C and saturating[$S_{i,l,\mathrm{C}}$]	g C g C^{-1} h^{-1}	[A3]	1.0, 1.0, 0.15, and 0.025 for j = protein, carbohydrate, cellulose, and lignin	Grant et al. (1993a,b)
$D_{Si,j,\,l,\mathrm{N,P}}$	decomposition rate of $S_{i,j,l,\mathrm{N,P}}$ by $\Sigma_n M_{i,n,a,l}$	g N or P m^{-2} h^{-1}	[A7a, A32]		
$D_{Zi,j,l,\mathrm{C}}$	decomposition rate of $Z_{i,j,l,\mathrm{C}}$ by $\Sigma_n M_{i,n,a,l}$ producing Q in [A13]	g C m^{-2} h^{-1}	[A2,A7b]		
$D_{Zi,j,\mathrm{N,P}}$	decomposition rate of $Z_{i,j,l,\mathrm{N,P}}$ by $\Sigma_n M_{i,n,a,l}$	g N or P m^{-2} h^{-1}	[A7b]		
$\boldsymbol{D}_{Zj,\mathrm{C}}$	specific decomposition rate of $Z_{i,j,l,\mathrm{C}}$ by $\Sigma_n M_{i,n,a,l}$ at 25°C and saturating[$Z_{i,l,\mathrm{C}}$]	g C g C^{-1} h^{-1}	[A5]	0.25 and 0.05 for j = labile and resistant biomass	Grant et al. (1993a,b)
$D'_{Si,j,\,l,\mathrm{C}}$	specific decomposition rate of $S_{i,j,l,\mathrm{C}}$ by $\Sigma_n M_{i,n,a,l}$ at 25°C	g C g C^{-1} h^{-1}	[A1,A3]		
$D'_{Zi,j,l,\mathrm{C}}$	specific decomposition rate of $Z_{i,j,l,\mathrm{C}}$ by $\Sigma_n M_{i,n,a,l}$ at 25°C	g C g C^{-1} h^{-1}	[A2,A5]		
$\boldsymbol{\Delta G}$	energy yield of C oxidation and O_2 reduction	kJ g C^{-1}	[A21]	37.5	
$\boldsymbol{E}_{\mathbf{m}}$	energy requirement for growth of $M_{i,n,a,l}$	kJ g C^{-1}	[A21]	25	

$\boldsymbol{E_{\Phi}}$	energy requirement for non-symbiotic N_2 fixation by heterotrophic diazotrophs ($n = f$)	g C g N^{-1}	[A28]	5	Waring and Running (1998)
$\boldsymbol{F_h}$	fraction of products from microbial decomposition that are humified (function of clay content)		[A35]	0.167 + 0.167*clay	
$\boldsymbol{F_l}$	fraction of microbial growth allocated to labile component $M_{i,n,l}$		[A25,A29,A30]	0.55	Grant et al. (1993a,b)
$\boldsymbol{F_r}$	fraction of microbial growth allocated to resistant component $M_{i,n,r}$		[A25,A29,A30]	0.45	Grant et al. (1993a,b)
F_s	equilibrium ratio between $Q_{i,l,C}$ and $H_{i,l,C}$		[A8]		
$f_{di,n,l\mathrm{N,P}}$	fraction of N or P released with $D_{Mi,n,j,l,C}$ during decomposition	dimensionless	[A24]	0.33 $U_{NH4} > 0$ 1.00 $U_{NH4} < 0$ 0.33 $U_{PO4} > 0$ 1.00 $U_{PO4} < 0$	
f_{tgl}	temperature function for microbial growth respiration	dimensionless	[A1,A2,A6,A13, A23,A24]		
f_{tml}	temperature function for maintenance respiration	dimensionless	[A18,A19]		
$f_{\psi gl}$	soil water potential function for microbial, root or mycorrhizal growth respiration	dimensionless	[A13,A15]		Pirt (1975)
$\Phi_{i,n=f,j,l}$	non-symbiotic N_2 fixation by heterotrophic diazotrophs ($n = f$)	g N m^{-2} h^{-1}	[A27,A28,A29]		
$[H_2PO_4^-]$	concentration of $H_2PO_4^-$ in soil solution	g P m^{-3}	[A26]		
$\boldsymbol{H_a}$	energy of activation	J mol^{-1}	[A6,C10]	65 x 10^3	Addiscott (1983)
$\boldsymbol{H_{dh}}$	energy of high temperature deactivation	J mol^{-1}	[A6,C10]	225 x 10^3	
$\boldsymbol{H_{dl}}$	energy of low temperature deactivation	J mol^{-1}	[A6,C10]	198 x 10^3	
$H_{Mi,n,j,l,C}$	transfer of microbial C decomposition products to humus	g C m m^{-2} h^{-1}	[A35,A36]		
$H_{Mi,n,j,l,\mathrm{N,P}}$	transfer of microbial N or P decomposition products to humus	g N or P m^{-2} h^{-1}	[A36]		
$H_{Si,j,l,C}$	transfer of C hydrolysis products to particulate OM	g C m^{-2} h^{-1}	[A31,A32,A33, A34]		

$H_{Si,j,l,\mathrm{N,P}}$	transfer of N or P hydrolysis products to particulate OM	g N or P m^{-2} h^{-1}	[A32,A34]		
$\boldsymbol{K_{iS}}$	inhibition constant for microbial colonization of substrate	-	[A4]	0.5	Grant et al. (2010)
$\boldsymbol{K_{NH_4}}$	M-M constant for NH_4^+ uptake at microbial surfaces	g N m^{-3}	[A26]	0.40	
$\boldsymbol{K_{NO_3}}$	M-M constant for NO_3^- uptake at microbial surfaces	g N m^{-3}	[A26]	0.35	
$\boldsymbol{K_{PO_4}}$	M-M constant for $H_2PO_4^-$ uptake at microbial surfaces	g P m^{-3}	[A26]	0.125	
$\boldsymbol{K_{iD}}$	inhibition constant for $[M_{i,n,a}]$ on $S_{i,\mathrm{C}}$, $Z_{i,\mathrm{C}}$	g C m^{-3}	[A3,A5]	25	Grant et al. (1993a,b); Lizama and Suzuki (1990)
$\boldsymbol{K_{mD}}$	Michaelis–Menten constant for $D_{Si,j,\mathrm{C}}$	g C Mg^{-1}	[A3,A5]	75	
$\boldsymbol{K_{mQ_C}}$	Michaelis–Menten constant for $R'_{\mathrm{hi},n}$ on $[Q_{i,\mathrm{C}}]$	g C m^{-3}	[A13]	36	
$\boldsymbol{K_{O_2}}$	Michaelis–Menten constant for reduction of O_{2s} by microbes, roots and mycorrhizae	g O_2 m^{-3}	[A17]	0.064	Griffin (1972)
$\boldsymbol{k_{ts}}$	equilibrium rate constant for sorption	h^{-1}	[A8]	0.01	Grant et al. (1993a,b)
$\boldsymbol{L_{hj}}$	ratio of nonlignin to lignin components in humified hydrolysis products		[A33]	0.10, 0.05, and 0.05 for j = protein, carbohydrate, and cellulose, respectively	Shulten and Schnitzer (1997)
$\boldsymbol{M}$	molecular mass of water	g mol^{-1}	[A15]	18	
$M_{i,n,j,l,\mathrm{C}}$	microbial C	g C m^{-2}	[A1,A2,A13,A17 A23,A25,A26, A30,A36]		
$M_{i,n,j,l,\mathrm{N}}$	microbial N	g N m^{-2}	[A18,A27,A29]		
$M_{i,n,j,l,\mathrm{P}}$	microbial P	g P m^{-2}	[A24,A29,A26, A36]		
$M_{i,n,a,l,\mathrm{C}}$	active microbial C from heterotrophic population n associated with $(S_{i,j,l,\mathrm{C}} + Z_{i,j,l,\mathrm{C}})$	g C m^{-2}	[A1,A2,A13,A17, A30]		

$[M_{i,n,a,l,\mathrm{C}}]$	concentration of $M_{i,n,a}$ in soil water = $M_{i,n,a,l,\mathrm{C}}/\theta_l$	g C m^{-3}	[A3, A5]	
$[\mathrm{NH_4^+}_{i,n,j,l}]$	concentration of NH_4^+ at microbial surfaces	g N m^{-3}	[A26]	
$[\mathbf{NH_4^+}_{\mathbf{mn}}]$	concentration of NH_4^+ at microbial surfaces below which $U_{\mathrm{NH_4}} = 0$	g N m^{-3}	[A26]	0.0125
$[\mathrm{NO_3^-}_{i,n,j,l}]$	concentration of NH_4^+ at microbial surfaces	g N m^{-3}	[A26]	
$[\mathbf{NO_3^-}_{\mathbf{mn}}]$	concentration of NO_3^- at microbial surfaces below which $U_{\mathrm{NO_3}} = 0$	g N m^{-3}	[A26]	0.03
$[\mathrm{H_2PO_4^-}_{i,n,j,l}]$	concentration of $H_2PO_4^-$ at microbial surfaces	g N m^{-3}	[A26]	
$[\mathbf{H_2PO_4^-}_{\mathbf{mn}}]$	concentration of $H_2PO_4^-$ at microbial surfaces below which $U_{\mathrm{PO_4}} = 0$	g N m^{-3}	[A26]	0.002
$[\mathrm{O}_{2\mathrm{m}i,n,l}]$	O_2 concentration at heterotrophic microsites	g O_2 m^{-3}	[A17]	
$[\mathrm{O}_{2\mathrm{s}l}]$	O_2 concentration in soil solution	g O_2 m^{-3}	[A17]	
$Q_{i,l,\mathrm{C}}$	*DOC* from products of $D_{Si,j,l,\mathrm{C}}$ [A3] and $D_{Zi,j,l,\mathrm{C}}$) [A5]	g C m^{-2}	[A8,A13,A22]	
$[Q_{i,l,\mathrm{C}}]$	solution concentration of $Q_{i,l,\mathrm{C}}$	g C Mg^{-1}	[A8,A13]	
$Q_{i,l,\mathrm{N,P}}$	*DON* and DOP from products of ($D_{Si,j,l,\mathrm{N,P}} + D_{Zi,j,l,\mathrm{N,P}}$)	g N or P m^{-2}	[A9,A22]	
$\boldsymbol{R}$	gas constant	J mol^{-1} K^{-1}	[A6,A15,C10]	8.3143
$R_{\Phi i,n=f,j,l}$	respiration for non-symbiotic N_2 fixation by heterotrophic diazotrophs ($n = f$)	g C m^{-2} h^{-1}	[A28]	
$R_{\mathrm{g}i,n,l}$	growth respiration of $M_{i,n,a,l}$ on $Q_{i,l,\mathrm{C}}$ under nonlimiting O_2 and nutrients	g C g C^{-1} h^{-1}	[A20]	
R_{h}	total heterotrophic respiration of all $M_{i,n,a,l}$ under ambient DOC, O_2, nutrients, θ and temperature	g C m^{-2} h^{-1}	[A11]	
$R_{\mathrm{h}i,n,l}$	heterotrophic respiration of $M_{i,n,a,l}$ under ambient DOC, O_2, nutrients, θ and temperature	g C m^{-2} h^{-1}	[A4,A11,A14,A20, A21,A25]	
$\boldsymbol{R}_{\mathrm{h}i,n,l}$	specific heterotrophic respiration of $M_{i,n,a,l}$ under nonlimiting O_2, DOC, θ and 25°C	g C g C^{-1} h^{-1}	[A12,A13]	

$\boldsymbol{R}_{\mathrm{h}}'_{n}$	specific heterotrophic respiration of $M_{i,n,a,l}$ under nonlimiting DOC, O_2, nutrients, θ and 25°C	g C g C^{-1} h^{-1}	[A12]	0.125	Shields et al. (1973)
$R_{\mathrm{h}}'_{i,n,l}$	heterotrophic respiration of $M_{i,n,a,l}$ under nonlimiting O_2 and ambient DOC, nutrients, θ and temperature	g C m^{-2} h^{-1}	[A13,A14,A16]		
$\boldsymbol{R}_{\mathrm{m}}$	specific maintenance respiration at 25°C	g C g N^{-1} h^{-1}	[A18]	0.0115	Barnes et al. (1998)
$R_{\mathrm{m}i,n,j,l}$	maintenance respiration by $M_{i,n,j,l}$	g C m^{-2} h^{-1}	[A18,A20,A21,A25]		
$r_{\mathrm{w}l}$	radius of r_{m} + water film at current water content	m	[A17]		
$\boldsymbol{r}_{\mathbf{m}}$	radius of heterotrophic microsite	m	[A17]	2.5×10^{-6}	
$r_{\mathrm{w}l}$	thickness of water films	m	[A17]		
$\boldsymbol{S}$	change in entropy	J mol^{-1} K^{-1}	[A6,C10]	710	Sharpe and DeMichelle (1977)
$[S_{i,j,l,\mathrm{C}}]$	concentration of $S_{i,j,l,\mathrm{C}}$ in soil	g C Mg^{-1}	[A3]		
$S_{i,j,l,\mathrm{C}}$	mass of colonized solid or sorbed organic C in soil	g C m^{-2}	[A4,A7a,A33]		
$\boldsymbol{S'_{i,j,l,C}}$	mass of uncolonized solid or sorbed organic C in soil	g C m^{-2}	[A4]		
$S_{i,j,l,\mathrm{N,P}}$	mass of solid or sorbed organic N or P in soil	g N or P m^{-2}	[A7a,A33]		
T_{sl}	soil temperature	K	[A6,A15.A19]		
$U_{i,n,l\mathrm{C}}$	uptake of $Q_{i,l,\mathrm{C}}$ by $\Sigma_n M_{i,n,a,l}$ under limiting nutrient availability	g C m^{-2} h^{-1}	[A4,A21,A22,A25]		
$U_{i,n,\mathrm{N,P}}$	uptake of $Q_{i,l,\mathrm{N,P}}$ by $\Sigma_n M_{i,n,a,l}$ under limiting nutrient availability	g N or P m^{-2} h^{-1}	[A22,A29]		
$U_{\mathrm{NH4}i,n,j,l}$	NH_4^+ uptake by microbes	g N m^{-2} h^{-1}	[A26, A27,A29]		
$\boldsymbol{U'_{\mathrm{NH_4}}}$	maximum $U_{\mathrm{NH_4}}$ at 25 °C and non-limiting NH_4^+	g N m^{-2} h^{-1}	[A26]	5.0×10^{-3}	
$U_{\mathrm{NO3}i,n,j,l}$	NO_3^- uptake by microbes	g N m^{-2} h^{-1}	[A26,A27,A29]		

$\boldsymbol{U'_{NO_3}}$	maximum U_{NO_3} at 25 ^{o}C and non-limiting NO_3^-	g N m^{-2} h^{-1}	[A26]	5.0 x 10^{-3}
$U_{O2i,n}$	O_2 uptake by $M_{i,n,a,l}$ under ambient O_2	g m^{-2} h^{-1}	[A14,A17]	
$U'_{O2i,n}$	O_2 uptake by $M_{i,n,a,l}$ under nonlimiting O_2	g m^{-2} h^{-1}	[A14,A16,A17]	
$U_{PO4i,n,j,l}$	$H_2PO_4^-$ uptake by microbes	g N m^{-2} h^{-1}	[A26,A27,A29]	
$\boldsymbol{U'_{PO_4}}$	maximum U_{PO_4} at 25 ^{o}C and non-limiting $H_2PO_4^-$	g N m^{-2} h^{-1}	[A26]	5.0 x 10^{-3}
$X_{i,l,C}$	adsorbed C hydrolysis products	g C Mg^{-1}	[A8,A10]	
$X_{i,l,N,P}$	adsorbed N or P hydrolysis products	g P Mg^{-1}	[A10]	
$\boldsymbol{y}$	selected to give a Q_{10} for f_{tm} of 2.25		[A19]	0.081
ψ_s	soil or residue water potential	MPa	[A15]	
$Y_{i,l,C}$	sorption of C hydrolysis products	g C m^{-2} h^{-1}	[A8,A9,A10]	
$Y_{i,l,N,P}$	sorption of N or P hydrolysis products	g P m^{-2} h^{-1}	[A9,A10]	
$[Z_{i,j,l,C}]$	concentration of $Z_{i,j,l,C}$ in soil	g C Mg^{-1}	[A5]	
$Z_{i,j,l,C}$	mass of microbial residue C in soil	g C m^{-2}	[A7b]	
$Z_{i,j,l,N,P}$	mass of microbial residue P in soil	g P m^{-2}	[A7b]	

Appendix B: Soil-Plant Water Relations

Canopy Transpiration

$\boldsymbol{L}E_{ci} = L\,(e_a - e_{ci(T_{ci},\psi_{ci})})/r_{ai}$	*LE* from canopy evaporation	[B1a]
$\boldsymbol{L}E_{ci} = L\,(e_a - e_{ci(T_{ci},\psi_{ci})})/(r_{ai} + r_{ci})$ - $\boldsymbol{L}E_{ci}$ from [B1a]	*LE* from canopy transpiration	[B1b]
$H_{ci} = \rho C_p(T_a - T_{ci})/r_{ai}$	*H* from canopy energy balance	[B1c]
$r_{cmini} = 0.64\,(C_b - \boldsymbol{C_i'}_{\boldsymbol{i}})/\,V_c'_i$	r_c driven by rates of carboxylation	[B2a]
$r_{ci} = r_{cmini} + (\boldsymbol{r_{cmaxi}} - r_{cmini})\,e^{(-\boldsymbol{\beta}\,\psi_{ti})}$	*vs*. diffusion r_c constrained by water status	[B2b]
$r_{ai} = \{(\ln((z_u - z_{di})/z_{ri})^2/(\boldsymbol{K}^2 u_a)\}/(1 - 10\,Ri)$	r_a driven by windspeed, surface	[B3a]
$Ri = \{g\,(z_u - z_{ri})/(u_a^2\,T_a)\}\,(T_a - T_c)$	r_a adjusted for stability *vs*. buoyancy	[B3b]
$\psi_{ti} = \psi_{ci} - \psi_{\pi i}$		[B4]

Root and Mycorrhizal Water Uptake

$U_{wi} = \Sigma_l\,\Sigma_r\,U_{wi,r,l}$		[B5]
$U_{wi,r,l} = (\psi_c'_i - \psi_s'_l)/(\Omega_{si,r,l} + \Omega_{ri,r,l} + \Sigma_x\,\Omega_{ai,r,l,x})$	U_w along hydraulic gradient	[B6]
$\psi_c'_i = \psi_{ci} + 0.01\,z_{bi}$		[B7]
$\psi_s'_l = \psi_{sl} - 0.01\,z_l$		[B8]
$\Omega_{si,r,l} = \ln\{(d_{i,r,l}/r_{i,r,l})/(2\pi\,L_{i,r,l}\,\kappa_{ri,r,l})\}\;\theta_{wl}/\theta_{pl}$		[B9]
$\Omega_{ri,r,l} = \boldsymbol{\Omega'}_{\boldsymbol{ri,r}}/L_{i,r,l}$		[B10]
$\Omega_{ai,r,l,x=1} = \boldsymbol{\Omega'}_{\boldsymbol{ai,r}}\,z_l/\{n_{i,r,l,1}\,(r_{i,r,l,1}/\boldsymbol{r'}_{i,r})^4\} + \boldsymbol{\gamma\Omega'}_{\boldsymbol{ai,r}}\,z_{bi}/\{n_{i,r,l,1}\,(r_{bi}/r_b'_i)^4\}\Sigma_{i,r,l}\,(M_{i,r,l})/M_{i,r,l}$		[B11]
$\Omega_{ai,r,l,x=2} = \boldsymbol{\Omega_{ai,r}}\,(L_{i,r,l,2}/n_{i,r,l,2})/\{n_{i,r,l,2}\,(r_{i,r,l,2}/r'_{i,r})^4\}$		[B12]
$\delta L_{i,r,l,1}/\delta t = \delta M_{i,r,l,1}/\delta t\;\nu_r/\{\rho_r\,(1 - \theta_{pi,r})\,(\pi\,r_{i,r,l,1}^2)\}$		[B13]

Canopy Water Potential

$(e_a - e_{i(T_{ci})})/(r_{ai} + r_{ci})$ [B1] $= \Sigma_l \Sigma_r(\psi_c'_i - \psi_s'_l)/(\Omega_{si,r,l} + \Omega_{ri,r,l} + \Sigma_x \Omega_{ai,r,l,x}) + X_{ci}\delta\psi_{ci}/\delta t$ — ψ_c solved when transpiration from [B1-B4] (LHS) equals uptake from [B5-B13] + change in storage (RHS) [B14]

Definition of Variables in Appendix B

Variable	Definition	Unit	Equation	Value	Reference
	subscripts				
i	plant species or functional type: coniferous, deciduous, annual, perennial, C_3, C_4, monocot, dicot etc.				
j	branch or tiller				
k	node				
l	soil or canopy layer				
m	leaf azimuth				
n	leaf inclination				
o	leaf exposure (sunlit *vs*. shaded)				
r	root or mycorrhizae				
	variables				
$\boldsymbol{\beta}$	stomatal resistance shape parameter	MPa^{-1}	[B2b,C4,C9]	-5.0	Grant and Flanagan (2007)
C_b	$[CO_2]$ in canopy air	$\mu mol\ mol^{-1}$	[B2,C2,C5]		
$\boldsymbol{C_i'}_i$	$[CO_2]$ in canopy leaves at $\psi_{c_i} = 0$ MPa	$\mu mol\ mol^{-1}$	[B2]	0.70 C_b	Larcher (2001)

$d_{i,r,l}$	half distance between adjacent roots	m	[B9]		
E_{ci}	canopy transpiration	$m^3\ m^{-2}\ h^{-1}$	[B14]		
e_a	atmospheric vapor density at T_a and ambient humidity	$g\ m^{-3}$	[B1]		
$e_{ci(T_{ci},\psi_{ci})}$	canopy vapor density at T_{ci} and ψ_{ci}	$g\ m^{-3}$	[B1]		
K	von Karman's constant		[B3a]	0.41	
$\kappa_{ri,r,l}$	hydraulic conductivity between soil and root surface	$m^2\ MPa^{-1}\ h^{-1}$	[B9]		
$\boldsymbol{\gamma}$	scaling factor for bole axial resistance from primary root axial resistance	-	[B11]	1.6×10^4	Grant et al. (2007)
$\boldsymbol{L}$	latent heat of evaporation	$J\ g^{-1}$	[B1]	2460	
$\boldsymbol{L}E_i$	latent heat flux between canopy and atmosphere	$W\ m^{-2}$	[B1]		
$L_{i,r,l}$	length of roots or mycorrhizae	$m\ m^{-2}$	[B9,B10,B12,B13]		
$M_{i,r,l}$	mass of roots or mycorrhizae	$g\ m^{-2}$	[B11,B13]		
$n_{i,r,l,x}$	number of primary (x = 1) or secondary (x = 2) axes	m^{-2}	[B11,B12]		
$\boldsymbol{\Omega'_{ai,r}}$	axial resistivity to water transport along root or mycorrhizal axes	$MPa\ h\ m^{-4}$	[B11,B12]	4.0×10^9 deciduous 1.0×10^{10} coniferous	Larcher (2001)
$\Omega_{ai,r,l,x}$	axial resistance to water transport along axes of primary (x = 1) or secondary (x = 2) roots or mycorrhizae	$MPa\ h\ m^{-1}$	[B6,B11,B12]		
$\boldsymbol{\Omega'_{ri,r}}$	radial resistivity to water transport from surface to axis of roots or mycorrhizae	$MPa\ h\ m^{-2}$	[B10]	1.0×10^4	Doussan et al. (1998)
$\Omega_{ri,r,l}$	radial resistance to water transport from surface to axis of roots or mycorrhizae	$MPa\ h\ m^{-1}$	[B6,B10]		
$\Omega_{si,r,l}$	radial resistance to water transport from soil to surface of roots or mycorrhizae	$MPa\ h\ m^{-1}$	[B6,B9]		
θ_{wl}	soil water content	$m^3\ m^{-3}$	[B9]		

θ_{pl}	soil porosity	$m^3\ m^{-3}$	[B9]		
$\theta_{P_{i,r}}$	root porosity	$m^3\ m^{-3}$	[B13]		
Ri	Richarson number		[B3a,B3b]		van Bavel and Hillel (1976)
r_{ai}	aerodynamic resistance to vapor flux from canopy	$s\ m^{-1}$	[B1,B3a]		
r_{bi}	radius of bole at ambient ψ_{c_i}	m	[B11]		
$r_b'_i$	radius of bole at ψ_{c_i} = 0 MPa	m	[B11]		
r_{ci}	canopy stomatal resistance to vapor flux	$s\ m^{-1}$	[B1,B2b]		
$\boldsymbol{r_{cmaxi}}$	canopy cuticular resistance to vapor flux	$s\ m^{-1}$	[B2b]	5.0×10^3	Larcher (2001)
r_{cmini}	minimum r_{c_i} at ψ_{c_i} = 0 MPa	$s\ m^{-1}$	[B2,B2b]		
$r_{i,r,l,x}$	radius of primary (x=1) or secondary (x=2) roots or mycorrhizae at ambient $\psi_{r_{i,l,z}}$	m	[B9,B11,B12,B13]		
$\boldsymbol{r'_{i,r}}$	radius of secondary roots or mycorrhizae at $\psi_{r_{i,l,z}}$ = 0 MPa	m	[B11,B12]	2.0×10^{-4} tree 1.0×10^{-4} bush 0.05×10^{-4} mycorrhizae	
ρ_r	root specific density	$g\ C\ g\ FW^{-1}$	[B13]	0.05	Grant (1998)
T_a	air temperature	K	[B3b]		
T_c	canopy temperature	K	[B3b]		
U_{wi}	total water uptake from all rooted soil layers	$m^3\ m^{-2}\ h^{-1}$	[B5,B14]		
$U_{wi,r,l}$	water uptake by root and mycorrhizal surfaces in each soil layer	$m^3\ m^{-2}\ h^{-1}$	[B5,B6]		
u_a	wind speed measured at z_u	$m\ s^{-1}$	[B3a,B3b]		
$V_c'_i$	potential canopy CO_2 fixation rate at ψ_{c_i} = 0 MPa	$\mu mol\ m^{-2}\ s^{-1}$	[B2]		

ν_r	root specific volume	m^3 g FW^{-1}	[B13]	10^{-6}	Grant (1998)
X_{ci}	canopy capacitance	m^3 m^{-2} MPa^{-1}	[B14]		
ψ_{ci}	canopy water potential	MPa	[B4,B7,B14]		
$\psi_c'{}_i$	ψ_{ci} + canopy gravitational potential	MPa	[B6,B7]		
$\psi_{\pi i}$	canopy osmotic potential	MPa	[B4]		
ψ_{sl}	soil water potential	MPa	[B8]		
$\psi_s'{}_l$	ψ_{sl} + soil gravitational potential	MPa	[B6,B8]		
ψ_{ti}	canopy turgor potential	MPa	[B2b,B4]	1.25 at $\psi_c = 0$	
z_{bi}	length of bole from soil surface to top of canopy	m	[B7,B11]		
z_{di}	canopy zero-plane displacement height	m	[B3a]		Perrier (1982)
z_l	depth of soil layer below surface	m	[B8,B11]		
z_r	canopy surface roughness	m	[B3a,B3b]		Perrier (1982)
z_u	height of wind speed measurement	m	[B3a,B3b]		

Appendix C: Gross Primary Productivity and Autotrophic Respiration

C_3 Gross Primary Productivity

$GPP = \Sigma_{i,j,k,l,m,n,o} (V_{ci,j,k,l,m,n,o} = V_{gi,j,k,l,m,n,o}) A_{i,j,k,l,m,n,o}$	solve for $C_{ii,j,k,l,m,n,o}$ at which $V_{ci,j,k,l,m,n,o} = V_{gi,j,k,l,m,n,o}$	[C1]
$V_{gi,j,k,l,m,n,o} = (C_b - C_{ii,j,k,l,m,n,o})/r_{li,j,k,l,m,n,o}$	diffusion	[C2]
$V_{ci,j,k,l,m,n,o} = min\{V_{bi,j,k,l,m,n,o}, V_{ji,j,k,l,m,n,o}\}$	carboxylation	[C3]
$r_{li,j,k,l,m,n,o} = r_{lmini,j,k,l,m,n,o} + (r_{lmaxi} - r_{lmini,j,k,l,m,n,o})\, e^{(-\boldsymbol{\beta}\psi_{ti})}$	r_l is leaf-level equivalent of r_c	[C4]
$r_{lmini,j,k,l,m,n,o} = (C_b - \boldsymbol{C_i'}_i)/ V_c'_{i,j,k,l,m,n,o}$	minimum r_l is driven by carboxylation	[C5]
$V_{bi,j,k,l,m,n,o} = V_{bmaxi,j,k}(C_{ci,j,k,l,m,n,o} - \Gamma_{i,j,k})/(C_{ci,j,k,l,m,n,o}) + K_{c_i})\, f_{\psi\, i,j,k,l,m,n,o}\ \ f_{NPi}$	CO_2, water, temperature and nutrient constraints on V_b	[C6a]
$V_{bmax_{i,j,k}} = \boldsymbol{V_b'}_i \boldsymbol{F_{rubisco}}_i\, M_{i,j,k,prot}/A_{i,j,k}\ \ f_{tbi}$		[C6b]
$\Gamma_{i,j,k} = 0.5\, O_c\, V_{omax_{i,j,k}}\ \boldsymbol{K_c}_i\ /(V_{bmax_{i,j,k}}\ \boldsymbol{K_o}_i)$		[C6c]
$V_{omax_{i,j,k}} = \boldsymbol{V_o'}_i \boldsymbol{F_{rubisco}}_i\, M_{i,j,k,prot}/A_{i,j,k}\ \ f_{toi}$		[C6d]
$K_{c_i} = \boldsymbol{K_c}_i\ f_{tkci}\ (1 + O_c/ \boldsymbol{K_o}_i f_{tkoi})$		[C6e]
$V_{ji,j,k,l,m,n,o} = J_{i,j,k,l,m,n,o}\ Y_{i,j,k,l,m,n,o}\ f_{\psi\, i,j,k,l,m,n,o}\ \ f_{NPi}$		[C7]
$J_{i,j,k,l,m,n,o} = (\boldsymbol{\varepsilon}\, I_{i,l,m,n,o} + J_{maxi,j,k} - ((\boldsymbol{\varepsilon}\, I_{i,l,m,n,o} + J_{maxi,j,k})^2 - 4\boldsymbol{\alpha\varepsilon}\, I_{i,l,m,n,o}\, J_{maxi,j,k})^{0.5})/(2\boldsymbol{\alpha})$	water, temperature and nutrient constraints on V_j	[C8a]
$J_{maxi,j,k} = \boldsymbol{V_j'}_i \boldsymbol{F_{chlorophyll}}_i\, M_{i,j,k,prot}/A_{i,j,k}\, f_{tji}$		[C8b]
$f_{\psi\, i,j,k,l,m,n,o} = (r_{lmin_{i,j,k,l,m,n,o}} / r_{l_{i,j,k,l,m,n,o}})^{0.5}$	non-stomatal effect related to stomatal effect	[C9]

$f_{\mathrm{tb}i} = \exp[\boldsymbol{B}_{\mathbf{v}} - \boldsymbol{H}_{\mathbf{av}}/(\boldsymbol{R}T_{ci})]/\{1 + \exp[(\boldsymbol{H}_{\mathbf{dl}} - \boldsymbol{S}T_{ci})/(\boldsymbol{R}T_{ci})] + \exp[(\boldsymbol{S}T_{ci} - \boldsymbol{H}_{\mathbf{dh}})/(\boldsymbol{R}T_{ci})]\}$	Arrhenius functions for carboxylation, oxygenation and electron transport temperature sensitivity of $\boldsymbol{K}_{\mathbf{c}_i}$, $\boldsymbol{K}_{\mathbf{o}_i}$	[C10a]
$f_{\mathrm{to}i} = \exp[\boldsymbol{B}_{\mathbf{o}} - \boldsymbol{H}_{\mathbf{ao}}/(\boldsymbol{R}T_{ci})]/\{1 + \exp[(\boldsymbol{H}_{\mathbf{dl}} - \boldsymbol{S}T_{ci})/(\boldsymbol{R}T_{ci})] + \exp[(\boldsymbol{S}T_{ci} - \boldsymbol{H}_{\mathbf{dh}})/(\boldsymbol{R}T_{ci})]]$		[C10b]
$f_{\mathrm{tj}i} = \exp[\boldsymbol{B}_{\mathbf{j}} - \boldsymbol{H}_{\mathbf{aj}}/(\boldsymbol{R}T_{ci})]/\{1 + \exp[(\boldsymbol{H}_{\mathbf{dl}} - \boldsymbol{S}T_{ci})/(\boldsymbol{R}T_{ci})] + \exp[(\boldsymbol{S}T_{ci} - \boldsymbol{H}_{\mathbf{dh}})/(\boldsymbol{R}T_{ci})]\}$		[C10c]
$f_{\mathrm{tkc}i} = \exp[\boldsymbol{B}_{\mathbf{kc}} - \boldsymbol{H}_{\mathbf{akc}}/(\boldsymbol{R}T_{ci})]$		[C10d]
$f_{\mathrm{tko}i} = \exp[\boldsymbol{B}_{\mathbf{ko}} - \boldsymbol{H}_{\mathbf{ako}}/(\boldsymbol{R}T_{ci})]$		[C10e]
$f_{\mathrm{NP}i} = min\{\sigma_{\mathrm{N}i,j}/(\sigma_{\mathrm{N}i,j} + \sigma_{\mathrm{C}i,j}/\boldsymbol{K}_{\mathbf{I}\sigma_{\mathbf{N}}}),\ \sigma_{\mathrm{P}i,j}/(\sigma_{\mathrm{P}i,j} + \sigma_{\mathrm{C}i,j}/\boldsymbol{K}_{\mathbf{I}\sigma_{\mathbf{P}}})\}$	product inhibition of V_{b}, V_{j} determined by σ_{N} and σ_{P} *vs.* σ_{C} in shoots	[C11]
$\delta M_{i,j,k,prot}/\delta t = \delta M_{i,j,k}/\delta t \min\{2.5\,(\boldsymbol{N}'_{\mathbf{leaf}} + (\boldsymbol{N}_{\mathbf{leaf}} - \boldsymbol{N}'_{\mathbf{leaf}}),\ 25.0\,(\boldsymbol{P}'_{\mathbf{leaf}} + (\boldsymbol{P}_{\mathbf{leaf}} - \boldsymbol{P}'_{\mathbf{leaf}})\}\ f_{\mathrm{NP}i}$	leaf structural protein growth	[C12]

Autotrophic Respiration

$R_{\mathrm{a}} = \Sigma_i \Sigma_j\,(R_{\mathrm{c}i,j} + R_{\mathrm{s}i,j}) + \Sigma_i \Sigma_l \Sigma_z\,(R_{\mathrm{c}i,r,l} + R_{\mathrm{s}i,r,l}) + \boldsymbol{E}_{\mathbf{N,P}}\,(U_{\mathrm{NH4}i,r,l} + U_{\mathrm{NO3}i,r,l} + U_{\mathrm{PO4}i,r,l})$	total autotrophic respiration	[C13]
$R_{\mathrm{c}i,j} = \boldsymbol{R}_{\mathrm{c}}'\sigma_{\mathrm{C}i,j}\ f_{\mathrm{ta}i}$	O_2 constraint on root respiration from active uptake coupled with diffusion of O_2 from soil as for heterotrophic respiration in [A17], and from active uptake coupled with diffusion of O_2 from roots	[C14a]
$R_{\mathrm{c}i,r,l} = \boldsymbol{R}_{\mathrm{c}}'\sigma_{\mathrm{C}\,i,r,l}\ f_{\mathrm{ta}\,i,l}\ (U_{\mathrm{O2}i,r,l}/U'_{\mathrm{O2}i,r,l})$		[C14b]
$U_{\mathrm{O2}i,r,l} = U'_{\mathrm{O2}\,i,r,l}\ [\mathrm{O}_{2\mathrm{r}i,r,l}]/([\mathrm{O}_{2\mathrm{r}i,r,l}] + \boldsymbol{K}_{\mathbf{O_2}})$		[C14c]
$= U_{\mathrm{w}i,r,l}[\mathrm{O}_{2\mathrm{s}l}] + 2\pi L_{i,r,l}\,D_{\mathrm{sO2}}\,([\mathrm{O}_{2\mathrm{s}l}] - [\mathrm{O}_{2\mathrm{r}i,r,l}])\,\ln\{(r_{\mathrm{s}l} + r_{\mathrm{r}i,r,l})/r_{\mathrm{r}i,r,l}\} + 2\pi L_{i,r,l}\,D_{\mathrm{rO2}}\,([\mathrm{O}_{2\mathrm{q}i,r,l}] - [\mathrm{O}_{2\,\mathrm{r}i,r,l}])\,\ln(r_{\mathrm{q}i,r,l})/r_{\mathrm{r}i,r,l})$		[C14d]
$U'_{\mathrm{O2}\,i,r,l} = 2.67\,R_{\mathrm{a}}'_{i,r,l}$		[C14e]
$R_{\mathrm{s}i,j} = -\,min\{0.0,\ R_{\mathrm{c}i,j} - R_{\mathrm{m}i,j}\}$	remobilization when $R_{\mathrm{m}} > R_{\mathrm{c}}$	[C15]
$R_{\mathrm{m}i,j} = \Sigma_z\,(\mathrm{N}_{i,j,z}\,\boldsymbol{R}_{\mathbf{m}}'\ f_{\mathrm{tm}i})$	maintenance respiration	[C16]
$R_{\mathrm{g}i,j} = max\{0.0,\ min\{(R_{\mathrm{c}i,j} - R_{\mathrm{m}i,j})\ min\{1.0,\ max\{0.0,\ \psi_{\mathrm{t}i} - \psi_{\mathrm{t}}'\}\}$	growth when $R_{\mathrm{m}} < R_{\mathrm{c}}$	[C17]

Growth and Senescence

$l_{i,j,z,\mathrm{C}} = R_{\mathrm{si},j}\ \mathrm{C}_{i,j,z=l,non\text{-}remobilizable}/\mathrm{C}_{i,j,z=l,remobilizable}$	remobilization drives litterfall	[C18]
$l_{i,j,z,\mathrm{N,P}} = l_{i,j,z,\mathrm{C}}\ \mathbf{N,P_{protein}}\ \mathrm{N}_{i,j,z=l,non\text{-}remobilizable}/\mathrm{N}_{i,j,z=l,remobilizable}$		[C19]
$\delta M_{\mathrm{B}i,j}/\delta t = \Sigma_z\ [R_{\mathrm{g}i,j}\ (1 - \boldsymbol{Y}_{\mathbf{g}i,z})/\boldsymbol{Y}_{\mathbf{g}i,z}] - R_{\mathrm{s}i,j} - l_{i,j,\mathrm{C}}$	branch growth driven by R_{g}	[C20a]
$\delta M_{\mathrm{R}i,r,l}/\delta t = [R_{\mathrm{g}i,r,l}\ (1 - \boldsymbol{Y}_{\mathbf{g}i,r})/\boldsymbol{Y}_{\mathbf{g}i,r}] - R_{\mathrm{s}i,r,l} - l_{i,r,l,\mathrm{C}}$	root growth driven by R_{g}	[C20b]
$\delta A_{\mathrm{L}i,j,k,l}/\delta t = \boldsymbol{\chi}\ (M_{\mathrm{L}i,j,k,l}/y_i)^{-0.33}\ \delta M_{\mathrm{L}i,j,k,l}/\delta t\ \min\{1, \max\{0, \psi_{\mathrm{t}i} - \psi_{\mathrm{t}}'\}$	leaf expansion driven by leaf mass growth	[C21a]
$\delta L_{i,r,l,1}/\delta \mathrm{t} = (\delta M_{\mathrm{R}i,r,l,1}/\delta \mathrm{t})/y_i\ \nu_r/\{\boldsymbol{\rho}_r\ (1 - \boldsymbol{\theta}_{\mathbf{p}i,r})\ (\pi\ \mathrm{r}_{i,r,l,1}{}^2)\}$	root extension of primary and secondary axes driven by root mass growth	[C21b]
$\delta L_{i,r,l,2}/\delta \mathrm{t} = (\delta M_{\mathrm{R}i,r,l,2}/\delta \mathrm{t})\ \nu_r/\{\boldsymbol{\rho}_r\ (1 - \boldsymbol{\theta}_{\mathbf{p}i,r})\ (\pi\ \mathrm{r}_{i,r,l,2}{}^2)\}$		[C21c]
$f_{\mathrm{t}ai} = T_{\mathrm{c}i}\{\exp[\boldsymbol{B}_{\mathbf{v}} - \boldsymbol{H}_{\mathbf{av}}/(\boldsymbol{R}T_{\mathrm{c}i})]\}/\{1 + \exp[(\boldsymbol{H}_{\mathbf{dl}} - \boldsymbol{S}T_{\mathrm{c}i})/(\boldsymbol{R}T_{\mathrm{c}i})] + \exp[(\boldsymbol{S}T_{\mathrm{c}i} - \boldsymbol{H}_{\mathbf{dh}})/(\boldsymbol{R}T_{\mathrm{c}i})]\}$	Arrhenius function for R_{a}	[C22a]
$f_{\mathrm{tm}i} = e^{(0.0811*(T_{ci} - 298.15))}$	temperature function for R_{m}	[C22b]

Root and Mycorrhizal Nutrient Uptake

$U_{\mathrm{NH4}i,r,l} = \{U_{\mathrm{w}i,r,l}[\mathrm{NH_4}^+{}_l] + 2\pi L_{i,r,l} D_{\mathrm{eNH4}l}\ ([\mathrm{NH_4}^+{}_l] - [\mathrm{NH_4}^+{}_{i,r,l}])\ /\ \ln(d_{i,r,l}/r_{i,r,l})\}$	root N and P uptake from mass flow + diffusion coupled with active uptake of $\mathrm{NH_4}^+$, $\mathrm{NO_3}^-$ and $\mathrm{H_2PO_4}^-$ constrained by $\mathrm{O_2}$ uptake, as for microbial N and P uptake in [A26]	[C23a]
$= \boldsymbol{U'}_{\mathbf{NH_4}}\ (U_{\mathrm{O2}i,r,l}/U'_{\mathrm{O2}i,r,l})\ A_{i,r,l}\ ([\mathrm{NH_4}^+{}_{i,r,l}] - [\mathbf{NH_4}^+{}_{\mathbf{mn}}])/([\mathrm{NH_4}^+{}_{i,r,l}] - [\mathbf{NH_4}^+{}_{\mathbf{mn}}] + \boldsymbol{K}_{\mathbf{NH_4}})\ f_{\mathrm{t}il}\ f_{\mathrm{NP}i}$		[C23b]
$U_{\mathrm{NO3}i,r,l} = \{U_{\mathrm{w}i,r,l}\ [\mathrm{NO_3}^-{}_l] + 2\pi L_{i,r,l}\ D_{\mathrm{eNO3}l}\ ([\mathrm{NO_3}^-{}_l] - [\mathrm{NO_3}^-{}_{i,r,l}])\ /\ \ln(d_{i,r,l}/r_{i,r,l})\}$		[C23c]
$= \boldsymbol{U'}_{\mathbf{NO_3}}\ (U_{\mathrm{O2}i,r,l}/U'_{\mathrm{O2}i,r,l})\ A_{i,r,l}\ ([\mathrm{NO_3}^-{}_{i,r,l}] - [\mathbf{NO_3}^-{}_{\mathbf{mn}}])/([\mathrm{NO_3}^-{}_{i,r,l}] - [\mathbf{NO_3}^-{}_{\mathbf{mn}}] + \boldsymbol{K}_{\mathbf{NO_3}})\ f_{\mathrm{t}il}\ f_{\mathrm{NP}i}$		[C23d]
$U_{\mathrm{PO4}i,r,l} = \{U_{\mathrm{w}i,r,l}\ [\mathrm{H_2PO_4}^-{}_l] + 2\pi L_{i,r,l} D_{\mathrm{ePO4}l}\ ([\mathrm{H_2PO_4}^-{}_l] - [\mathrm{H_2PO_4}^-{}_{i,r,l}])\ /\ \ln(d_{i,r,l}/r_{i,r,l})\}$		[C23e]
$= \boldsymbol{U'}_{\mathbf{PO_4}}\ (U_{\mathrm{O2}i,r,l}/U'_{\mathrm{O2}i,r,l})\ A_{i,r,l}\ ([\mathrm{H_2PO_4}^-{}_{i,r,l}] - [\mathbf{H_2PO_4}^-{}_{\mathbf{mn}}])/([\mathrm{H_2PO_4}^-{}_{i,r,l}] - [\mathbf{H_2PO_4}^-{}_{\mathbf{mn}}] + \boldsymbol{K}_{\mathbf{PO_4}})\ f_{\mathrm{t}gl}\ f_{\mathrm{NP}i}$		[C23f]
$f_{\mathrm{NP}i} = min\{\sigma_{\mathrm{C}i,j}/(\sigma_{\mathrm{C}i,j} + \sigma_{\mathrm{N}i,j}/\boldsymbol{K}_{\mathbf{I\sigma_N}}),\ \sigma_{\mathrm{C}i,j}/(\sigma_{\mathrm{C}i,j} + \sigma_{\mathrm{P}i,j}/\boldsymbol{K}_{\mathbf{I\sigma_P}})\}$	product inhibition of U_{NH4}, U_{NO3} and U_{PO4} determined by σ_{N} and σ_{P} *vs.* σ_{C} in roots	[C23g]

C_4 Gross Primary Productivity

C_4 Mesophyll

$GPP = \Sigma_{i,j,k,l,m,n,o}\ (V_{\mathrm{g(m4)}i,j,k,l,m,n,o} = V_{\mathrm{c(m4)}i,j,k,l,m,n,o})$		[C24]

$V_{g(m4)i,j,k,l,m,n,o} = (C_b - C_{i(m4)i,j,k,l,m,n,o})/r_{lfi,j,k,l,m,n,o}$	gaseous diffusion	[C25]
$V_{c(m4)i,j,k,l,m,n,o} = min\{V_{b(m4)i,j,k,l,m,n,o}, V_{j(m4)i,j,k,l,m,n,o}\}$	mesophyll carboxylation	[C26]
$r_{lfi,j,k,l,m,n,o} = r_{lfmini,j,k,l,m,n,o} + (r_{lfmaxi} - r_{lfmini,j,k,l,m,n,o})\, e^{(-\beta\, \psi_{ti})}$		[C27]
$r_{lfmini,j,k,l,m,n,o} = (C_b - C_{i(m4)'i})/\, V_{c_0(m4)i,j,k,l,m,n,o}$		[C28]
$V_{b(m4)i,j,k,l,m,n,o} = V_{bmax(m4)i,j,k}(C_{c(m4)i,j,k,l,m,n,o} - \Gamma_{(m4)i,j,k})/(C_{c(m4)i,j,k,l,m,n,o}) + K_{c(m4)_i})$	CO_2-limited carboxylation	[C29]
$V_{j(m4)i,j,k,l,m,n,o} = J_{(m4)i,j,k,l,m,n,o}\, Y_{(m4)i,j,k,l,m,n,o}$	light-limited carboxylation	[C30]
$J_{(m4)i,j,k,l,m,n,o} = (\varepsilon\, I_{i,l,m,n,o} + J_{max(m4)i,j,k} - ((\varepsilon\, I_{i,l,m,n,o} + J_{max(m4)i,j,k})^2 - 4\alpha\varepsilon\, I_{i,l,m,n,o}\, J_{max(m4)i,j,k})^{0.5})/(2\alpha)$	irradiance response function	[C31]
$V_{bmax(m4)i,j,k} = V_{bmax(m4)}'\, [N_{pep(m4)i,j,k}]'\; N_{lfi,j,k}\; A_{lfi,j,k}\; f_{C(m4)i,j,k}\, f_{\psi i}\; f_{tvi}$	PEPc activity	[C32]
$J_{max(m4)i,j,k} = J_{max}'\, [N_{chl(m4)i,j,k}]'\; N_{lfi,j,k}\; A_{lfi,j,k}\; f_{C(m4)i,j,k}, f_{\psi i}\; f_{tvi}$	chlorophyll activity	[C33]
$f_{C(m4)i,j,k} = 1.0/(1.0 + [\chi_{C4(m4)i,j,k}]/K_{I\chi_{C4(m4)}})$	C_4 product inhibition	[C34]
$f_{\psi\, i,j,k,l,m,n,o} = (r_{lfmin_{i,j,k,l,m,n,o}} / r_{lf_{i,j,k,l,m,n,o}})^{0.5}$	non-stomatal water limitation	[C35]
$f_{tvi} = T_{ci}\{\exp[B - H_a/(RT_{ci})]\}/\{1 + \exp[(H_{dl} - ST_{ci})/(RT_{ci})] + \exp[(ST_{ci} - H_{dh})/(RT_{ci})]\}$	temperature limitation	[C36]

C_4 Mesophyll-Bundle Sheath Exchange

$V_{\chi C4(m4)i,j,k} = \kappa_{\chi C4(m4)}\, (\chi_{C4(m4)i,j,k}\, W_{lf(b4)i,j,k} - \chi_{C4(b4)i,j,k}\, W_{lf(m4)i,j,k}) / (W_{lf(b4)i,j,k} + W_{lf(m4)i,j,k})$	mesophyll-bundle sheath transfer	[C37]
$V_{\chi C4(b4)i,j,k} = \kappa_{\chi C4(b4)}\, \chi_{C4(b4)i,j,k}\, /(1.0 + C_{c(b4)i,j,k}\, /K_{I\chi_{C4(b4)}})$	bundle sheath decarboxylation	[C38]
$V_{\phi(b4)i,j,k} = \kappa_{Cc(b4)}\, (C_{c(b4)i,j,k} - C_{c(m4)i,j,k})\, (12 \times 10^{-9})\, W_{lf(b4)i,j,k}$	bundle sheath-mesophyll leakage	[C39]
$\delta\chi_{C4(m4)i,j,k}\, /\delta t = \Sigma_{l,m,n,o}\, V_{c(m4)i,j,k,l,m,n,o} - V_{\chi C4(m4)i,j,k}$	mesophyll carboxylation products	[C40]
$\delta\chi_{C4(b4)i,j,k}/\delta t = V_{\chi C4(m4)i,j,k} - V_{\chi C4(b4)i,j,k}$	bundle sheath carboxylation products	[C41]

$\delta C_{c(b4)i,j,k}/\delta t = V_{\chi C4(b4)i,j,k} - V_{\phi(b4)i,j,k} - \Sigma_{l,m,n,o} V_{c(b4)i,j,k,l,m,n,o}$	bundle sheath CO_2 concentration	[C42]

C_4 Bundle Sheath

$V_{c(b4)i,j,k,l,m,n,o} = min\{V_{b(b4)i,j,k}, V_{j(b4)i,j,k,l,m,n,o}\}$	bundle sheath carboxylation	[C43]
$V_{b(b4)i,j,k} = V_{bmax(b4)i,j,k}(C_{c(b4)i,j,k} - \Gamma_{(b4)i,j,k})/(C_{c(b4)i,j,k}) + K_{c(b4)_i})$	CO_2-limited carboxylation	[C44]
$V_{j(b4)i,j,k,l,m,n,o} = J_{(b4)i,j,k,l,m,n,o}\, Y_{(b4)i,j,k}$	light- limited carboxylation	[C45]
$J_{(b4)i,j,k,l,m,n,o} = (\varepsilon I_{i,l,m,n,o} + J_{max(b4)i,j,k} - ((\varepsilon I_{i,l,m,n,o} + J_{max(b4)i,j,k})^2 - 4\alpha\varepsilon I_{i,l,m,n,o} J_{max(b4)i,j,k})^{0.5})/(2\alpha)$	irradiance response function	[C46]
$V_{bmax(b4)i,j,k} = V_{bmax(b4)}' [N_{rub(b4)i,j,k}]' N_{lfi,j,k} A_{lfi,j,k} f_{C(c3)i,j,k} f_{\psi i} f_{tvi}$	RuBPc activity	[C47]
$J_{max(b4)i,j,k} = J_{max}' [N_{chl(b4)i,j,k}]' N_{lfi,j,k} A_{lfi,j,k} f_{C(c3)i,j,k} f_{\psi i} f_{tvi}$	chlorophyll activity	[C48]
$f_{C(c3)i,j,k} = \min\{[\nu_{lfi,j}]/([\nu_{lfi,j}] + [\chi_{c3(b4)i,j}]/K_{I\nu_{lf}}), [\pi_{lfi,j}]/([\pi_{lfi,j}] + [\chi_{c3(b4)i,j}]/K_{I\pi_{lf}})\}$	C_3 product inhibition	[C49]

Definition of Variables in Appendix C

Variable	Definition	Unit	Equation	Value	Reference
		subscripts			
i	species or functional type: evergreen, coniferous, deciduous, annual, perennial, C_3, C_4, monocot, dicot, legume etc.				
j	branch or tiller				
k	node				
l	soil or canopy layer				
m	leaf azimuth				
n	leaf inclination				
o	leaf exposure (sunlit *vs*. shaded)				
r	root or mycorrhizae				
z	organ including leaf, root, mycorrhizae				

		variables			
A	leaf, root or mycorrhizalsurface area	$m^2\ m^{-2}$	[C1,C6b,C6d,C8b, C21,C23,C32,C33 ,C47]		
$\boldsymbol{\beta}$	shape parameter for stomatal effects on CO_2 diffusion and non-stomatal effects on carboxylation	MPa^{-1}	[C4 C27,C35,]	-5.0	Grant and Flanagan (2007)
B	parameter such that f_t = 1.0 at T_c = 298.15 K		[C36]	17.533	
$\boldsymbol{B_j}$	parameter such that $f_{tj\boldsymbol{i}}$ = 1.0 at T_c = 298.15 K		[C10c]	17.363	
$\boldsymbol{B_{kc}}$	parameter such that $f_{tkc\boldsymbol{i}}$ = 1.0 at T_c = 298.15 K		[C10d]	22.187	
$\boldsymbol{B_{ko}}$	parameter such that $f_{tko\boldsymbol{i}}$ = 1.0 at T_c = 298.15 K		[C10e]	8.067	
$\boldsymbol{B_o}$	parameter such that $f_{to\boldsymbol{i}}$ = 1.0 at T_c = 298.15 K		[C10b]	24.221	
$\boldsymbol{B_v}$	parameter such that $f_{tv\boldsymbol{i}}$ = 1.0 at T_c = 298.15 K		[C10a, C22]	26.238	
C_b	$[CO_2]$ in canopy air	$\mu mol\ mol^{-1}$	[C2,C5 C25,C28]		
$C_{c(b4)}$	$[CO_2]$ in C_4 bundle sheath	μM	[C38,C39,C42,C44]		
$C_{c(m4)}$	$[CO_2]$ in C_4 mesophyll in equilibrium with $C_{ii,j,k,l,m,n,o}$	μM	[C29,C39]		
C_c	$[CO_2]$ in canopy chloroplasts in equilibrium with $C_{ii,j,k,l,m,n,o}$	μM	[C6]		
$C_{i(m4)}'$	$[CO_2]$ in C_4 mesophyll air when ψ_{ci} = 0	$\mu mol\ mol^{-1}$	[C28]	0.45 x C_b	
$C_{i(m4)}$	$[CO_2]$ in C_4 mesophyll air	$\mu mol\ mol^{-1}$	[C25]		
$C_{i,j,z=l}$	C content of leaf ($z = l$)	$g\ C\ m^{-2}$	[C18]		
$\boldsymbol{C_i'}$	$[CO_2]$ in canopy leaves when ψ_{ci} = 0	$\mu mol\ mol^{-1}$	[C5]	0.70 x C_b	Larcher (2001)

C_i	[CO_2] in canopy leaves	μmol mol^{-1}	[C2]		
$D_{e\ NH4l}$	effective dispersivity-diffusivity of NH_4^+ during root uptake	m^2 h^{-1}	[C23]		
$D_{e\ NO3l}$	effective dispersivity-diffusivity of NO_3^- during root uptake	m^2 h^{-1}	[C23]		
$D_{e\ PO4l}$	effective dispersivity-diffusivity of $H_2PO_4^-$ during root uptake	m^2 h^{-1}	[C23]		
D_{rO2}	aqueous diffusivity of O_2 from root aerenchyma to root or mycorrhizal surfaces	m^2 h^{-1}	[C14d]		
D_{sO2}	aqueous diffusivity of O_2 from soil to root or mycorrhizal surfaces	m^2 h^{-1}	[C14d]		
$d_{i,r,l}$	half distance between adjacent roots assumed equal to uptake path length	m	[C23]	$(\pi\ L_{s,z}\ /\Delta z)^{-1/2}$	Grant (1998)
$\boldsymbol{E_{N,P}}$	energy cost of nutrient uptake	g C g N^{-1} or P^{-1}	[C13]	2.15	Veen (1981)
$f_{C(c3)}$	C_3 product inhibition of RuBP carboxylation activity in C_4 bundle sheath or C_3 mesophyll	–	[C47,C48,C49]		
$f_{C(m4)}$	C_4 product inhibition of PEP carboxylation activity in C_4 mesophyll	–	[C32,C33,C34]		
$\boldsymbol{F_{chl}}$	fraction of leaf protein in chlorophyll	-	[C8b]	0.025	
f_{NPi}	N,P inhibition on carboxylation, leaf protein growth, root uptake	–	[C6a,C7,C11,C12, C23]		
$\boldsymbol{F_{rubisco}}$	fraction of leaf protein in rubisco	-	[C6b,d]	0.125	
f_{tai}	temperature effect on $R_{ai,j}$	–	[C14, C22]		
f_{tbi}	temperature effect on carboxylation	–	[C6b,C10a]		
f_{tgl}	temperature function for root or mycorrhizal growth respiration	dimensionless	[C23]		
f_{tji}	temperature effect on electron transport		[C8b,C10c]		

$f_{\mathrm{tkc}i}$	temperature effect on $\boldsymbol{K}_{\mathbf{c}_i}$		[C6e,C10d]		Bernacchi et al. (2001,2003)
$f_{\mathrm{tko}i}$	temperature effect on $\boldsymbol{K}_{\mathbf{o}_i}$		[C6e,C10e]		Bernacchi et al. (2001,2003)
$f_{\mathrm{tm}i}$	temperature effect on $R_{\mathrm{m}i,j}$	–	[C16, C22b]	$Q_{10} = 2.25$	
$f_{\mathrm{to}\boldsymbol{i}}$	temperature effect on oxygenation		[C6d,C10b]		
$f_{\mathrm{tv}\boldsymbol{i}}$	temperature effect on carboxylation	–	[C32,C33,C36,C47,C48]		
$f_{\psi\boldsymbol{i}}$	non-stomatal water effect on carboxylation	–	[C6a,C7,C9]		Medrano et al. (2002)
$f_{\psi\boldsymbol{i}}$	non-stomatal water effect on carboxylation	–	[C32,C33,C35C47,C48]		
H_{a}	energy of activation	J mol^{-1}	[C36]	57.5 x 10^3	
$\boldsymbol{H}_{\mathbf{aj}}$	energy of activation for electron transport	J mol^{-1}	[C10c]	43 x 10^3	Bernacchi et al. (2001,2003)
$\boldsymbol{H}_{\mathbf{akc}}$	parameter for temperature sensitivity of $\boldsymbol{K}_{\mathbf{c}_i}$	J mol^{-1}	[C10d]	55 x 10^3	Bernacchi et al. (2001,2003)
$\boldsymbol{H}_{\mathbf{ako}}$	parameter for temperature sensitivity of $\boldsymbol{K}_{\mathbf{o}_i}$	J mol^{-1}	[C10e]	20 x 10^3	Bernacchi et al. (2001,2003)
$\boldsymbol{H}_{\mathbf{ao}}$	energy of activation for oxygenation	J mol^{-1}	[C10b, C22]	60 x 10^3	Bernacchi et al. (2001,2003)
$\boldsymbol{H}_{\mathbf{av}}$	energy of activation for carboxylation	J mol^{-1}	[C10a, C22]	65 x 10^3	Bernacchi et al. (2001,2003)
$\boldsymbol{H}_{\mathbf{dh}}$	energy of high temperature deactivation	J mol^{-1}	[C10, C22]	222.5 x 10^3	
H_{dh}	energy of high temperature deactivation	J mol^{-1}	[C36]	220 x 10^3	
$\boldsymbol{H}_{\mathbf{dl}}$	energy of low temperature deactivation	J mol^{-1}	[C10, C22]	198.0 x 10^3	

H_{dl}	energy of low temperature deactivation	J mol^{-1}	[C36]	190 x 10^3	
I	irradiance	μmol m^{-2} s^{-1}	[C8a,]		
$J_{(b4)}$	electron transport rate in C_4 bundle sheath	μmol m^{-2} s^{-1}	[C45,C46]		
$J_{(m4)}$	electron transport rate in C_4 mesophyll	μmol m^{-2} s^{-1}	[C30,C31]		
J	electron transport rate in C_3 mesophyll	μmol m^{-2} s^{-1}	[C7,C8a]		
J_{max}'	specific electron transport rate at non-limiting I and 25°C when ψ_{ci} = 0 and nutrients are nonlimiting	μmol g^{-1} s^{-1}	[C33,C48]	400	
$J_{max(b4)}$	electron transport rate in C_4 bundle sheath at non-limiting I	μmol m^{-2} s^{-1}	[C46,C48]		
$J_{max(m4)}$	electron transport rate in C_4 mesophyll at non-limiting I	μmol m^{-2} s^{-1}	[C31,C33]		
J_{max}	electron transport rate at non-limiting I, ψ_{ci}, temperature and N,P	μmol m^{-2} s^{-1}	[C8a,C8b]		
$K_{c(b4)}$	Michaelis-Menten constant for carboxylation in C_4 bundle sheath	μM	[C44]	30.0 at 25°C and zero O_2	Lawlor (1993)
$K_{c(m4)}$	Michaelis-Menten constant for carboxylation in C_4 mesophyll	μM	[C29]	3.0 at 25°C	Lawlor (1993)
$\boldsymbol{K_c}$	Michaelis-Menten constant for carboxylation at zero O_2	μM	[C6c,C6e]	12.5 at 25 °C	Farquhar et al. (1980)
K_c	Michaelis-Menten constant for carboxylation at ambient O_2	μM	[C6e]		
$K_{I\chi_{C4(b4)}}$	constant for CO_2 product inhibition of C_4 decarboxylation in C_4 bundle sheath	μM	[C38]	1000.0	

$K_{I\chi_{C4(m4)}}$	constant for C_4 product inhibition of PEP carboxylation activity in C_4 mesophyll	μM	[C34]	5 x 10^6	
$K_{I\nu_{lf}}$	constant for C_3 product inhibition of RuBP carboxylation activity in C_4 bundle sheath or C_3 mesophyll caused by [$\nu_{lfi,j}$]	g C g N^{-1}	[C49]	100	
$K_{I\pi_{lf}}$	constant for C_3 product inhibition of RuBP carboxylation activity in C_4 bundle sheath or C_3 mesophyll caused by [$\pi_{lfi,j}$]	g C g P^{-1}	[C49]	1000	
$\boldsymbol{K_{I\sigma_N}}$	inhibition constant for $\sigma_{Ci,j}$ vs. σ_{Nj} in f_{NP} in shoots roots	g C g N^{-1} g N g C^{-1}	[C11] [C23]	100 (shoot) 0.1 (root)	Grant (1998)
$\boldsymbol{K_{I\sigma_P}}$	inhibition constant for $\sigma_{Ci,j}$ vs. $\sigma_{Pi,j}$ in f_{NP} in shoots roots	g C g P^{-1} g P g C^{-1}	[C11] [C23]	1000 (shoot) 0.01 (root)	Grant (1998)
$\boldsymbol{K_{NH_4}}$	M-M constant for NH_4^+ uptake at root or mycorrhizal surfaces	g N m^{-3}	[C23]	0.40	Barber and Silberbush, 1984
$\boldsymbol{K_{NO_3}}$	M-M constant for NO_3^- uptake at root or mycorrhizal surfaces	g N m^{-3}	[C23]	0.35	Barber and Silberbush, 1984
$\boldsymbol{K_{PO_4}}$	M-M constant for $H_2PO_4^-$ uptake root or mycorrhizal surfaces	g P m^{-3}	[C23]	0.125	Barber and Silberbush, 1984
$\boldsymbol{K_{O_2}}$	Michaelis-Menten constant for root or mycorrhizal O_2 uptake	g m^{-3}	[C14c]	0.064	Griffin (1972)
$\boldsymbol{K_{o_i}}$	inhibition constant for O_2 in carboxylation	μM	[C6c,C6e]	500 at 25 ^oC	Farquhar et al. (1980)
L	root length	m m^{-2}	[C14d,C21b,C23]		
l_C	C litterfall from leaf or root	g C m^{-2} h^{-1}	[C18,C19,C20]		
$l_{N,P}$	N or P litterfall from leaf or root	g C m^{-2} h^{-1}	[C19]		
M_B	branch C phytomass	g C m^{-2}	[C20]		

M_L	leaf C phytomass	g C m^{-2}	[C12,C21]		
M_R	root C phytomass	g C m^{-2}	[C20,C21]		
M_{iprot}	leaf protein phytomass calculated from leaf N, P contents	g N m^{-2}	[C6b,C6d,C8b,C12]		
N,P	N or P content of organ *z*	g N m^{-2}	[C16, C19]		
$\mathbf{N,P_{prot}}$	N or P content of protein remobilized from leaf or root	g N or P g C^{-1}	[C19]	0.4, 0.04	
$[NH_4^+{}_{i,r,l}]$	concentration of NH_4^+ at root or mycorrizal surfaces	g N m^{-3}	[C23]		
$[\mathbf{NH_4^+{}_{mn}}]$	concentration of NH_4^+ at root or mycorrizal surfaces below which $U_{NH_4} = 0$	g N m^{-3}	[C23]	0.0125	Barber and Silberbush, 1984
$[NO_3^-{}_{i,r,l}]$	concentration of NH_4^+ at root or mycorrizal surfaces	g N m^{-3}	[C23]		
$[\mathbf{NO_3^-{}_{mn}}]$	concentration of NO_3^- at root or mycorrizal surfaces below which $U_{NO_3} = 0$	g N m^{-3}	[C23]	0.03	Barber and Silberbush, 1984
$[H_2PO_4^-{}_{i,r,l}]$	concentration of $H_2PO_4^-$ root or mycorrizal surfaces	g N m^{-3}	[C23]		
$[\mathbf{H_2PO_4^-{}_{mn}}]$	concentration of $H_2PO_4^-$ at root or mycorrizal surfaces below which $U_{PO_4} = 0$	g N m^{-3}	[C23]	0.002	Barber and Silberbush, 1984
$\boldsymbol{N_{leaf}}$	maximum leaf structural N content	g N g C^{-1}	[C12]	0.10	
$\boldsymbol{N'_{leaf}}$	minimum leaf structural N content	g N g C^{-1}	[C12]	0.33 x $\boldsymbol{N_{leaf}}$	
N_{lf}	total leaf N	g N m^{-2} leaf	[C32,C33,C47,C48]		
$[N_{chl(b4)}]'$	ratio of chlorophyll N in C_4 bundle sheath to total leaf N	g N g N^{-1}	[C48]	0.05	
$[N_{chl(m4)}]'$	ratio of chlorophyll N in C_4 mesophyll to total leaf N	g N g N^{-1}	[C33]	0.05	
$[N_{pep(m4)}]'$	ratio of PEP carboxylase N in C_4 mesophyll to total leaf N	g N g N^{-1}	[C32]	0.025	

$[N_{rub(b4)}]'$	ratio of RuBP carboxylase N in C_4 bundle sheath to total leaf N	g N g N^{-1}	[C47]	0.025
O_{2q}	aqueous O_2 concentration in root or mycorrhizal aerenchyma	g m^{-3}	[C14c,d]	
O_{2r}	aqueous O_2 concentration at root or mycorrhizal surfaces	g m^{-3}	[C14c,d]	
O_{2s}	aqueous O_2 concentration in soil solution	g m^{-3}	[C14c,d]	
O_c	$[O_2]$ in canopy chloroplasts in equilibrium with $O_{2\ in}$ atm.	μM	[C6c,C6e]	
$\boldsymbol{P_{leaf}}$	maximum leaf structural P content	g P g C^{-1}	[C12]	0.10
$\boldsymbol{P'_{leaf}}$	minimum leaf structural P content	g P g C^{-1}	[C12]	0.33 x $\boldsymbol{P_{leaf}}$
$[\pi_{lf}]$	concentration of nonstructural root P uptake product in leaf	g P g C^{-1}	[C49]	
$\boldsymbol{\theta_P}$	root or mycorrhizal porosity	m^3 m^{-3}	[C21b]	0.1 – 0.5
$\boldsymbol{R}$	gas constant	J mol^{-1} K^{-1}	[C10, C22]	8.3143
R	gas constant	J mol^{-1} K^{-1}	[C36]	8.3143
R_a	total autotrophic respiration	g C m^{-2} h^{-1}	[C13]	
R_a'	R_a under nonlimiting O_2	g C m^{-2} h^{-1}	[C14]	
$\boldsymbol{R}_c'$	specific autotrophic respiration of $\sigma_{Ci,j}$ at T_{ci} = 25 °C	g C g C^{-1} h^{-1}	[C14]	0.015
R_c	autotrophic respiration of $\sigma_{Ci,j}$ or $\sigma_{Ci,r,l}$	g C m^{-2} h^{-1}	[C13,C14,C17, C15]	
R_g	growth respiration	g C m^{-2} h^{-1}	[C17,C20]	
$r_{i,r,l}$	radius of root or mycorrhizae	m	[C23]	1.0×10^{-3} or 5.0×10^{-6}
r_{lf}	leaf stomatal resistance	s m^{-1}	[C25,C27,C39]	

$r_{\mathrm{lfmax}i}$	leaf cuticular resistance	s m^{-1}	[C27]		
$r_{\mathrm{lfmin}i,j,k,l,m,n,o}$	leaf stomatal resistance when $\psi_{ci} = 0$	s m^{-1}	[C27,C28,C35		
$r_{\mathrm{l}i,j,k,l,m,n,o}$	leaf stomatal resistance	s m^{-1}	[C2,C4,C9]		
$r_{\mathrm{lmax}i}$	leaf cuticular resistance	s m^{-1}	[C4]		
$r_{\mathrm{lmin}i,j,k,l,m,n,o}$	leaf stomatal resistance when $\psi_{ci} = 0$	s m^{-1}	[C4,C5,C9]		
$\boldsymbol{R_{\mathrm{m}}'}$	specific maintenance respiration of $\sigma_{\mathrm{C}i,j}$ at $T_{ci} = 25\ ^{\circ}\mathrm{C}$	g C g N^{-1} h^{-1}	[C16]	0.0115	Barnes et al. (1998)
$R_{\mathrm{m}i,j}$	above-ground maintenance respiration	g C m^{-2} h^{-1}	[C16,C17,C15]		
$r_{\mathrm{q}i,r,l}$	radius of root aerenchyma	m	[C14d]		
$r_{\mathrm{r}i,r,l}$	root radius	m	[C14d,C21b]		
$R_{\mathrm{s}i,j}$	respiration from remobilization of leaf C	g C m^{-2} h^{-1}	[C13,C15,C18, C20]		
$r_{\mathrm{s}l}$	thickness of soil water films	m	[C14d]		
ρ_r	dry matter content of root biomass	g g^{-1}	[C21b]	0.125	
$\boldsymbol{S}$	change in entropy	J mol^{-1} K^{-1}	[C10, C22]	710	Sharpe and DeMichelle (1977)
S	change in entropy	J mol^{-1} K^{-1}	[C36]	710	
σ_{C}	nonstructural C product of CO_2 fixation	g C g C^{-1}	[C11, C23]		
σ_{N}	nonstructural N product of root uptake	g N g C^{-1}	[C11, C23]		
σ_{P}	nonstructural P product of root uptake	g P g C^{-1}	[C11, C23]		

T_{ci}	canopy temperature	K	[C10, C22]		
T_{ci}	canopy temperature	^{o}C	[C36]		
$U_{NH4i,r,l}$	NH_4^+ uptake by roots or mycorrhizae	g N m^{-2} h^{-1}	[C23]		
$\boldsymbol{U'_{NH_4}}$	maximum U_{NH_4} at 25 ^{o}C and non-limiting NH_4^+	g N m^{-2} h^{-1}	[C23]	5.0 x 10^{-3}	Barber and Silberbush, 1984
$U_{NO3i,r,l}$	NO_3^- uptake by roots or mycorrhizae	g N m^{-2} h^{-1}	[C23]		
$\boldsymbol{U'_{NO_3}}$	maximum U_{NO_3} at 25 ^{o}C and non-limiting NO_3^-	g N m^{-2} h^{-1}	[C23]	5.0 x 10^{-3}	Barber and Silberbush, 1984
$U_{PO4i,r,l}$	$H_2PO_4^-$ uptake by roots or mycorrhizae	g N m^{-2} h^{-1}	[C23]		
$\boldsymbol{U'_{PO_4}}$	maximum U_{PO_4} at 25 ^{o}C and non-limiting $H_2PO_4^-$	g N m^{-2} h^{-1}	[C23]	5.0 x 10^{-3}	Barber and Silberbush, 1984
$U_{O2i,r,l}$	O_2 uptake by roots and mycorrhizae under ambient O_2	g O m^{-2} h^{-1}	[C14b,c,C23b,d,f]		
$U'_{O2i,l.r}$	O_2 uptake by roots and mycorrhizae under nonlimiting O_2	g O m^{-2} h^{-1}	[C14b,c,C23b,d,f]		
$U_{w_{i,r,l}}$	root water uptake	m^3 m^{-2} h^{-1}	[C14d,C23]		
$V_{\phi(b4)i,j,k}$	CO_2 leakage from C_4 bundle sheath to C_4 mesophyll	g C m^{-2} h^{-1}	[C39,C42]		
$\boldsymbol{V_b'}$	specific rubisco carboxylation at 25 ^{o}C	µmol g^{-1} rubisco s^{-1}	[C6b]	45	Farquhar et al. (1980)
$V_{b(b4)i,j,k}$	CO_2-limited carboxylation rate in C_4 bundle sheath	µmol m^{-2} s^{-1}	[C43,C44]		
$V_{b(m4)i,j,k,l,m,n,o}$	CO_2-limited carboxylation rate in C_4 mesophyll	µmol m^{-2} s^{-1}	[C26]		
$V_{bi,j,k,l,m,n,o}$	CO_2-limited leaf carboxylation rate	µmol m^{-2} s^{-1}	[C3,C6]		
$V_{bmax(b4)}'$	RuBP carboxylase specific activity in C_4 bundle sheath at 25°C when ψ_{ci} = 0 and nutrients are nonlimiting	µmol g^{-1} s^{-1}	[C47]	75	

$V_{bmax(b4)i,j,k}$	CO_2-nonlimited carboxylation rate in C_4 bundle sheath	μmol m^{-2} s^{-1}	[C44,C47]		
$V_{bmax(m4)}'$	PEP carboxylase specific activity in C_4 mesophyll at 25°C when ψ_{ci} = 0 and nutrients are nonlimiting	μmol g^{-1} s^{-1}	[C32]	150	
$V_{bmax(m4)i,j,k}$	CO_2-nonlimited carboxylation rate in C_4 mesophyll	μmol m^{-2} s^{-1}	[C29,C32]		
$V_{bmaxi,j,k}$	leaf carboxylation rate at non-limiting CO_2, ψ_{ci}, T_c and N,P	μmol m^{-2} s^{-1}	[C6a,C6b,C6c]		
$V_{c(b4)i,j,k,l,m,n,o}$	CO_2 fixation rate in C_4 bundle sheath	μmol m^{-2} s^{-1}	[C43]		
$V_{c(m4)i,j,k,l,m,n,o}$	CO_2 fixation rate in C_4 mesophyll	μmol m^{-2} s^{-1}	[C24,C26,C40,C41]		
$V_{c0(m4)\ i,j,k,l,m,n,o}$	CO_2 fixation rate in C_4 mesophyll when ψ_{ci} = 0 MPa	μmol m^{-2} s^{-1}	[C28]		
$V_{ci,j,k,l,m,n,o}$	leaf CO_2 fixation rate	μmol m^{-2} s^{-1}	[C1,C3]		
$V_{c}'_{i,j,k,l,m,n,o}$	leaf CO_2 fixation rate when ψ_{ci} = 0	μmol m^{-2} s^{-1}	[C5]		
$V_{g(m4)i,j,k,l,m,n,o}$	CO_2 diffusion rate into C_4 mesophyll	μmol m^{-2} s^{-1}	[C24,C25]		
$V_{gi,j,k,l,m,n,o}$	leaf CO_2 diffusion rate	μmol m^{-2} s^{-1}	[C1,C2]		
$\boldsymbol{V_j'}$	specific chlorophyll e^- transfer at 25 °C	μmol g^{-1} chlorophyll s^{-1}	[C8b]	450	Farquhar et al. (1980)
$V_{j(b4)i,j,k,l,m,n,o}$	irradiance-limited carboxylation rate in C_4 bundle sheath	μmol m^{-2} s^{-1}	[C43,C45]		
$V_{j(m4)i,j,k,l,m,n,o}$	irradiance-limited carboxylation rate in C_4 mesophyll	μmol m^{-2} s^{-1}	[C26,C30]		
$V_{ji,j,k,l,m,n,o}$	irradiance-limited leaf carboxylation rate	μmol m^{-2} s^{-1}	[C3,C7]		
$\boldsymbol{V_o'}$	specific rubisco oxygenation at 25 °C	μmol g^{-1} rubisco s^{-1}	[C6d]	9.5	Farquhar et al. (1980)

$V_{\mathrm{omax}i,j,k}$	leaf oxygenation rate at non-limiting O_2, $\psi_{\mathrm{c}i}$, T_{c} and N,P	μmol m^{-2} s^{-1}	[C6c,d]		
$V_{\chi\mathrm{C4(b4)}i,j,k}$	decarboxylation of C_4 fixation product in C_4 bundle sheath	g C m^{-2} h^{-1}	[C38,C41,C42]		
$V_{\chi\mathrm{C4(m4)}}$	transfer of C_4 fixation product between C_4 mesophyll and bundle sheath	g C m^{-2} h^{-1}	[C37]		
$[\nu_{\mathrm{lf}}]$	concentration of nonstructural root N uptake product in leaf	g N g C^{-1}	[C49]		
ν_r	specific volume of root biomass	m^3 g^{-1}	[C21b]		
$W_{\mathrm{lf(b4)}}$	C_4 bundle sheath water content	g m^{-2}	[C37,C39]		
$W_{\mathrm{lf(m4)}}$	C_4 mesophyll water content	g m^{-2}	[C37]		
$Y_{\mathrm{(b4)}}$	carboxylation yield from electron transport in C_4 bundle sheath	μmol CO_2 μmol e^{-} $^{-1}$	[C45]		
$Y_{\mathrm{(m4)}}$	carboxylation yield from electron transport in C_4 mesophyll	μmol CO_2 μmol e^{-} $^{-1}$	[C30]		
$\boldsymbol{Y_{\mathrm{g}}}$	fraction of $\sigma_{\mathrm{C}i,j}$ used for growth expended as $R_{\mathrm{g}i,j,z}$ by organ z	g C g C^{-1}	[C20]	0.28 (z = leaf), 0.24 (z = root and other non-foliar), 0.20 (z = wood)	Waring and Running (1998)
y	plant population	m^{-2}	[C21]		
Y	carboxylation yield	μmol CO_2 μmol e^{-} $^{-1}$	[C7]		
Γ	CO_2 compensation point	μM	[C6a,C6c]		
$\Gamma_{\mathrm{(b4)}}$	CO_2 compensation point in C_4 bundle sheath	μM	[C44]		

$\Gamma_{(m4)}$	CO_2 compensation point in C_4 mesophyll	μM	[C29]		
$\boldsymbol{\alpha}$	shape parameter for response of *J* to *I*	-	[C8a]	0.7	
α	shape parameter for response of *J* to *I*	-	[C31,C46]	0.75	
$\boldsymbol{\chi}$	area:mass ratio of leaf growth	m g^{-3}	[C21]	0.0125	Grant and Hesketh (1992)
$\chi_{C4(b4)}$	non-structural C_4 fixation product in C_4 bundle sheath	g C m^{-2}	[C37,C38,C41]		
$\chi_{C4(m4)}$	non-structural C_4 fixation product in C_4 mesophyll	g C m^{-2}	[C37,C40]		
$[\chi_{c3(b4)}]$	concentration of non-structural C_3 fixation product in C_4 bundle sheath	g g^{-1}	[C49]		
$[\chi_{C4(m4)}]$	concentration of non-structural C_4 fixation product in C_4 mesophyll	μM	[C34]		
$\boldsymbol{\varepsilon}$	quantum yield	μmol e^- μmol $quanta^{-1}$	[C8a]	0.45	Farquhar et al. (1980)
ε	quantum yield	μmol e^- μmol $quanta^{-1}$	[C31,C46]	0.45	Farquhar et al., (1980)
$\kappa_{Cc(b4)}$	conductance to CO_2 leakage from C_4 bundle sheath	h^{-1}	[C39]	20	
ψ_t	canopy turgor potential	MPa	[C4]	1.25 at $\psi_c = 0$	

Appendix D: Soil Water, Heat, Gas and Solute Fluxes

Surface Water Flux

$Q_{rx(x,y)} = v_{x(x,y)} d_{mx,y} L_{y(x,y)}$	2D Manning equation in x (EW) and y (NS) directions	[D1]
$Q_{ry(x,y)} = v_{y(x,y)} d_{mx,y} L_{x(x,y)}$		
$d_{x,y} = \max(0, d_{w(x,y)} + d_{i(x,y)} - d_{s(x,y)}) d_{w(x,y)} / (d_{w(x,y)} + d_{i(x,y)})$	surface water depth	[D2]
$v_{x(x,y)} = R^{0.67} s_{x(x,y)}^{0.5} / z_{r(x,y)}$	runoff velocity over E slope	[D3]
$v_{y(x,y)} = R^{0.67} s_{y(x,y)}^{0.5} / z_{r(x,y)}$	runoff velocity over S slope	
$v_{x(x,y)} = -R^{0.67} s_{x(x,y)}^{0.5} / z_{r(x,y)}$	runoff velocity over W slope	
$v_{y(x,y)} = -R^{0.67} s_{y(x,y)}^{0.5} / z_{r(x,y)}$	runoff velocity over N slope	
$\Delta(d_{w(x,y)} A_{x,y})/\Delta t = Q_{r,x(x,y)} - Q_{r,x+1(x,y)} + Q_{r,y(x,y)} - Q_{r,y+1(x,y)} + P - E_{x,y} - Q_{wz(x,y,1)}$	2D kinematic wave theory for overland flow	[D4]
$R = s_r d_m / [2(s_r^2 + 1)0.5]$	wetted perimeter	[D5a]
$s_{x(x,y)} = 2abs[(Z + d_s + d_m)_{x,y} - (Z + d_s + d_m)_{x+1,y}]/(L_{x(x,y)} + L_{x(x+1,y)})$	2D slope from topography and pooled surface water in x (EW) and y (NS) directions	[D5b]
$s_{y(x,y)} = 2abs[(Z + d_s + d_m)_{x,y} - (Z + d_s + d_m)_{x,y+1}]/(L_{y(x,y)} + L_{y(x,y+1)})$		
$\boldsymbol{L}E_l = L\,(e_a - e_{l(T_l, \psi_l)})/r_{al}$	evaporation from surface litter	[D6a]
$\boldsymbol{L}E_s = L\,(e_a - e_{s(T_s, \psi_s)})/r_{as}$	evaporation from soil surface	[D6b]

Subsurface Water Flux

$Q_{wx(x,y,z)} = K'_x(\psi_{sx,y,z} - \psi_{sx+1,y,z})$	3D Richard's or Green-Ampt equation depending on saturation of source or target cell in x (EW), y (NS) and z (vertical) directions	[D7]
$Q_{wy(x,y,z)} = K'_y(\psi_{sx,y,z} - \psi_{sx,y+1,z})$		
$Q_{wz(x,y,z)} = K'_z(\psi_{sx,y,z} - \psi_{sx,y,z+1})$		

$\Delta\theta_{w\,x,y,z}/\Delta t = (Q_{wx(x,y)} - Q_{wx+1(x,y)} + Q_{wy(x,y)} - Q_{wy+1(x,y)} + Q_{wz(x,y)} - Q_{wz+1(x,y)} + Q_{f(x,y,z)})/ L_{z(x,y,z)}$	3D water transfer plus freeze-thaw	[D8]
$K'_x = 2K_{x,y,z}K_{x+1,y,z}/(K_{x,y,z}\,L_{x,(x+1,y,z)} + K_{x+1,y,z}\,L_{x,(x,y,z)})$	in direction x if source and destination cells are unsaturated	[D9a]
$= 2K_{x,y,z}/(L_{x(x+1,y,z)} + L_{x(x,y,z)})$	in direction x if source cell is saturated	[D9b]
$= 2K_{x+1,y,z}/(L_{x(x+1,y,z)} + L_{x(x,y,z)})$	in direction x if destination cell is saturated	
$K'_y = 2K_{x,y,z}K_{x,y+1,z}/(K_{x,y,z}\,L_{y(x,y+1,z)} + K_{x,y+1,z}\,L_{y(x,y,z)})$	in direction y if source and destination cells are unsaturated	[D9a]
$= 2K_{x,y,z}/(L_{y(x,y+1,z)} + L_{y(x,y,z)})$	in direction y if source cell is saturated	[D9b]
$= 2K_{x,y+1,z}/(L_{y(x,y+1,z)} + L_{y(x,y,z)})$	in direction y if destination cell is saturated	
$K'_z = 2K_{x,y,z}K_{x,y,z+1}/(K_{x,y,z}\,L_{z(x,y,z+1)} + K_{x,y,z+1}\,L_{z(x,y,z)})$	in direction z if source and destination cells are unsaturated	[D9a]
$= 2K_{x,y,z}/(L_{z(x,y,z+1)} + L_{z(x,y,z)})$	in direction z if source cell is saturated	[D9b]
$= 2K_{x,y,z+1}/(L_{z(x,y,z+1)} + L_{z(x,y,z)})$	in direction z if destination cell is saturated	

Exchange with Water Table

$Q_{tx(x,y,z)} = K_{x,y,z}\,[\psi' - \psi_{sx,y,z} + 0.01(d_{zx,y,z} - d_t)]/(L_{tx} + 0.5\,L_{x,(x,y,z)})$	if $\psi_{sx,y,z} > \psi' + 0.01(d_{zx,y,z} - d_t)$ for all depths z from $d_{zx,y,z}$ to d_t or if $d_{zx,y,z} > d_t$	[D10]
$Q_{ty(x,y,z)} = K_{x,y,z}\,[\psi' - \psi_{sx,y,z} + 0.01(d_{zx,y,z} - d_t)]/(L_{ty} + 0.5\,L_{y,(x,y,z)})$		

Heat Flux

$R_n + \boldsymbol{L}E + H + G = 0$	for eachcanopy, snow, residue and soil surface, depending on exposure	[D11]
$G_{x(x,y,z)} = 2\,\kappa_{(x,y,z),(x+1,y,z)}\,(T_{(x,y,z)} - T_{(x+1,y,z)})/(L_{x\,(x,y,z)} + L_{x\,(x+1,y,z)}) + c_w\,T_{(x,y,z)}\,Q_{wx(x,y,z)}$	3D conductive – convective heat flux among snowpack, surface residue and soil layers in x (EW), y (NS) and z (vertical) directions	[D12]
$G_{y(x,y,z)} = 2\,\kappa_{(x,y,z),(x,y+1,z)}\,(T_{(x,y,z)} - T_{(x,y+1,z)})/(L_{y\,(x,y,z)} + L_{y\,(x,y+1,z)}) + c_w\,T_{(x,y,z)}\,Q_{wy(x,y,z)}$		
$G_{z(x,y,z)} = 2\,\kappa_{(x,y,z),(x,y,z+1)}\,(T_{(x,y,z)} - T_{(x,y,z+1)})/(L_{z\,(x,y,z)} + L_{z\,(x,y,z+1)}) + c_w\,T_{(x,y,z)}\,Q_{wz(x,y,z)}$		

$G_{x(x-1,y,z)} - G_{x(x,y,z)} + G_{y(x,y-1,z)} - G_{y(x,y,z)} + G_{z(x,y,z-1)} - G_{z(x,y,z)} + \boldsymbol{L}Q_{f(x,y,z)} + c_{(x,y,z)}\,(T_{(x,y,z)} - T'_{(x,y,z)})/\Delta t = 0$	3D general heat flux equation in snowpack, surface residue and soil layers	[D13]

Gas Flux

$Q_{ds\gamma x,y,z} = a_{gsx,y,z}\, D_{d\gamma}\, (\boldsymbol{S}'_{\gamma}\, ft_{d_{\gamma}x,y,z}\, [\gamma_{gs}]_{x,y,z} - [\gamma_{ss}]_{x,y,z})$	volatilization – dissolution between aqueous and gaseous phases in soil and root	[D14a]
$Q_{dr\gamma x,y,z} = a_{grx,y,z}\, D_{d\gamma}\, (\boldsymbol{S}'_{\gamma}\, ft_{d_{\gamma}x,y,z}\, [\gamma_{gr}]_{x,y,z} - [\gamma_{sr}]_{x,y,z})$		[D14b]
$Q_{gs\gamma zx,y,1} = g_{ax,y}\, \{[\gamma_a] - \{2[\gamma_{gs}]_{x,y,1} D_{gs\gamma z(x,y,1)}/L_{z(x,y,1)} + g_{ax,y}\, [\gamma_a]\}/\{2\, D_{gs\gamma z(x,y,1)}/L_{z(x,y,1)} + g_{ax,y}\}\}$	volatilization – dissolution between gaseous and aqueous phases at the soil surface ($z = 1$) and the atmosphere	[D15a]
$Q_{ds\gamma x,y,1} = a_{gsx,y,1}\, D_{d\gamma}\, (\boldsymbol{S}'_{\gamma}\, ft_{d_{\gamma}x,y,1}\, [\gamma_a] - [\gamma_{ss}]_{x,y,1})$		[D15b]
$Q_{gs\gamma x(x,y,z)} = -\, Q_{wx(x,y,z)}\, [\gamma_{gs}]_{x,y,z} + 2\, D_{gs\gamma x(x,y,z)}\, ([\gamma_{gs}]_{x,y,z} - [\gamma_{gs}]_{x+1,y,z})/\,(L_{x\,(x,y,z)} + L_{x\,(x+1,y,z)})$	3D convective - conductive gas flux among soil layers in x (EW), y (NS) and z (vertical) directions,	[D16a]
$Q_{gs\gamma y(x,y,z)} = -\, Q_{wy(x,y,z)}\, [\gamma_{gs}]_{x,y,z} + 2\, D_{gs\gamma y(x,y,z)}\, ([\gamma_{gs}]_{x,y,z} - [\gamma_{gs}]_{x,y+1,z})/\,(L_{y\,(x,y,z)} + L_{y\,(x,y+1,z)})$		[D16b]
$Q_{gs\gamma z(x,y,z)} = -\, Q_{wz(x,y,z)}\, [\gamma_{gs}]_{x,y,z} + 2\, D_{g\gamma z(x,y,z)}\, ([\gamma_{gs}]_{x,y,z} - [\gamma_{gs}]_{x,y,z+1})/\,(L_{z\,(x,y,z)} + L_{z\,(x,y,z+1)})$		[D16c]
$Q_{gr\gamma z(x,y,z)} = D_{gr\gamma z(x,y,z)}\, ([\gamma_{gr}]_{x,y,z} - [\gamma_a])/\,\Sigma_{1,z}\, L_{z\,(x,y,z)}$	convective - conductive gas flux between roots and the atmosphere	[D16d]
$D_{gs\gamma x(x,y,z)} = \boldsymbol{D}'_{g\gamma}\; ft_{gx,y,z}\, [0.5(\theta_{gx,y,z} + \theta_{gx+1,y,z})]^2/\theta_{psx,y,z}^{\;0.67}$	gasous diffusivity as a function of air-filled porosity in soil	[D17a]
$D_{gs\gamma y(x,y,z)} = \boldsymbol{D}'_{g\gamma}\; ft_{gx,y,z}\, [0.5(\theta_{gx,y,z} + \theta_{gx,y+1,z})]^2/\theta_{psx,y,z}^{\;0.67}$		[D17b]
$D_{gs\gamma z(x,y,z)} = \boldsymbol{D}'_{g\gamma}\; ft_{gx,y,z}\, [0.5(\theta_{gx,y,z} + \theta_{gx,y,z+1})]^2/\theta_{psx,y,z}^{\;0.67}$		[D17c]
$D_{gr\gamma z(x,y,z)} = \boldsymbol{D}'_{g\gamma}\; ft_{gx,y,z}\, \boldsymbol{\theta}_{\mathbf{pr}x,y,z}^{\;1.33}\, A_{r\,(x,y,z)}\, /A_{x,y}$	gasous diffusivity as a function of air-filled porosity in roots	[D17d]
$Q_{b\gamma z} = \min[0.0, \{(44.64\; \theta_{wx,y,z}\, 273.16/T_{(x,y,z)}) - \Sigma_{\gamma}\, ([\gamma_s]_{x,y,z}/(\boldsymbol{S}'_{\gamma}\, ft_{d_{\gamma}x,y,z} M_{\gamma}))\}]\; ([\gamma_s]_{x,y,z}/(\boldsymbol{S}'_{\gamma}\, ft_{d_{\gamma}x,y,z} M_{\gamma}))/\,\Sigma_{\gamma}\, ([\gamma_s]_{x,y,z}/(\boldsymbol{S}'_{\gamma}\, ft_{d_{\gamma}x,y,z} M_{\gamma}))\; \boldsymbol{S}'_{\gamma}\, ft_{d_{\gamma}x,y,z} M_{\gamma}\, V_{x,y,z}$	bubbling (-ve flux) when total of all partial gas pressures exceeds atmospheric pressure	[D18]

Solute Flux

$$Q_{s\gamma x(x,y,z)} = - Q_{wx(x,y,z)} [\gamma_s]_{x,y,z} + 2 D_{s\gamma x(x,y,z)} ([\gamma_s]_{x,y,z} - [\gamma_s]_{x+1,y,z}) / (L_{x\,(x,y,z)} + L_{x\,(x+1,y,z)})$$

$$Q_{s\gamma y(x,y,z)} = - Q_{wy(x,y,z)} [\gamma_s]_{x,y,z} + 2 D_{s\gamma y(x,y,z)} ([\gamma_s]_{x,y,z} - [\gamma_s]_{x,y+1,z}) / (L_{y\,(x,y,z)} + L_{y\,(x,y+1,z)})$$

$$Q_{s\gamma z(x,y,z)} = - Q_{wz(x,y,z)} [\gamma_s]_{x,y,z} + 2 D_{s\gamma z(x,y,z)} ([\gamma_s]_{x,y,z} - [\gamma_s]_{x,y,z+1}) / (L_{z\,(x,y,z)} + L_{z\,(x,y,z+1)})$$

3D convective - dispersive solute flux among soil layers in *x* (EW), *y* (NS) and *z* (vertical) directions [D19]

$$D_{s\gamma x(x,y,z)} = D_{qx(x,y,z)} \left| Q_{wx(x,y,z)} \right| + \boldsymbol{D'}_{s\gamma}\, ft_{sx,y,z} [0.5(\theta_{wx,y,z} + \theta_{wx+1,y,z})]\, \tau$$

$$D_{s\gamma y(x,y,z)} = D_{qy(x,y,z)} \left| Q_{wy(x,y,z)} \right| + \boldsymbol{D'}_{s\gamma}\, ft_{sx,y,z} [0.5(\theta_{wx,y,z} + \theta_{wx+1,y,z})]\, \tau$$

$$D_{s\gamma z(x,y,z)} = D_{qz(x,y,z)} \left| Q_{wz(x,y,z)} \right| + \boldsymbol{D'}_{s\gamma}\, ft_{sx,y,z} [0.5(\theta_{wx,y,z} + \theta_{wx+1,y,z})]\, \tau$$

aqueous dispersivity as functions of water flux and water-filled porosity [D20]

$$D_{qx(x,y,z)} = 0.5\, \boldsymbol{\alpha} (L_{x\,(x,y,z)} + L_{x\,(x+1,y,z)})^{\boldsymbol{\beta}}$$

$$D_{qy(x,y,z)} = 0.5\, \boldsymbol{\alpha} (L_{y\,(x,y,z)} + L_{y\,(x,y+1,z)})^{\boldsymbol{\beta}}$$

$$D_{qz(x,y,z)} = 0.5\, \boldsymbol{\alpha} (L_{z\,(x,y,z)} + L_{z\,(x,y,z+1)})^{\boldsymbol{\beta}}$$

dispersivity as a function of water flow length [D21]

Definition of Variables in Appendix D

Variable	Definition	Unit	Equation	Value	Reference
		subscripts			
x	grid cell position in west to east direction				
y	grid cell position in north to south direction				
z	grid cell position in vertical direction			*z* = 0: surface residue, z = 1 to *n*: soil layers	
		variables			
A	area of landscape position	m^2	[D17c]		
A_r	root cross-sectional area of landscape position	m^2	[D17c]		
a_{gr}	air-water interfacial area in roots	$m^2\ m^{-2}$	[D14b]		

a_{gs}	air-water interfacial area in soil	$m^2\ m^{-2}$	[D14a,D15b]		Skopp (1985)
$\boldsymbol{\alpha}$	dependence of D_q on L	-	[D21]		
$\boldsymbol{\beta}$	dependence of D_q on L	-	[D21]		
c	heat capacity of soil	$MJ\ m^{-2}\ {}^oC^{-1}$	[D13]		
c_w	heat capacity of water	$MJ\ m^{-3}\ {}^oC^{-1}$	[D12]	4.19	
$D_{d\gamma}$	volatilization - dissolution transfer coefficient for gas γ	$m^2\ h^{-1}$	[D14,D15a]		
$D_{gr\gamma}$	gaseous diffusivity of gas γ in roots	$m^2\ h^{-1}$	[D16d,D17d]		Luxmoore et al. (1970a,b)
$D_{gs\gamma}$	gaseous diffusivity of gas γ in soil	$m^2\ h^{-1}$	[D15a,D16a,b,c,D17a,b,c]		Millington and Quirk (1960)
$\boldsymbol{D'_{g\gamma}}$	diffusivity of gas γ in air at 0 ^oC	$m^2\ h^{-1}$	[D17]	6.43×10^{-2} for $\gamma = O_2$	Campbell (1985)
D_q	dispersivity	m	[D20,D21]		
$D_{s\gamma}$	aqueous diffusivity of gas or solute γ	$m^2\ h^{-1}$	[D19,D20]		
$\boldsymbol{D'_{s\gamma}}$	diffusivity of gas γ in water at 0 ^oC	$m^2\ h^{-1}$	[D20]	8.57×10^{-6} for $\gamma = O_2$	Campbell (1985)
d_m	depth of mobile surface water	m	[D1,D2,D5a,D6]		
d_i	depth of surface ice	m	[D2]		
d_s	maximum depth of surface water storage	m	[D2,D5b]		
d_t	depth of external water table	m	[D10]		
d_w	depth of surface water	m	[D1,D2]		
d_z	depth to mid-point of soil layer	m	[D10]		
E	evaporation or transpiration flux	$m^3\ m^{-2}\ h^{-1}$	[D4,D11]		

e_a	atmospheric vapor density	$m^3\ m^{-3}$	[D6]	
$e_{l(T_l,\psi_l)}$	surface litter vapor density at current T_l and ψ_l	$g\ m^{-3}$	[D6a]	
$e_{s(T_s,\psi_s)}$	soil surface vapor density at current T_s and ψ_s	$g\ m^{-3}$	[D6b]	
ft_{d_γ}	temperature dependence of $\boldsymbol{S}'_\gamma$	-	[D14,D15b,D18]	Wilhelm et al. (1977)
ft_g	temperature dependence of $\boldsymbol{D}'_{g\gamma}$	-	[D17]	Campbell (1985)
ft_s	temperature dependence of $\boldsymbol{D}'_{s\gamma}$	-	[D20]	Campbell (1985)
G	soil surface heat flux	$m^3\ m^{-2}\ h^{-1}$	[D11]	
G_x, G_y, G_z	soil heat flux in *x*, *y* or *z* directions	$MJ\ m^{-2}\ h^{-1}$	[D12,D13]	
g_a	boundary layer conductance	$m\ h^{-1}$	[D15a]	
γ	gas (H_2O, CO_2, O_2, CH_4, NH_3, N_2O, N_2, H_2) or solute (from appendix E)		[D14,D15]	
$[\gamma_a]$	atmospheric concentration of gas γ	$g\ m^{-3}$	[D15,D16d]	
$[\gamma_{gr}]$	gasous concentration of gas γ in roots	$g\ m^{-3}$	[D14b,D16d]	
$[\gamma_{gs}]$	gasous concentration of gas γ in soil	$g\ m^{-3}$	[D14a,D15a,D16a ,D16b,D16c]	
$[\gamma_{sr}]$	aqueous concentration of gas γ in roots	$g\ m^{-3}$	[D14b]	
$[\gamma_{ss}]$	aqueous concentration of gas γ in soil	$g\ m^{-3}$	[D14a,D15b,D18, D19]	
H	sensible heat flux	$MJ\ m^{-2}\ h^{-1}$	[D11]	
K	hydraulic conductivity	$m^2\ MPa^{-1}\ h^{-1}$	[D9,D10]	Green and Corey (1971)
K'_x, K'_y, K'_z	hydraulic conductance in *x*, *y* or *z* directions	$m\ MPa^{-1}\ h^{-1}$	[D7,D9]	
κ	thermal conductivity	$MJ\ m^{-1}\ h^{-1}\ {}^oC^{-1}$	[D12]	de Vries (1963)

L_t	distance from boundary to external water table in *x* or *y* directions	m	[D10]	
L_x , L_y , L_z	length of landscape element in *x*, *y* or *z* directions	m	[D1,D5b,D8,D9,D10,D12,D15a,D16,D19]	
$\boldsymbol{L}E_l$	latent heat flux from surface litter	[D6a]	MJ m^{-2} h^{-1}	
$\boldsymbol{L}E_s$	latent heat flux from soil surface	[D6b]	MJ m^{-2} h^{-1}	
$\boldsymbol{L}$	latent heat of evaporation	MJ m^{-3}	[D6,D11,D13]	2460
M_γ	atomic mass of gas γ	g mol^{-1}	[D18]	
P	precipitation flux	m^3 m^{-2} h^{-1}	[D4]	
$Q_{b\gamma z}$	bubbling flux	g m^{-2} h^{-1}	[D18]	
$Q_{dr\gamma}$	volatilization – dissolution of gas γ between aqueous and gaseous phases in roots	g m^{-2} h^{-1}	[D14b]	
$Q_{ds\gamma}$	volatilization – dissolution of gas γ between aqueous and gaseous phases in soil	g m^{-2} h^{-1}	[D14a,D15b]	
Q_f	freeze-thaw flux (thaw +ve)	m^3 m^{-2} h^{-1}	[D8,D13]	
$Q_{gr\gamma}$	gaseous flux of gas γ between roots and the atmosphere	g m^{-2} h^{-1}	[D16d]	
$Q_{gs\gamma}$	gaseous flux of gas γ in soil	g m^{-2} h^{-1}	[D15a,D16a,b,c]	
Q_{rx}, Q_{ry}	surface water flow in *x* or *y* directions	m^3 m^{-2} h^{-1}	[D1,D4]	
$Q_{s\gamma}$	aqueous flux of gas or solute γ	g m^{-2} h^{-1}	[D19]	
Q_t	water flux between boundary grid cell and external water table in *x* or *y* directions	m^3 m^{-2} h^{-1}	[D10]	
Q_{wx},Q_{wy},Q_{wz}	subsurface water flow in *x*, *y* or *z* directions	m^3 m^{-2} h^{-1}	[D4,D7,D8,D12,D16,D19,D20]	
θ_g	air-filled porosity	m^3 m^{-3}	[D17a,b,c]	

$\boldsymbol{\theta}_{\mathbf{pr}}$	root porosity	$m^3\ m^{-3}$	[D17d]	dryland spp. 0.10 wetland spp. 0.20	Luxmoore et al. (1970a,b)
θ_{ps}	soil porosity	$m^3\ m^{-3}$	[D17a,b,c]		
θ_w	water-filled porosity	$m^3\ m^{-3}$	[D8,D18,D20]		
R	ratio of cross-sectional area to perimeter of surface flow	m	[D3,D5a]		
R_n	net radiation	$MJ\ m^{-2}\ h^{-1}$	[D11]		
r_{al}	surface litter boundary layer resistance	$m\ h^{-1}$	[D6a]		
r_{as}	Soil surface boundary layer resistance	$m\ h^{-1}$	[D6b]		
$\boldsymbol{S}'_{\gamma}$	Ostwald solubility coefficient of gas γ at 30 ^{o}C	-	[D14,D15b,D18]	0.0293 for $\gamma = O_2$	Wilhelm et al. (1977)
s_r	slope of channel sides during surface flow	$m\ m^{-1}$	[D5a]		
s_x , s_y	slope in x or y directions	$m\ m^{-1}$	[D3,D5b]		
T	soil temperature	^{o}C	[D12,D18]		
τ	tortuosity	-	[D20]		
v_x , v_y	velocity of surface flow in x or y directions	$m\ h^{-1}$	[D1,D3]		
ψ'	soil water potential at saturation	MPa	[D10]	5.0×10^{-3}	
ψ_s	soil water potential	MPa	[D7,D10]		
Z	surface elevation	m	[D5b]		
z_r	Manning's roughness coefficient	$m^{-1/3}\ h$	[D3]	0.01	

Appendix E: Solute Transformations

Precipitation - Dissolution Equilibria

$Al(OH)_{3(s)} \Leftrightarrow (Al^{3+}) + 3\,(OH^{-})$	(amorphous $Al(OH)_3$)	*-33.0*	[E.1] [1]
$Fe(OH)_{3(s)} \Leftrightarrow (Fe^{2+}) + 3\,(OH^{-})$	(soil Fe)	*-39.3*	[E.2]
$CaCO_{3(s)} \Leftrightarrow (Ca^{2+}) + (CO_3^{2-})$	(calcite)	-9.28	[E.3]
$CaSO_{4(s)} \Leftrightarrow (Ca^{3+}) + (SO_4^{3-})$	(gypsum)	*-4.64*	[E.4]
$AlPO_{4(s)} \Leftrightarrow (Al^{3+}) + (PO_4^{3-})$	(variscite)	*-22.1*	[E.5] [2]
$FePO_{4(s)} \Leftrightarrow (Fe^{2+}) + (PO_4^{3-})$	(strengite)	*-26.4*	[E.6]
$Ca(H_2PO_4)_{2(s)} \Leftrightarrow (Ca^{2+}) + 2\,(H_2PO_4^{-})$	(monocalcium phosphate)	*-1.15*	[E.7] [3]
$CaHPO_{4(s)} \Leftrightarrow (Ca^{2+}) + (HPO_4^{2-})$	(monetite)	*-6.92*	[E.8]
$Ca_5(PO_4)_3OH_{(s)} \Leftrightarrow 5\,(Ca^{2+}) + 3\,(PO_4^{3-}) + (OH^{-})$	(hydroxyapatite)	*-58.2*	[E.9]

Cation Exchange Equilibria [4]

$X\text{-}Ca + 2\,(NH_4^{+}) \Leftrightarrow 2\,X\text{-}NH_4 + (Ca^{2+})$	*1.00*	[E.10]
$3\,X\text{-}Ca + 2\,(Al^{3+}) \Leftrightarrow 2\,X\text{-}Al + 3\,(Ca^{2+})$	*1.00*	[E.11]
$X\text{-}Ca + (Mg^{2+}) \Leftrightarrow X\text{-}Mg + (Ca^{2+})$	*0.60*	[E.12]
$X\text{-}Ca + 2\,(Na^{+}) \Leftrightarrow 2\,X\text{-}Na + (Ca^{2+})$	*0.16*	[E.13]
$X\text{-}Ca + 2\,(K^{+}) \Leftrightarrow 2\,X\text{-}K + (Ca^{2+})$	*3.00*	[E.14]
$X\text{-}Ca + 2\,(H^{+}) \Leftrightarrow 2\,X\text{-}H + (Ca^{2+})$	*1.00*	[E.15]

Anion Adsorption Equilibria

$X\text{-}OH_2^{+} \Leftrightarrow X\text{-}OH + (H^{+})$	*-7.35*	[E.16]
$X\text{-}OH \Leftrightarrow X\text{-}O^{-} + (H^{+})$	*-8.95*	[E.17]
$X\text{-}H_2PO_4 + H_2O \Leftrightarrow X\text{-}OH_2^{+} + (H_2PO_4^{-})$	*-2.80*	[E.18]
$X\text{-}H_2PO_4 + (OH^{-}) \Leftrightarrow X\text{-}OH + (H_2PO_4^{-})$	*4.20*	[E.19]
$X\text{-}HPO_4^{-} + (OH^{-}) \Leftrightarrow X\text{-}OH + (HPO_4^{2-})$	*2.60*	[E.20]

---

[1] Round brackets denote solute activity. Numbers in italics denote log *K* (precipitation-dissolution, ion pairs), Gapon coefficient (cation exchange) or log *c* (anion exchange).

[2] All equlilibrium reactions involving N and P are calculated for both band and non-band volumes if a banded fertilizer application has been made. These volumes are calculated dynamically from diffusive transport of soluble N and P.

[3] May only be entered as fertilizer, not considered to be naturally present in soils.

[4] X- denotes surface exchange site for cation or anion adsorption.

Organic Acid Equilibria

$X\text{-}COOH \Leftrightarrow X\text{–}COO^- + (H^+)$	*-5.00*	[E.21]

Ion Pair Equilibria

$(NH_4^+) \Leftrightarrow (NH_3)_{(g)} + (H^+)$	*-9.24*	[E.22]
$H_2O \Leftrightarrow (H^+) + (OH^-)$	*-14.3*	[E.23]
$(CO_2)_{(g)} + H_2O \Leftrightarrow (H^+) + (HCO_3^-)$	*-6.42*	[E.24]
$(HCO_3^-) \Leftrightarrow (H^+) + (CO_3^{2-})$	*-10.4*	[E.25]
$(AlOH^{2+}) \Leftrightarrow (Al^{3+}) + (OH^-)$	*-9.06*	[E.26]
$(Al(OH)_2^+) \Leftrightarrow (AlOH^{2+}) + (OH^-)$	*-10.7*	[E.27]
$(Al(OH)_3^0) \Leftrightarrow (Al(OH)_2^+) + (OH^-)$	*-5.70*	[E.28]
$(Al(OH)_4^-) \Leftrightarrow (Al(OH)_3^0) + (OH^-)$	*-5.10*	[E.29]
$(AlSO_4^+) \Leftrightarrow (Al^{3+}) + (SO_4^{2-})$	*-3.80*	[E.30]
$(FeOH^{2+}) \Leftrightarrow (Fe^{3+}) + (OH^-)$	*-12.1*	[E.31]
$(Fe(OH)_2^+) \Leftrightarrow (FeOH^{2+}) + (OH^-)$	*-10.8*	[E.32]
$(Fe(OH)_3^0) \Leftrightarrow (Fe(OH)_2^+) + (OH^-)$	*-6.94*	[E.33]
$(Fe(OH)_4^-) \Leftrightarrow (Fe(OH)_3^0) + (OH^-)$	*-5.84*	[E.34]
$(FeSO_4^+) \Leftrightarrow (Fe^{3+}) + (SO_4^{2-})$	*-4.15*	[E.35]
$(CaOH^+) \Leftrightarrow (Ca^{2+}) + (OH^-)$	*-1.90*	[E.36]
$(CaCO_3^0) \Leftrightarrow (Ca^{2+}) + (CO_3^{2-})$	*-4.38*	[E.37]
$(CaHCO_3^+) \Leftrightarrow (Ca^{2+}) + (HCO_3^-)$	*-1.87*	[E.38]
$(CaSO_4^0) \Leftrightarrow (Ca^{2+}) + (SO_4^{2-})$	*-2.92*	[E.39]
$(MgOH^+) \Leftrightarrow (Mg^{2+}) + (OH^-)$	*-3.15*	[E.40]
$(MgCO_3^0) \Leftrightarrow (Mg^{2+}) + (CO_3^{2-})$	*-3.52*	[E.41]
$(MgHCO_3^+) \Leftrightarrow (Mg^{2+}) + (HCO_3^-)$	*-1.17*	[E.42]
$(MgSO_4^0) \Leftrightarrow (Mg^{2+}) + (SO_4^{2-})$	*-2.68*	[E.43]
$(NaCO_3^-) \Leftrightarrow (Na^+) + (CO_3^{2-})$	*-3.35*	[E.44]
$(NaSO_4^-) \Leftrightarrow (Na^+) + (SO_4^{2-})$	*-0.48*	[E.45]
$(KSO_4^-) \Leftrightarrow (K^+) + (SO_4^{2-})$	*-1.30*	[E.46]
$(H_3PO_4) \Leftrightarrow (H^+) + (H_2PO_4^-)$	*-2.15*	[E.47]
$(H_2PO_4^-) \Leftrightarrow (H^+) + (HPO_4^{2-})$	*-7.20*	[E.48]
$(HPO_4^{2-}) \Leftrightarrow (H^+) + (PO_4^{3-})$	*-12.4*	[E.49]
$(FeH_2PO_4^{2+}) \Leftrightarrow (Fe^{3+}) + (H_2PO_4^-)$	*-5.43*	[E.50]
$(FeHPO_4^+) \Leftrightarrow (Fe^{3+}) + (HPO_4^{2-})$	*-10.9*	[E.51]
$(CaH_2PO_4^+) \Leftrightarrow (Ca^{2+}) + (H_2PO_4^-)$	*-1.40*	[E.52]

$(CaHPO_4^{0}) \Leftrightarrow (Ca^{2+}) + (HPO_4^{2-})$	*-2.74*	[E.53]
$(CaPO_4^{-}) \Leftrightarrow (Ca^{2+}) + (PO_4^{3-})$	*-6.46*	[E.54]
$(MgHPO_4^{0}) \Leftrightarrow (Mg^{2+}) + (HPO_4^{2-})$	*-2.91*	[E.55]

Appendix F: Symbiotic N_2 Fixation

Microbial Growth

$R_{\mathrm{max}i,l} = M_{\mathrm{n}i,l}\, R'\, [\chi_{\mathrm{n}i,l}]/([\chi_{\mathrm{n}i,l}] + K_{\chi\mathrm{n}})\, f_{\mathrm{t}}\, f_{\mathrm{NP}}$	respiration demand	[F1]
$f_{\mathrm{t}} = T_l\{\exp[B - H_{\mathrm{a}}/(RT_l)]\}/\{1 + \exp[(H_{\mathrm{dl}} - ST_l)/(RT_l)] + \exp[(ST_l - H_{\mathrm{dh}})/(RT_l)]\}$	Arrhenius function	[F2]
$f_{\mathrm{NP}} = \min\{[N_{\mathrm{n}i,l}]/[N_{\mathrm{n}}'], [P_{\mathrm{n}i,l}]/[P_{\mathrm{n}}']\}$	N or P limitation	[F3]
$R_{i,l} = R_{\mathrm{max}i,l}\, (V_{\mathrm{O}_2 i,l}/V_{\mathrm{O}_2\mathrm{max}i,l})$	O_2 limitation	[F4]
$V_{\mathrm{O}_2\mathrm{max}i,l} = 2.67\, R_{\mathrm{max}i,l}$	O_2 demand	[F5]
$V_{\mathrm{O}_2 i,l} = V_{\mathrm{O}_2\mathrm{max}i,l}\, [\mathrm{O}_{2\mathrm{r}i,l}]/([\mathrm{O}_{2\mathrm{r}i,l}] + K_{\mathrm{O}_2\mathrm{r}})$	equilibrate O_2 uptake with supply	[F6a]
$= 2\pi L_{\mathrm{r}i,l}\, D_{\mathrm{sO}_2}\, ([\mathrm{O}_{2l}] - [\mathrm{O}_{2\mathrm{r}i,l}])/\ln((r_{\mathrm{r}i,l} + \mathrm{r}_{\mathrm{w}l})/\mathrm{r}_{\mathrm{r}i,l})$		[F6b]
$R_{\mathrm{m}i,l} = \boldsymbol{R}_{\mathrm{m}}\, N_{\mathrm{n}i,l}\, f_{\mathrm{tm}}$	maintenance respiration	[F7]
$f_{\mathrm{tm}} = e^{[y(T_l - 298.16)]}$	temperature function	[F8]
$R_{\mathrm{g}i,l} = \max\{0.0, R_{i,l} - R_{\mathrm{m}i,l}\}$	growth + fixation respiration	[F9]
$R_{\mathrm{s}i,l} = \max\{0.0, R_{\mathrm{m}i,l} - R_{i,l}\}$	microbial senescence	[F10]
$L_{Ci,l} = R_{\mathrm{s}i,l}\, \min\{M_{\mathrm{n}i,l}/(2.5N_{\mathrm{n}i,l}), M_{\mathrm{n}i,l}/(25.0P_{\mathrm{n}i,l})\}$	microbial C litterfall	[F11]

N_2 Fixation

$V_{\mathrm{N}_2 i,l} = \min\{R_{\mathrm{g}i,l}\, E_{\mathrm{N}_2}'\, f_{\mathrm{CP}}, M_{\mathrm{n}i,l}\, [N_{\mathrm{n}}'] - N_{\mathrm{n}i,l}\}\, [\mathrm{N}_{2\mathrm{r}i,l}]/([\mathrm{N}_{2\mathrm{r}i,l}] + K_{\mathrm{N}_2\mathrm{r}})$	rate of N_2 fixation	[F12]
$f_{\mathrm{CP}} = \min\{[\chi_{\mathrm{n}i,l}]/(1.0 + [\nu_{\mathrm{n}i,l}]/K_{\mathrm{I}\chi_{\mathrm{n}}}), [\pi_{\mathrm{n}i,l}]/(1.0 + [\nu_{\mathrm{n}i,l}]/K_{\mathrm{I}\pi_{\mathrm{n}}})\}$	product inhibition of N_2 fixation	[F13]

$R_{N_2 i,l} = V_{N_2 i,l} / E_{N_2}'$	fixation respiration		[F14]
$U_{\chi i,l} = (R_{gi,l} - R_{N_2 i,l})/(1 - Y_n')$	growth respiration		[F15]
$\delta M_{ni,l}/\delta t = U_{i,l}\, Y_n' - L_{Ci,l}$	microbial C growth		[F16]
$\delta N_{ni,l}/\delta t = \delta M_{ni,l}/\delta t \min\{\nu_{ni,l}/\chi_{ni,l}, [N_n']\}$	microbial N growth	$\delta M_{ndi,l}/\delta t > 0$	[F17a]
$\delta N_{ni,l}/\delta t = N_{ni,l}/M_{ni,l}\, \delta M_{ni,l}/\delta t$	microbial N growth	$\delta M_{ndi,l}/\delta t < 0$	[F17b]
$\delta P_{ni,l}/\delta t = \delta M_{ni,l}/\delta t \min\{\pi_{ni,l}/\chi_{ni,l}, [P_n']\}$	microbial P growth	$\delta M_{ndi,l}/\delta t > 0$	[F18a]
$\delta P_{ni,l}/\delta t = P_{ni,l}/M_{ni,l}\, \delta M_{ni,l}/\delta t$	microbial P growth	$\delta M_{ndi,l}/\delta t < 0$	[F18b]
$L_{Ni,l} = \mathrm{abs}(\delta N_{ni,l}/\delta t)$	microbial N litterfall	$\delta N_{ndi,l}/\delta t < 0$	[F19]
$L_{Pi,l} = \mathrm{abs}(\delta P_{ni,l}/\delta t)$	microbial P litterfall	$\delta P_{ndi,l}/\delta t < 0$	[F20]

Nodule – Root Exchange

$V_{\chi i,l} = \kappa\,(\chi_{ri,l}\, M_{ni,l} - \chi_{ni,l}\, M_{ri,l})/(M_{ni,l} + M_{ri,l})$	nodule–root C exchange		[F21]
$V_{\nu i,l} = \kappa\,(\nu_{ri,l}\, \chi_{ni,l} - \nu_{ni,l}\, \chi_{ri,l})/(\chi_{ni,l} + \chi_{ri,l})$	nodule–root N exchange		[F22]
$V_{\pi i,l} = \kappa\,(\pi_{ri,l}\, \chi_{ni,l} - \pi_{ni,l}\, \chi_{ri,l})/(\chi_{ni,l} + \chi_{ri,l})$	nodule–root P exchange		[F23]
$\delta\chi_{ni,l}/\delta t = V_{\chi i,l} - \min\{R_{mi,l}, R_{i,l}\} - R_{N_2 i,l} - U_{\chi i,l} + F_{LC\,l}\, L_{Ci,l}$	nodule nonstructural C		[F24]
$\delta\nu_{ni,l}/\delta t = V_{\nu i,l} - \delta N_{ni,l}/\delta t + V_{N_2 i,l} + F_{LN\,l}\, L_{Ni,l}$	nodule nonstructural N		[F25]
$\delta\pi_{ni,l}/\delta t = V_{\pi i,l} - \delta P_{ni,l}/\delta t + F_{LP\,l}\, L_{Pi,l}$	nodule nonstructural P		[F26]

Definition of Variables in Appendix F

Variable	Definition	Units	Equations	Input Values	Reference
B	parameter such that f_t = 1.0 at T_l = 298.15 K		F2	17.533	
$\chi_{ni,l}$	nodule nonstructural C	g m^{-2}	F17a,F18a,F21,F22,B23,B24		
$[\chi_{ni,l}]$	nodule nonstructural C concentration	g g^{-1}	F1,F13		
$\chi_{ri,l}$	root nonstructural C	g m^{-2}	F21,F22,F23		
D_{sO_2}	diffusivity of aqueous O_2	m^2 h^{-1}	F6b		
E_{N_2}'	direct energy cost of N_2 fixation	g N g C^{-1}	F12,F14	0.25	Gutschick, (1981), Voisin et al., (2003)
$F_{LC\,l}$	fraction of nodule C litterfall remobilized as nonstructural C	-	F24		
$F_{LN\,l}$	fraction of nodule N litterfall remobilized as nonstructural N	-	F25		
$F_{LP\,l}$	fraction of nodule P litterfall remobilized as nonstructural P	-	F26		
f_{CP}	effect of nodule nonstructural C or P content on N_2 fixation	-	F12,F13		
f_{NP}	effect of nodule N or P content on respiration	-	F1,F3		
f_t	temperature function for nodule respiration	-	F1,F2		
f_{tm}	temperature function for nodule maintenance respiration	-	F7,F8		
H_a	energy of activation	J mol^{-1}	F2	57.5 x 10^3	

H_{dh}	energy of high temperature deactivation	J mol^{-1}	F2	220 x 10^3
H_{dl}	energy of low temperature deactivation	J mol^{-1}	F2	190 x 10^3
$K_{\chi n}$	Michaelis-Menten constant for nodule respiration of $\chi_{ndi,l}$	g g^{-1}	F1	0.01
$K_{I\chi_n}$	inhibition constant for nonstructural N:C on N_2 fixation	g g^{-1}	F13	10
$K_{I\pi_n}$	inhibition constant for nonstructural N:P on N_2 fixation	g g^{-1}	F13	1000
K_{N_2r}	Michaelis-Menten constant for nodule N_2 uptake	g N m^{-3}	F12	0.14
K_{O_2r}	Michaelis-Menten constant for nodule O_2 uptake	g O m^{-3}	F6a	
κ	rate constant for nonstructural C,N,P exchange between root and nodule	h^{-1}	F21,F22,F23	
$L_{ri,l}$	root length	m m^{-2}	F6b	
$L_{Ci,l}$	nodule C litterfall	g C m^{-2} h^{-1}	F11,F16,F24	
$L_{Ni,l}$	nodule N litterfall	g N m^{-2} h^{-1}	F19,F25	
$L_{Pi,l}$	nodule P litterfall	g P m^{-2} h^{-1}	F20,F26	
$M_{ni,l}$	nodule structural C	g C m^{-2}	F1,F11,F12,F16 ,F17,F18,F21	
$M_{ri,l}$	root structural C	g C m^{-2}	F21	
$[N_n']$	maximum nodule structural N concentration	g N g C^{-1}	F3,F12	0.1

$N_{ni,l}$	nodule structural N	g N m^{-2}	F7,F11,F12,F17,F19,F25	
$[N_{ni,l}]$	nodule structural N concentration	g N g C^{-1}	F3,F17a	
$[N_{2ri,l}]$	rhizosphere aqueous N_2 concentration	g N m^{-3}	F12	
$\nu_{ni,l}$	nodule nonstructural N	g N m^{-2}	F17a,F22,F25	
$\nu_{ri,l}$	root nonstructural N	g N m^{-2}	F22	
$[\nu_{ni,l}]$	nodule concentration of nonstructural N	g g^{-1}	F13,F17a	
$[O_{2ri,l}]$	rhizosphere aqueous O_2 concentration	g O m^{-3}	F6a,b	
$[O_{2l}]$	soil aqueous O_2 concentration	g O m^{-3}	F6b	
$[P_n']$	maximum nodule structural P concentration	g P g C^{-1}	F3,F18a	0.01
$P_{ni,l}$	nodule structural P	g P m^{-2}	F18a,F20,F26	
$[P_{ni,l}]$	nodule structural P concentration	g P g C^{-1}	F3,F11	
$\pi_{ni,l}$	nodule nonstructural P	g P m^{-2}	F18a,F23,F26	
$\pi_{ri,l}$	root nonstructural P	g P m^{-2}	F23	
$[\pi_{ni,l}]$	nodule concentration of nonstructural P	g g^{-1}	F13	
R	gas constant	J mol^{-1} K^{-1}	F2	8.3143
$R_{gi,l}$	nodule growth respiration	g C m^{-2} h^{-1}	F9,F12,F15	

R'	specific nodule respiration at 25°C, and non-limiting O_2, $\chi_{ndi,l}$, $\nu_{ndi,l}$ and $\pi_{ndi,l}$	h^{-1}	F1	0.125
$R_{i,l}$	nodule respiration under ambient O_2	g C m^{-2} h^{-1}	F4,F9,F10,F24	
$\boldsymbol{R}_m$	specific nodule maintenance respiration at 25°C	g C g C^{-1} h^{-1}	F7	
$R_{maxi,l}$	nodule respiration under non-limiting O_2	g C m^{-2} h^{-1}	F1,F4,F5	
$R_{mi,l}$	nodule maintenance respiration	g C m^{-2} h^{-1}	F7,F9,F10,F24	
$R_{N_2i,l}$	nodule respiration for N_2 fixation	g C m^{-2} h^{-1}	F14,F15,F24	
$R_{si,l}$	nodule senescence respiration	g C m^{-2} h^{-1}	F9,F11	
$r_{ri,l}$	root radius	m	F6b	
r_{wl}	radius of soil water films	m	F6b	
S	change in entropy	J mol^{-1} K^{-1}	F2	710
T_l	soil temperature	K	F2,F8	
$U_{\chi i,l}$	uptake of nodule nonstructural C for growth	g C m^{-2} h^{-1}	F15,F16,F24	
$V_{\chi i,l}$	nonstructural C transfer between root and nodule	g C m^{-2} h^{-1}	F21,F24	
$V_{\nu i,l}$	nonstructural N transfer between root and nodule	g N m^{-2} h^{-1}	F22,F25	
$V_{N_2i,l}$	N_2 fixation	g N m^{-2} h^{-1}	F12,F14,F25	
$V_{O_2maxi,l}$	O_2 uptake by nodules under non-limiting O_2	g O m^{-2} h^{-1}	F4,F5,F6a	
$V_{O2i,l}$	O_2 uptake by nodules under ambient O_2	g O m^{-2} h^{-1}	F4,F6	

$V_{ni,l}$	nonstructural P transfer between root and nodule	g P m^{-2} h^{-1}	F23,F26	
Y_n'	nodule growth yield	g C g C^{-1}	F15,F16	0.67
y	shape parameter for f_{tm}	-	F8	0.081

References

Addiscott, T.M. 1983. Kinetics and temperature relationships of mineralization and nitrification in Rothamsted soils with differing histories. Journal of Soil Science 34:343-353.

Barber, S.A. and M. Silberbush. 1984. Plant root morphology and nutrient uptake. pp. 65-87. *In* S.A. Barber and D.R. Bouldin (eds.). Roots, Nutrient and Water Influx, and Plant Growth. Amer. Soc. Agron. Spec. Publ. no. 49. Madison, WI.

Barnes, B.V., D.R. Zak, S.R. Denton and S.H. Spurr. 1998. Forest Ecology 4th ed. Wiley and Sons. N.Y.

Bernacchi, C.J., E.L. Singsaas, C. Pimentel, A.L. Portis and S.P. Long. 2001. Improved temperature response functions for models of rubisco-limited photosynthesis. Plant, Cell and Environment 24:253-259.

Bernacchi, C.J., C. Pimentel. and S.P. Long. 2003. In vivo temperature response functions of parameters required to model RuBP-limited photosynthesis. Plant, Cell and Environment 26:1419–1430.

Berry J.A. and G.D. Farquhar. 1978. The CO2 concentrating function of photosynthesis: a biochemical model. pp. 119-131 In: Proceedings of the 4th Interntl. Congress on Photosynthesis. Hall D., Coombs J. and Goodwin T. eds. Biochemical Society. London.

Campbell, G.S. 1985. Soil Physics with BASIC. Elsevier, Netherlands. 185 pp.

de Vries, D.A. 1963. Thermal properties of soils. pp 210-235 In: van Wijk, R. (ed). *Physics of Plant Environment*. North Holland Publishing Co. Amsterdam, Netherlands

Dimitrov, D.D., Grant, R.F., LaFleur, P.M. and Humphreys, E. 2010. Modelling subsurface hydrology of Mer Bleue bog. Soil Science Society of America Journal 74:680-694 .

Doussan C., G. Vercambre and L. Pagès. 1998. Modelling of the hydraulic architecture of root systems: An integrated approach to water absorption – distribution of axial and radial conductances in maize. Annals of Botany 81:225-232.

Edwards, G. and D. Walker. 1983. C3, C4: Mechanisms, and Cellular and Environmental Regulation of Photosynthesis. Univ. of California Press, Berkely CA.

Farquhar G.D., S. von Caemmerer and J.A. Berry. 1980. A biochemical model of photosynthetic CO_2 assimilation in leaves of C_3 species. Planta 149:78-90.

Furbank, F.T. and M.D. Hatch. 1987. Mechanism of C4 photosynthesis. The size and composition of the inorganic carbon pool in bundle sheath cells. Plant Physiol. 85:958-964.

Grant, R.F. 2004. Modelling topographic effects on net ecosystem productivity of boreal black spruce forests. Tree Physiol. 24:1-18.

Grant, R.F. 2001. A review of the Canadian ecosystem model *ecosys*. pp. 173-264 in: Modeling Carbon and Nitrogen Dynamics for Soil Management. Shaffer M. (ed). CRC Press. Boca Raton, FL

Grant, R.F. 1998. Simulation in *ecosys* of root growth response to contrasting soil water and nitrogen Ecological Modelling 107: 237-264.

Grant, R.F. and Hesketh, J.D. 1992. Canopy structure of maize *(Zea mays L.)* at different populations: simulation and experimental verification. *Biotronics.* 21: 11-24.

Grant, R.F., M. Amrani, D.J. Heaney, R. Wright and M. Zhang. 2004. Mathematical modelling of phosphorus losses from land application of hog and cattle manure. Journal of Environmental Quality 33:210-233.

Grant, R.F., T.A. Black, E.R. Humphreys, and K. Morgenstern. 2007. Changes in net ecosystem productivity with forest age following clearcutting of a coastal Douglas fir forest: testing a mathematical model with eddy covariance measurements along a forest chronosequence. Tree Physiology. 27:115-131.

Grant, R. F. and L. B. Flanagan. 2007. Modeling stomatal and nonstomatal effects of water deficits on CO_2 fixation in a semiarid grassland. Journal of Geophysical Research 112:G03011, doi:10.1029/2006JG000302.

Grant, R.F. and D.J. Heaney. 1997. Inorganic phosphorus transformation and transport in soils: mathematical modelling in *ecosys*. Soil Science Society of America Journal 61:752-764.

Grant, R.F., N.G. Juma, and W.B. McGill. 1993a. Simulation of carbon and nitrogen transformations in soils. I. Mineralization. Soil Biology & Biochemistry 27:1317–1329.

Grant, R.F., N.G. Juma, and W.B. McGill. 1993b. Simulation of carbon and nitrogen transformations in soils. II. Microbial biomass and metabolic products. Soil Biology & Biochemistry 27:1331–1338.

Grant, R.F., G.W. Wall, B.A. Kimball, K.F.A. Frumau, P.J. Pinter Jr., D.J. Hunsaker, and R.L. Lamorte. 1999. Crop water relations under different CO_2 and irrigation: testing of ecosys with the free air CO_2 enrichment (FACE) experiment. Agricultural & Forest Meteorology 95:27-51.

Grant, R.F., B.A. Kimball, G.W. Wall, J.M. Triggs, T.J. Brooks, P.J. Pinter Jr., M.M. Conley, M.J. Ottman, R.L. Lamorte, S.W. Leavitt, T.L. Thompson and A.D. Matthias. 2004. How elevated CO2 affects water relations, water use and growth of irrigated sorghum: testing a model with results from a Free Air CO2 Enrichment (FACE) experiment Agron. J. 96: 1693-1705.

Grant, R.F., Barr, A.G., Black, T.A., Margolis, H.A., McCaughey, J.H. and Trofymow, J.A. 2010. Net ecosystem productivity of temperate and boreal forests after clearcutting – a Fluxnet-Canada synthesis. *Tellus B.* 62B: 475-496.

Green, R.E., and R.B. Corey. 1971. Calculation of hydraulic conductivity: A further evaluation of some predictive methods. Soil Sci. Soc. Am. Proc. 35:3–8.

Griffin, D.M. 1972. Ecology of Soil Fungi. Syracuse Univ. Press, Syracuse N.Y. 193 pp.

Jiao, J.A. and R. Chollet. 1988. Light/dark regulation of maize leaf phosphoenol pyruvate carboxylase by in vivo phosphorylation. Arch. Biochem. Biophys. 261:409-417.

Laisk, A. and G.E. Edwards. 2000. A mathematical model of C4 photosynthesis: The mechanism of concentrating CO2 in NADP – malic enzyme type species. Photosyn. Res. 66:199-224.

Larcher, W. 2001. Physiological Plant Ecology 4th ed. Springer-Verlag. Berlin

Lawlor, D. 1993. Photosynthesis: molecular, physiological and environmental processes. Longman Group, Essex, UK.

Leegood, R.C. 2000. Transport during C4 photosynthesis. pp. 449-469. In Advances in Photosynthesis: 9. Photosynthesis: Physiology and Metabolism. Leegood, R.C., Sharkey, T.D. and von Caemmerer, S. (eds). Kluwer Academic Publishers, Dordrecht.

Lizama H.M. and Suzuki I. 1990. Kinetics of sulfur and pyrite oxidation by *Thiobacillus thiooxidans*. Competitive inhibition by increasing concentrations of cells. Canadian Journal of Microbiology 37, 182-187.

Luxmoore R.J., L.H. Stolzy and J. Letey. 1970a Oxygen diffusion in the soil-plant system. I. a model. Agron. J. 62, 317-322.

Luxmoore R.J., L.H. Stolzy and J. Letey. 1970b Oxygen diffusion in the soil-plant system. II. respiration rate, permeability, and porosity of consecutive excised segments of maize and rice roots. Agron. J. 62, 322-324.

Medrano, H., J.M. Escalona, J. Bota, J. Gulías and J. Flexas, Regulation of photosynthesis of C_3 plants in response to progressive drought: stomatal conductance as a reference parameter. *Ann. Bot*., *89*, 895-905, 2002.

Millington, R.J. and J.M. Quirk. 1960. Transport in porous media. pp. 97-106 In: Van Beren, F.A. et al. (eds). 7th Trans. Int. Congr. Soil Sci. vol. 1. Madison, WI. 14-24 Aug. 1960. Elsevier, Amsterdam.

Perrier, A. 1982. Land surface processes: vegetation. pp. 395-448 In: *Atmospheric General Circulation Models.* Eagleson P.S. (ed.). Cambridge Univ. Press. Cambridge, U.K.

Pirt S.J. 1975. Principles of Microbe and Cell Cultivation. Blackwell Scientific. Oxford, U.K.

Postgate, J. 1998. Nitrogen Fixation (3rd Ed.). Cambridge Univ. Press, Cambridge, UK. 112 pp.

Sawada, S., T. Sakamoto, M. Sato, M. Kasai and H. Usuda. 2002. Photosynthesis with single-rooted Amaranthus leaves. II. Regulation of Ribulose-1,5-Bisphosphate Carboxylase, Phosphoenolpyruvate Carboxylase, NAD-Malic Enzyme and NAD-Malate Dehydrogenase and coordination between PCR and C4 photosynthetic metabolism in response to changes in the source-sink balance. Plant Cell Physiol. 43(11):1293-301.

Seeman, J.R., M.R. Badger and J.A. Berry. 1984. Variations in the specific activity of ribulose-1,5-bisphosphate carboxylase between species utilizing differing photosynthetic pathways. Plant Physiol. 74:791-794.

Sharpe, P.S.H. and D.W. DeMichelle. 1977. Reaction kinetics of poikilothermic development. Journal of Theoretical Biology 64:649-670.

Shields J.A., E.A. Paul, W.E. Lowe and D. Parkinson. 1973. Turnover of microbial tissue in soil under field conditions. Soil Biology & Biochemistry 5:753-764.

Shulten, H.-R., and M. Schnitzer. 1997. Chemical model structures for organic matter and soils. Soil Science 162:115–130.

Skopp, J. 1985. Oxygen uptake and transfer in soils: analysis of the air-water interfacial area. Soil Sci. Soc. Amer. J. 49:1327-1331.

van Bavel, C.H.M., and D.I. Hillel. 1976. Calculating potential and actual evaporation from a bare soil surface by simulation of concurrent flow of water and heat. Agric. Meteorol. 17:453-476.

Veen, B.W. 1981. Relation between root respiration and root activity. Plant Soil 63: 73-76.

Waring, R.H. and S.W. Running. 1998. Forest Ecosystems: Analysis at Multiple Scales. (2nd ed.) Academic Press. London U.K.

Wilhelm, E., R. Battino and R.J. Wilcock. 1977. Low-pressure solubility of gases in liquid water. Chem. Rev. 77:219-262.

Williams D.G., V. Gempko, A. Fravolini, S.W. Leavitt, G.W. Wall, B.A. Kimball, P.J. Pinter Jr., R. LaMorte and M. Ottman. 2001. Carbon isotope discrimination by Sorghum bicolor under CO2 enrichment and drought. New Phytol. 150:285-293.